Departamento de Bioquímica

Facultad de Medicina

Doctoral thesis

Patient-Derived Metastatic Models of Pancreatic Cancer: An *in-vivo* system for modeling metastasis and preclinical drug screening.

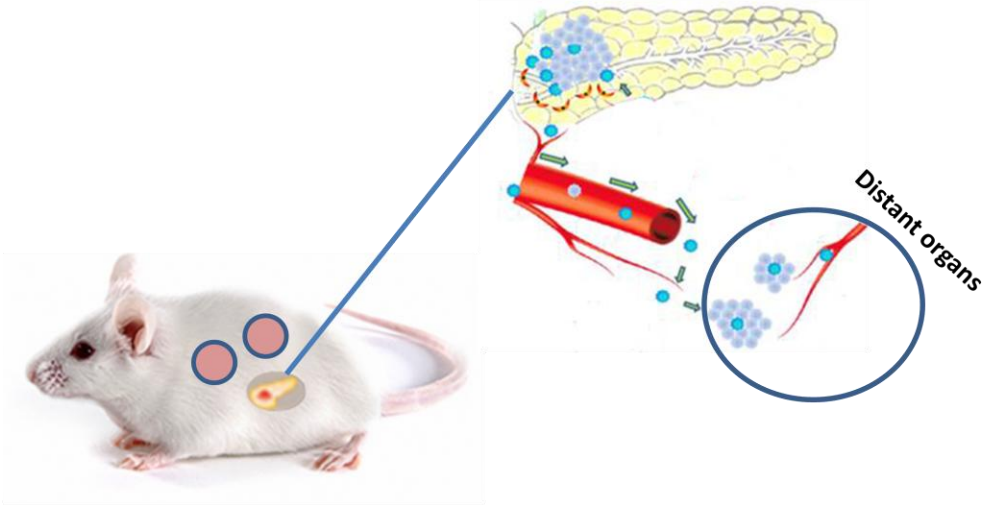

Spas Dimitrov Markov

Madrid, 2017

Departamento de Bioquímica
Facultad de Medicina

UNIVERSIDAD AUTÓNOMA DE MADRID

PATIENT-DERIVED METASTATIC MODELS OF PANCREATIC CANCER: AN *IN-VIVO* SYSTEM FOR MODELING METASTASIS AND PRECLINICAL DRUG SCREENING.

Doctoral thesis presented by the graduate in Molecular Biology

Spas Dimitrov Markov

Thesis Directores:
Dr. Manuel Hidalgo Medina
Dr. Pedro Pablo López Casas

Spanish National Cancer Research Centre (CNIO)
Madrid, Spain

“What doesn’t kill us makes us stronger.”

Friedrich Nietzsche

Acknowledgments

The completion of the doctoral thesis is a long term process, accompanied by hard working days, many weekends and holidays in the laboratory and many sleepless nights, but the funny moments were also part of this journey. Although my personal motivation and willing were the main driving force, the voluntary help of many people also contributed for the successful completion of this thesis.

First of all, I would like to thank to Dr. Manuel Hidalgo for giving me the opportunity to work on very motivating, exciting and promising projects, for his scientific and moral support, for his constructive advices, suggestions and ideas, and for his kindly treatment and amiable disposition. Also thanks to Dr. Pedro P. López for helping me with the experimental design, interpretation of the results and with optimization of different methods and protocols, for sharing with me his ideas and project proposals, which I constructively used to build some of the hypothesis and goals of the thesis. Thanks to Manuel Muñoz for teaching me many molecular and cell biology techniques and for providing his scientific experience for successful solution of different technical issues. Thanks to Natalia Baños, Victoria Bonilla, Camino Menéndez, Aurora Garcia, Yolanda Durán for teaching me many techniques and procedures, which involve working with experimental animals, for helping me with the *in-vivo* experiments and for backing me up during my annual holidays. Also, I want to express my sincere gratitude to you Viki for being one of the few persons, who had the courage to defend, support me and stay behind me in various occasions. I will never forget this nice gesture on your part. Thanks to Dr. Monica Musteanu for helping me with the optimization of the immunohistochemistry techniques. Thanks to Dr. Marina Mendiburu for sharing with me her experience in immunohistochemistry techniques. Thanks to Flow cytometry unit and especially to Dr. Miguel Sánchez for his help in experimental design and interpretation of flow cytometry data. Thanks to Dr. Fátima Al-Shahrour for her scientific support and advices on bioinformatic part of the thesis, and for providing tech support and help in interpretation of the results. Thanks to Javier Perales for his dedication in carrying out the computational part of the project and data analysis, for elaboration of the methodological part and some of the results, for preparation of some of the figures and of course for the long talks in social room. Thanks to Virginia Granda for helping me with the maintenance and the care of the mice colonies, and for the multiple funny moments in the Biomodule I. Thanks for Soraya Ruiz for teaching me to dominate the intravenous administration technique. Thanks to Maria Udriste

for her support and help with quantification and scanning of the immunohistochemical slides, and for the long talks and moments together. Thanks to Histopathology core unit for their excellent service throughout all these years and to Patricia González for the preparation of the methodological part of Alu protocol. Thanks to Dr. Hector Peinado and Dr. Susana Garcia for their scientific support and help with the exosome project. Thanks to Maria Pillar and Dr. Javier Muñoz from Proteomics core unit for their dedication in analysis and interpretation of the proteomic data. Thanks to Diego, Manu, Ximo from Confocal Microscopy core unit for their excellent service and helpful advices. Thanks to Dr. Manuel Valiente for the preparation of the brain tissue slides and for the acquisition of the fluorescence images. Thanks to Dr. Ana Dopazo and her team for their tech and scientific support on the genomic experiments. Many thanks to Inés Padura for providing me with hundreds of NSG mice to complete all In-vivo experiments. Last but not least, I would like to thank to my family and all my relatives and friends for their constant support throughout all these years. I want to thank to my brother Georgi Markov for his support, advices, his brother's love, generosity, and for all these funny moments that we spent together in Madrid. I also want to express my gratitude to him for coming back from USA to Madrid, when I was on trouble. He spent thousands of dollars for phone calls and flight tickets to help me overcome workplace and medical issues. I have the best brother on the world, who I love so much. I want to thanks to my mom Irina Markova and my dad Dimitar Markov for their infinite love, support, advices, long phone talks, gift surprises and for always being there for me. Thanks also to my uncle Stoyan Markov for providing me a financial support, when I arrived for the first time in Madrid and for the long talks about football and politics. Thanks to my uncle Vlado and my aunt Eli for their constant support, gift surprises, and for their kindly hospitality and treatment. To my cousans Dimitar, Sashko, Joro for their funny moments in Madrid and in Bulgaria. Thanks to my grandparents Georgi, Sofia, Spaska and Dimitar for supporting me, loving me, believing in me, praying for me and for successful outcome of the experiments. Thanks to my friends for their faithful friendship throughout all these years together.

Por último, quiero expresar en castellano mis más sinceras gracias a Reino de España, CNIO y la universidad Autónoma de Madrid por haber me dado la oportunidad de realizar los estudios de postgrado y la tesis doctoral.

Thank you.

Gracias.

Abstract

Although new chemotherapy regimens have shown significant survival improvement in patients with local, locally advanced and metastatic pancreatic ductal adenocarcinoma (PDAC), metastasis still remains the leading cause of cancer-related mortality in this disease. Therefore, discovery of novel drivers of metastasis for improvement of therapeutic options against metastasis is of crucial importance. Patient-derived xenografts (PDX) models have become a promising system for studying cancer diseases. Orthotopic models have been shown to better mimic the metastatic disease. However, to date, only few PDX orthotopic models of pancreatic cancer have been reported to establish distant metastasis. The metastatic incidence in these models still remains relatively low, therefore development of more efficient and reproducible model for studying metastasis is urgently needed.

In this thesis work, we developed several metastatic PDX models of PDAC by orthotopic transplantation of human pancreatic cancer specimens into immunodeficient NOD/SCID/IL2g-receptor null (NSG) mouse. Importantly, these preclinical models develop liver and/or lung metastasis with a high reproducibility rate. We further used these models as an *In-vivo* platform for isolation of the human tumor populations involved in metastatic process and their functional and single-cell transcriptomic characterization. In-vivo transplantation of the circulating tumor cells (CTCs) showed that they possess high tumorigenic and metastatic potential. Single-cell RNA sequencing analysis revealed that the CTCs cluster separately from their matched primary tumor and metastatic cells, displaying low expression of cell cycle- and ECM-associated genes and enrichment for genes involved in ribosome biogenesis. In addition, CTCs showed an increased expression of numerous cancer-related genes including Survivin, AURKA, and AURKB among others. Moreover, Survivin protein expression was detected in primary tumors and metastatic lesions of all metastatic models. Pre-clinical treatment with YM155 (survivin suppressor) decreased the metastatic tumor burden and showed beneficial effects on survival of the mice bearing metastatic ortotopic tumors. In addition, primary tumor resection in combination with YM155 resulted in significant improvement in median survival of the mice compared with control group. Finally, proteomic characterization of pancreatic cancer exosomes isolated from primary tumors and metastatic organs of PDX models revealed an organ-specific protein signatures with abundant expression of human proteins some of them reported to have a role in metastatic organotropism.

Resumen

Aunque los nuevos regímenes de quimioterapia han demostrado una mejora significativa de la supervivencia en pacientes con adenocarcinoma ductal pancreático local (ADP), localmente avanzado y metastásico, la metástasis sigue siendo la principal causa de mortalidad relacionada con esta enfermedad. Por lo tanto, el descubrimiento de nuevos ejecutores de metastasis para la mejora de las opciones terapéuticas contra la metástasis es de importancia crucial. Los xenoinjertos derivados de paciente (PDX) se han convertido en una plataforma muy prometedora para estudiar las enfermedades del cáncer. Se ha demostrado que los modelos ortotópicos mimetizan mejor la enfermedad metastásica. Sin embargo, hasta la fecha, sólo unos pocos modelos PDX ortotópicos de ADP se han reportado de establecer metástasis a distancia. La incidencia metastásica en estos modelos sigue siendo relativamente baja, por lo tanto, el desarrollo de un modelo más eficaz y reproducible para estudiar la metástasis es urgentemente necesario. En este trabajo de tesis, hemos desarrollado varios modelos metastásicos PDX de PDAC mediante trasplantación ortotopica de muestras pancreáticas tumorales humanas en ratones inmunodeficientes NOD / SCID / IL2g-null receptor (NSG). Es importante destacar que estos modelos preclínicos desarrollan metástasis hepática y/o pulmonar con una alta tasa de reproducibilidad. Además, hemos utilizado estos modelos como una plataforma *In-vivo* para el aislamiento de las poblaciones tumores humanas involucradas en el proceso metastásico y su caracterización funcional y transcriptómica al nivel individual. El trasplante *In vivo* de las células tumorales circulantes (CTC) mostró que poseen alto potencial tumorigénico y metastásico. Secuenciación individualizada del RNA reveló que las CTC se agrupan por separado de su correspondientes células tumorales primarias y metastásicas, mostrando baja expresión de genes asociados con el ciclo celular y el matriz extracelular y enriquecimiento de genes implicados en la biogénesis de ribosomas. Además, los CTC mostraron una expresión elevada de numerosos genes relacionados con el cáncer incluyendo Survivina, AurkA, y AurkB, entre otros. Por otra parte, la expresión de la proteína Survivina se detectó en los tumores primarios y las lesiones metastásicas de todos los modelos metastásicos. El tratamiento preclinico con YM155 (supresor de Survivina) disminuyó la carga tumoral metastásica y mostró efectos beneficiosos sobre la supervivencia de los ratones portadores de los tumores ortotópicos. Además, la resección del tumor primario en combinación con YM155 resultó en una mejora significativa en la supervivencia media de los ratones en comparación con el grupo control. Finalmente, la caracterización proteómica de los exosomas de cáncer pancreático aislados de los tumores primarios y los organos metastásicos de los modelos PDX reveló firmas proteómicas órgano-específicas con abundante expresión de proteínas humanas algunas de ellas reportadas de tener papel en el organotropismo metastatico.

Contents

Abbreviations

PDAC: Pancreatic ductal adenocarcinoma

PDX: Patient-derived xenografts

NSG: NOD/SCID/IL2g

CTCs: Circulating tumor cells

IPMNs: intraductual papillary mucinous neoplasia

MCNs: mucinous cystic neoplasia

PanINs: pancreatic intraepithelial neoplasia

MD: main duct

BD: branch duct

CDKN2A/p16: *cyclin-dependent kinase inhibitor 2A*

KRAS: *kristen rat sarcoma viral oncogen homolog*

SMAD4/DPC4: *SMAD family member 4*

TP53: *tumor protein p53*

TGF-β: *transforming growth factor, beta*

DTCs: disseminated tumor cells

LOH: Loss of heterogeneity.

MICs: metastasis initiating cells

EMT: epithelial-mesenchymal transition

ECM: extracellular matrix

MMP: matrix metalloproteinase

TEM: Transendothelial migration

ANGPTL4: ANGIOPOIETIN LIKE 4

VEGF: Vascular endothelial growth factor

COX-2: cicloxigenasa-2

BMDCs: bone marrow-derived cells

OPN: osteopontin

SDF 1: stromal cell-derived factor 1

Psap: prosaposin

Angpt2: Angiopoietin 2

DNA: Deoxyribonucleic acid

RNA: Ribonucleic acid

ITG: Integrin

GEMM: Genetically Engineered Mouse *Models*

scRNA-seq: Single-cell RNA sequencing

shRNAs: Short hairpin RNAs

KPC: $^{G12D/+}$; $p53^{R172H/+}$; PdxCre mice

SPARC: Secreted *Protein* Acidic And Cysteine Rich

WFA: Withaferin-A

IHC: immunohistochemistry

PCA: principal component analysis

CPM: copy per millions

PAGODA: pathway and gene set overdispersion analysis.

FN1: fibronectin 1

ITGB5: Integrin Subunit Beta 5

COL1a1: Collagen Type I Alpha 1

CNIO: Spanish National Cancer Research Centre

AURKA: Aurora Kinase A

AURKB: Aurora Kinase B

PLK-1: polo-like kinase 1

PAC-1: Promoter of caspase signaling

IHC: Immunohistochemistry

IF: Immunofluorescence

IL32: Interleukin 32

HSPB1: heat shock protein family B member 1

MTA2: Metastasis-associated protein 2

Gly12: Glycine 12

Gly13: Glycine 13

Gln61: Glutamine 61

MET: mesenchymal-epithelial transition

s.c: subcutaneously

CNIC: Centro Nacional de Investigaciones Cardiovasculares

Spas Dimitrov Markov

I. INTRODUCTION.

1.1.Pancreatic ductal adenocarcinoma.

1.1.1. Anatomy of pancreas and pancreatic cancer types.

The pancreas is a retroperitoneal organ located behind the stomach in the upper left abdomen. As illustrated in Figure 1, the pancreas is anatomically divided in head, neck, body and tail parts. The head is the widest and thickest part lying within the curve of the duodenum and over the inferior vena cava. The head is composed of an additional lobe called ucinate process, which is grooved by the superior mesenteric artery and the superior mesenteric vein. The neck connects the head to the body of the pancreas, it is grooved by the posterior mesenteric vessels, and it lies in front of the commencement of the portal vein. The body is the middle and longest part of the pancreas, that is located between the neck and the tail, where the mesenteric artery and vein pass behind this part of the pancreas. The tail is the narrowest part of the gland, located in the left side of the abdomen and its end contacts the splenic hilium. The pancreas is both an exocrine and an endocrine gland. The exocrine part is composed of acini cells, which secrete various digestive enzymes and bicarbonates. The endocrine pancreas is made up of the islets cells(called the islets of Langerhans), which are isolated clumps of endodermal cells divided into four cell types: alpha cells (produce glucagon), beta cells (produce insulin), delta cells (produce somatostatin) and PP cells (produce pancreatic polypeptides) [Figure1].

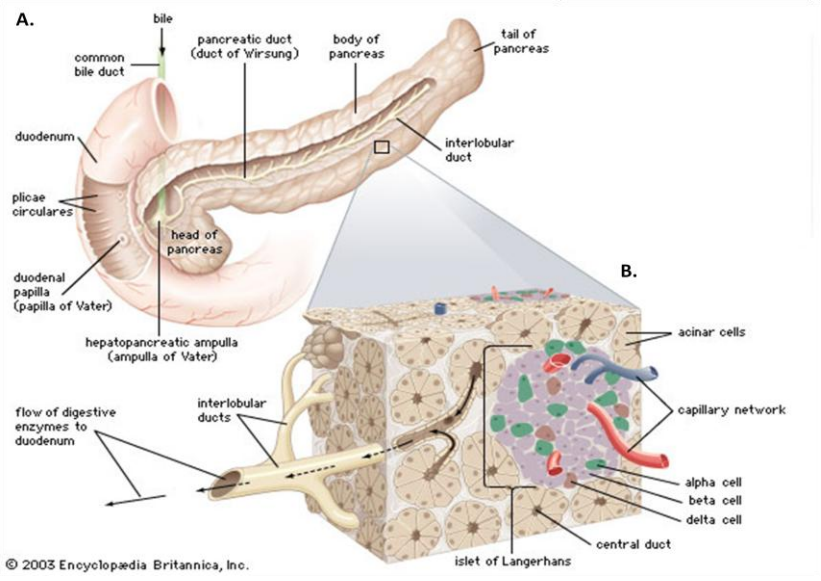

Figure 1. Anatomy of pancreas. (A). Gross anatomy of the pancreas indicating its close anatomical relationship with the duodenum and common bile duct. **(B).** The major components of the pancreatic parenchyma on a celular level. (Figure adapted from Encyclopaedia Britannica, Inc., © 2003.)

Pancreatic cancer is the third leading cause of cancer death in developed countries with a 5-year survival rate of only 5% [1,2]. There are several histological types of malignant tumors in the pancreas, with pancreatic ductal adenocarcinoma (PDAC) variant represents the most common type (80-90%). The other less frequent pancreatic exocrine and endocrine neoplasms are shown in Table 1.

Table 1. Histological classification of pancreatic neoplasms [3-5].

Histological type	Origin	Frequency
PDAC	Exocrine	80-90%
Acinar cell carcinoma	Exorcine	2%
Mucinous cystadenocarcinoma	Exocrine	3%
Serous cystadenocarcinoma	Exocrine	<1%
Intraductal papillary mucinous neoplasm	Exocrine	1-3%
Pseudopapillary carcinoma	Exocrine	<1%
Pancreatoblastoma	Exocrine	Rare
Gastrinoma	Endocrine	1-2%
Insulinoma	Endocrine	1-2%
Glucagonoma	Endocrine	<1%
Somatostatinoma	Endocrine	Rare
Vipoma	Endocrine	<1%

1.1.2. Staging classification of exocrine pancreatic cancer.

The most widely used staging system for exocrine pancreatic cancer was defined by the American Joint Committee on Cancer in agreement with the TMN Committee of the International Union Against Cancer [6]. This classification determines the anatomical extent of the disease, including the size and invasiveness of the primary tumor (T), the presence of regional nodal metastases (N), and the existence of distant metastasis (M). For pancreatic cancer, in particular, local extension of the primary tumor may result in unresectability. This is reflected in the staging system, where T3 primary tumors extends beyond the pancreas without involvement of unresectable structures, but T4 primary tumors involve structures such as celiac axis or superior mesenteric artery and they are classified as unresectable tumors. Table S1 illustrates the components of this staging system, including the anatomic stage of the disease and the prognostic groups.

1.1.3. Preneoplastic pancreatic lesions and their genetic features.

It has been shown that PDAC develops through a stepwise progression from preinvasive lesions, including intraductual papillary mucinous neoplasia (IPMNs), mucinous cystic neoplasia (MCNs), and pancreatic intraepithelial neoplasia (PanINs) to invasive neoplasms [7]. The IPMNs are mucin-producing epithelial neoplasms, which grow in the main duct (MD-IPMN) or branch duct (BD-IPMN) of the pancreas and are characterized by papillary architecture, intraductal proliferation of neoplastic duct epithelium, accompanied by mucin production. Based on their histological features, the IPMNs are subdivided in gastric, oncocytic, pancreatobiliary, and intestinal subtypes. On the other hand, the MCN precursor lesions mainly arise in women and are usually located in the pancreatic body and tail. In contrast to IPMNs, MCNs do not connect with the main pancreatic duct. Histologically, the MCNs are composed of mucinous epithelial lining, which consists of columnar cells with a varying degree of dysplasia and it is associated with an underlying ovarian-like stroma.

The third and best-characterized precursor lesion in the pancreas are the PanINs. Based on the degree of epithelial atypia, the PanINs are subdivided in four different grades: PanIN-1A, PanIN-1B, PanIN-2, and PanIN-3 [8]. PanIN-1 is a common incidental lesion, characterized by only minimal atypia and it may be found in up to 40% of noncancerous pancreata. Moreover, PanIN-1 lesions are divided into flat (PanIN-1A) and papillary (PanIN-1B) types. The lesions with moderate atypia are designated PanIN-2, whereas those with pronounced atypia are PanIN-3,

which is more closely associated with invasive carcinoma, and are detected in 30-50% of pancreata with infiltrating ductal carcinoma. Normally, it is difficult to follow the progression of PanINs to invasive carcinoma, because PanINs are radiographically undetectable and they are usually only seen in pancreatectomy specimens. However, a few clinical cases of progression have been reported [9-11], which further support the precursor nature of PanINs.

Most of the genetic alteration of infiltrating ductal carcinoma is identified at different stages in the PanINs progression. These alterations include telomere shortening and somatic mutations in the *KRAS* oncogene, *CDKN2A* (p16), TP53 and *SMAD4* tumour suppressor genes [12]. One of the earliest events in pancreatic tumorigenesis is a telomere shortening responsible for inducing genetic instability and activation of KRAS oncogene, mainly through single point mutations in codon 12. The tumor suppressor gene p16 is frequently found inactivated in early stages of PanIN progression. Mutations in two additional tumor suppressor genes, TP53 and SMAD4, are often associated with progression of PanIN-3 lesions to invasive ductal carcinoma. Figure 2 illustrates the progression model of pancreatic carcinoma and the mutation frequency of the genes in each of the PanINs lesions.

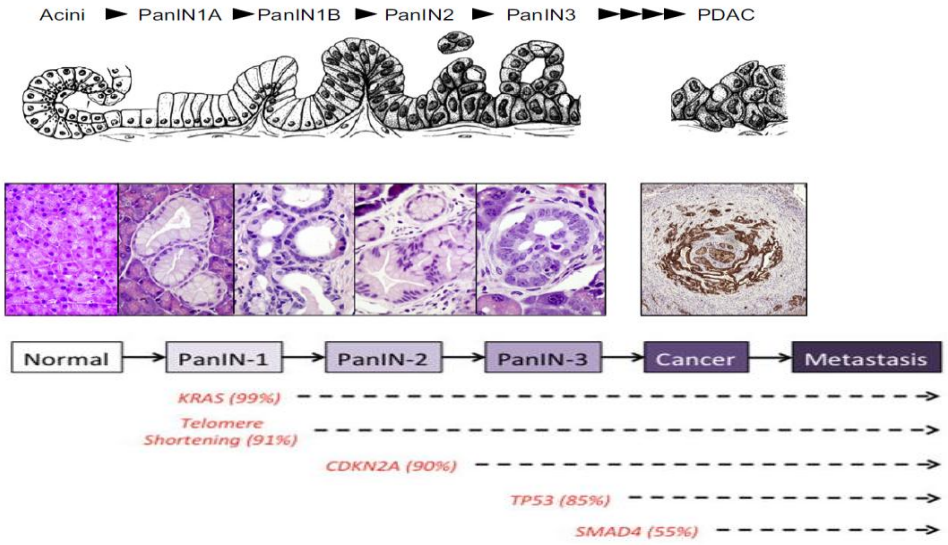

Figure 2. Progression model of pancreatic carcinogenesis. The top figure shows the morphologic progression model of pancreatic carcinogenesis. Illustrated from left to right are histological examples of a normal pancreatic duct, the PanINs classified in four groups, and infiltrating carcinoma, respectively. The bottom figure illustrates the genetic progression model of pancreatic cancer. The genetic alterations arising during pancreatic carcinogenesis are classified

into four events: early event - telomere shortening and constitutive activation of *KRAS* oncogene, intermediate event - inactivation of *CDKN2A* tumor suppressor gene and late event – inactivation of *TP53* and *SMAD4* events. The figures are taken from Feldmann Get et al.(2007) and Macgregor-Das et al. (2013). [12-13].

1.1.4. Molecular Genetics of Pancreatic cancer.

A great effort has been made in the past years to study the molecular mechanisms of this genetically complex disease. Numerous genetic alterations have been identified in pancreatic cancer, including amplifications and homozygous deletions, copy-number gains, chromosomal rearrangements and loss of heterozygosity (LOH) with and without copy number changes [10-13]. However, the spectrum of the altered genes and the types of alterations makes each pancreatic tumor distinctive.

The most frequent mutations in the PDAC are those described previously in the progression model, including the KRAS oncogene (99%) and tumor suppressor genes: CDKN2A/ p16 (90%), TP53 (85%) and SMAD4 / DPC4 (55%). K-ras (12p12.1) encodes a membrane-bound GTP-binding protein, which triggers various cellular functions, such as the transition through the G1 phase of the cell division cycle, survival, motility, and cytoskeletal remodeling. The K-ras activating mutations abrogate the GTP-binding pocket of the K-ras protein, which in turns converts the protein constitutively active. Somatic mutations of the codons Gly12, Gly13, or Gln61 are normally associated with permanently active K-ras. [18-19].

The second most frequent genetic alteration in pancreatic cancer occurs in *CDKN2A* (p16,9p21.3) gene, which is one of the most frequently mutated genes in cancer. P16 is considered as tumor suppressor gene, which regulates cell cycle progression by blocking the Rb phosphorylation through inhibition of cyclinD-CDK4/6 complex, whose function is mediating the commencement of the G1/S phase transition. The inactivation of p16 can occur through multiple mechanisms such as homozygous deletion, promoter hypermethylation or intragenic mutations [20-21]. Inactivation of p16 alone or in combination with activity of other oncogenes make a significant contribution to the formation of the pancreatic precursor lesions and their progression to pancreatic cancer.

TP53 (p53,1713.1) is another frequently mutated gene in pancreatic cancer. TP53 is tumor-suppressive gene, which main function is maintenance of a G2/M arrest and regulation of a G1/S

transition to facilitate normal cell cycle progression. Inactivating mutations in TP53 gene occur in more than 50% of sporadic pancreatic cancers, and they normally abolish the ability of the protein to bind to DNA and activate gene transcription [22-23]. In contrast to other tumor suppressor genes, homozygous deletions of TP53 are rarely identified; most of the alterations are missense mutations.

SMAD4 (18q21.1) is a tumor suppressor gene, that is commonly inactivated in approximately 45% of pancreatic cancers, mainly through homozygous deletion mutations [24-27]. SMAD4 is a member of TGFβ signaling and it has been shown to negatively regulates the tumor initiation and progression [28-29]. Functional characterization has demonstrated that the loss of SMAD4 promotes the TGFβ-mediated cancer cell growth and metastasis.

1.1.5. Treatment of PDAC.

Currently the most effective treatment is surgery, mainly due to the low success rate of most drug therapies. In this sense, various strategies are being investigated, based on the use of chemotherapy with or without radiotherapy, administered in the adjuvant or neoadjuvant settings. The current postsurgical treatments for PDAC are 5-fluorouracil, gemcitabine and nab-paclitaxel. Patient with metastatic pancreatic cancer are candidates for combination therapy with gemcitabine plus erlotinib, gemcitabine plus nab-paclitaxel, or the multidrug regimen of FOLFIRINOX (leucovorin, fluorouracil, irinotecan, and oxaliplatin) [30].

The median survival of patients treated with surgery is about two years, however this time decreases dramatically to 6-8 months in patients diagnosed with metastatic disease [31,32]. Therefore, alternative therapeutic strategies are urgently needed in PDAC.

1.2. Cancer metastasis.

The ability to develop metastasis is considered the most life-threatening feature of neoplastic cells and it is the first cause of cancer-related morbidity and mortality [33]. The metastases represent a subset of cells that escaped from primary tumor and colonized distant organs. This subset of metastatic cells is phenotypically distinct from the primary tumor cells, and the molecular mechanisms underlying these phenotypic characteristics of metastatic cells are currently being investigated.

1.2.1. Routes of dissemination.

Tumor dissemination may follow several routes, including local invasion, lymphatics or hematogenous spread, or direct seeding of body cavities. Another less common routes of spread have also been described, including dissemination of cancer cells trough the space between endothelium and basement membrane or perineural invasion in pancreatic and prostatic carcinomas. **In this doctoral thesis, the hematogenous dissemination is the principal focus of study.**

1.2.2. Metastasis progression models.

There are two distinct models which to some extend explain the phylogeny and progression of metastatic disease. These models are linear progression and parallel progression model and are discussed in the following chapter.

Linear progression model.

This model proposes that cancer cells can undergo multiple selective rounds of mutations within the primary tumor, and only a small subgroup of these tumor cell clones will acquire the genetic and epigenetic alterations necessary for generation of metastasis-competent cell clones (illustrated in Figure 3) [34]. The model also suggests that larger tumors may contain more metastasis-competent cells within the whole heterogeneous tumor population. Therefore, this fits well with TNM international classification system claiming that tumor size is associated with higher metastatic frequency. According to the model conception, metastasis founder cells usually spread at late stages of disease, and this is supported by evidences in the literature showing that the most invasive primary tumors exhibit a close genetic similitude with their corresponding metastases [35]. These metastatic cells can also disseminate from a first metastatic site to other organs, thus resulting in sequential development of multiple metastastatic lesions [36].

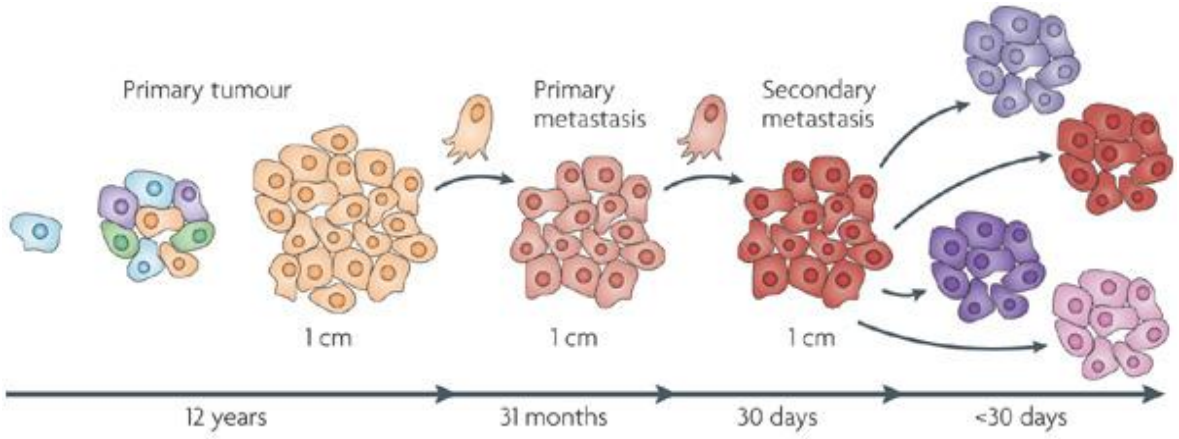

Figure 3. The linear progression model. Cancer cells within primary tumor cells continuously acquire numerous genetic alterations by which some of these cells can transform into metastasis-competent clones. At the late stage of primary tumor progression, metastatic clones within the primary tumors start to disseminate and subsequently develop into micro and overt macrometastases. Tumor cells from the first metastatic site may also colonize other organs, thus generating multiple and successive metastatic lesions. The Figure is taken from Klein, (2009) [39].

Several recent studies have shed new light on the genomic evolution during tumor progression. For example, Aparicio and collegues sequenced a breast cancer metastasis and its matched primary tumor, resected 9 years earlier and found that 11 out of 30 mutations that were identified in the metastatic lesions were also present in the primary tumor [37]. Therefore, this study demonstrated that some of the mutations in the primary tumor are also selected in the metastasis, but the genomic evolution occurring during metastatic progression is also prominent. In another study, Yachida and colleagues performed genomic sequencing studies to investigate the phylogenetic relationship between pancreatic primary tumors and their corresponding metastasis [38]. The authors suggest that metastasis is a late event in the genetic evolution of pancreatic cancer, showing that clonal populations which give rise to metastasis are also present within the primary tumor, but they are more genetically evolved than parental non-metastatic clone. Moreover, using mathematical modeling, they concluded that the appearance of metastasis-competent clones within the primary tumor takes place 10 years after tumor initiation and they spread 5 to 6 years later from the primary tumor.

In another in-depth study, Makohon-Moore and colleagues performed whole-genome sequencing of 39 samples including 26 metastatic lesions, up to 3 distinct regions of each primary tumor, and corresponding normal tissues obtained from untreated patients who died of metastatic pancreatic cancer [39]. They identified 614 somatic mutations, which they used to assess the genetic heterogeneity between primary tumors and metastases. The results showed that each patient harbored unique set of driver mutations that were present in both primary and metastatic tumors. Therefore, these findings indicate little variability of driver mutations in these PDAC patients and specific driver mutations of metastasis were not identified in this study.

McDonald and colleagues recently published a paper, where they used a large panel of matched primary and metastatic PDAC samples obtained from five untreated patients to study the impact of epigenetic heterogeneity on the pancreatic cancer progression [40]. Interestingly, the authors revealed massive epigenetic changes with chromatin modifications including global reprogramming of histone H3K9, DNA methylation within large heterochromatin domains (LOCKs) and gene regulatory modifications, both in the distant (liver lung) metastasis and in the primary tumor subclones they came from. They also discovered that distant metastases and their precursors processed glucose through the oxidative pentose phosphate pathway. Moreover analysis of all glycolytic and pentose phosphate metabolites identified a depletion of 6-phosphogluconic acid (6PG), which is the substrate for 6-phosphogluconate dehydrogenase (PGD) enzyme. To test whether PGD and the pentose phosphate pathway were tightly linked to the epigenetic changes, the researchers treated the tumor cells from different sites with 6-aminonicotinamide (6AN), which is a drug known to inhibit PGD but is not used in humans because of its severe side effects. They reported that this drug had no effect on the epigenetic state of DNA from the regional metastasis, but it reversed the epigenetic changes observed in cells from the distant metastasis, as well as reduced tumorigenicity in tumour forming assays, whereas normal and peritoneal metastatic cell were not affected by this treatment. Therefore, these two studies nicely demonstrated that there is little heterogeneity in driver mutations between primary and metastatic PDAC tumors, but there is considerable epigenetic reprogramming.

Parallel progression model.

In contrast to linear model, the parallel progression model proposes that primary tumor and metastatic lesions undergo an independent and parallel acquisition of genetic and epigenetic

alterations (illustrated in Figure 4) [41]. According to this model, the seeding of metastatic competent cells occurs very early, long before the primary tumor is clinically detectable. For example, Christoph Klein and colleagues observed that the genetic alterations in the DTCs in the bone marrow of patients with breast cancer are distinct from those in their corresponding primary tumors [42]. These data suggest that the genetic and epigenetic evolution may happen through multiple rounds of genetic diverseness and clonal selection mostly within the distant organ sites in which overt metastasis ultimately develop. Therefore, the parallel progression model suggests high genetic divergence between primary tumor and metastasis-competent cells, that may somehow explain their different response to systemically administered drugs, reported in several cancer types [43].

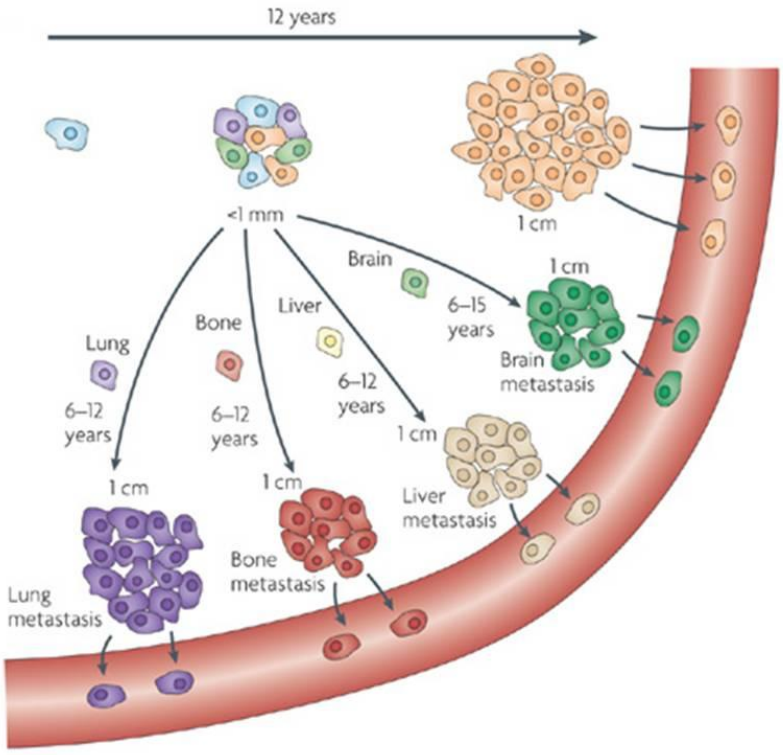

Figure 4. The parallel progression model.

The Figure shows the Metastasis Initiating Cells (MICs), which are spreading early from the primary tumor mass. According to this model, these metastatic cells evolve independently from primary tumor cells and acquire genetic alterations, that are specific for their target organ microenvironment. Before developing into overt macrometastasis, some of these metastatic cells

may enter into dormancy state in case of long metastatic latency. The Figure is adapted from Klein, (2009) [41].

1.2.3. The Metastatic cascade.

Metastasis is a complex process involving a series of steps by which a subset of metastatic tumor cells escape from the primary tumor site and disseminate to distant organs, where they form new lesions [44,45]. Some tumors are highly metastatic, capable of forming secondary lesions with high frequency (small-cell carcinoma of the lung, melanoma, pancreatic carcinoma), whereas others tumor types rarely metastasize to other organs, despite being locally invasive (basal cell carcinomas of the skin, glioblastoma multiforme). If a tumor cell with invasive properties cannot complete any step in the metastatic cascade, it cannot form a metastasis. Therefore, each tumor cell must complete every step of the metastatic cascade.

The metastatic cascade include the following steps:

A) Tumor Invasion.

Tumor invasion is the first step in the cancer dissemination, defined as the capacity of tumor cells to break the basement membrane and invade the surrounding stroma. This process requires important morphological and phenotypic changes, including adhesion, extracellular matrix (ECM) reorganization, and motility. An important biologic process, known as epithelial-mesenchymal transition (EMT) required for normal embryonic process, has also been implicated in tumor invasion. The EMT is characterized by transformation of a tumor cell with an epithelial-like morphology to a nonpolarized, motile and spindle-shaped tumor cell with a fibroblast-like morphology [46]. Normally, EMT is associated with downregulation of epithelial-specific E-cadherin and keratins and upregulations of mesenchymal markers including intermediate-filament vimentin, α-SMA, FSP1, and desmin among others. A key regulators of EMT are the zing finger transcriptional repressors Snail and Slug, which have been implicated in regulating EMT by their ability to repress E-cadherin transcription. Additional transcriptional factors such as TWIST, FOXC2, ZEB1, ZEB2 [47], non-codingRNAs including the *miR200* family (miR200a, miR200b, miR200c, miR141 and miR429), and the miR205 family [48] have been also reported to play a role in inducing the EMT program. In the absence of these EMT-inducing factors, tumor cells may also reverse the EMT process by undergoing a mesenchymal-epithelial transition (MET).

The ECM provides structural and biochemical support to the surrounding cells and regulates the cellular behaviour. The ECM can be remodelled by various enzymes, secreted by the tumor cells and surrounding stromal cells [49], which contributes to matrix degradation and tumor cell invasion. Proteolytic enzymes of many classes have been involved in tumor invasion, such as the serine proteinases, plasmin, plasminogen activator and matrix metalloproteinases (MMPs) among others. For example, it has been shown that upregulation of MMPs correlates with invasion, metastasis and poor prognosis in many cancer types. In addition, studies with animal models provide evidence for the importance of MMPs in cancer progression [50]. This scientific evidence describing the role of MMPs in tumor progression resulted in development and testing of synthetic MMPs inhibitors for cancer therapy [51]. However, these inhibitors did not show efficacy in clinical trials, probably due to issues with the inhibitor molecule or clinical trial design and a lack of knowledge about the broad spectrum of MMP activities.

B) Intravasation.

Intravasation of tumor cells is an active process that requires the distruption of endothelial junctions for the cancer cells to cross the endothelium of the blood vessels, a process known as transendothelial migration (TEM). Tumor blood vessels are highly abnormal, with weak endothelial junctions through which cancer cells can easily enter the bloodstream [52]. Various proteins have been described to play a role in intravasation. For example, COX2, EPIREGULIN, MMP1, and MMP2 participate in mediating breast cancer cell intravasation in the pulmonary parenchyma [53]. On the other hand, it has been recently described that the cytokine ANGIOPOIETIN LIKE 4 (ANGPTL4) is also able to trigger the infiltration of tumor cells into the lungs by inducing the dissociation of endothelial cell-cell junctions [54].

C) Transport through blood circulation.

The transport of tumor cells through circulatory system can be an active process governed by motility mechanisms or a passive process, where the tumor cells may be passively carried or pushed along with the blood flow. In blood circulation, many tumor cells are eradicated by the immune cells such as NK cells before seeding the secondary organs. Also, the tumor cells which were able to evade the immune system are often eliminated by exposure to shear forces generated by flowing blood [55]. In addition, the resistance and behavior of the tumor cells during transport

process often depend on whether they are present as single cells or as emboli. Generally, the embolization is divided in two types: homotypic (tumor cell-tumor cell) or heterotypic (tumor cell-leukocyte/platelet). The tumor cells present as emboli are usually more resistant to shear forces or immune attacks.

During the transport process, the tumor cells in blood circulation, known as circulating tumor cells (CTCs) are weakly adherent and subject to anoikis, which is a type of apoptosis, where the anchorage-dependent tumor cells are triggered to undergo programmed cell death [56]. In general, metastasis-competent cells are thought to be more resistant to anoikis than non-metastatic tumor cells.

D) Arrest

The physical entrapment within the small capillaries of distal organs and the arrest of CTCs in the microvasculature, as well as selective adhesion to the endothelium wall are two different processes. Both processes have been widely reported and the importance of these mechanisms in specific organs remains under debate. For instance, the specific adhesion of CTCs to microvessel endothelial cells at the future metastatic organs is considered to be one of the most important steps of the metastatic process, and this step is termed as organ-specific metastasis. Normally, the metastatic cancer cells, which exert higher rates of selective adhesion to microvessel endothelial cells result in higher metastatic incidence. In this regard, many *In vivo* and *In vitro* kinetic studies have demonstrated that the initial adhesion of CTCs takes place preferentially at endothelial cell junctions [57]. Moreover, it has been shown that the tumor cells frequently adhere at sites of inflammation and this is normally accompanied with modifications in cell surface components of endothelial cells at the sites of inflammation. Many tumor cells may also use common mechanisms to adhere to and pass through endothelium as the inflammatory cells.

G) Extravasation

During extravasation the tumor cells move from the interior of the vessels into parenchyma of the target organ. In general, the molecular mechanisms governing the extravasation process are similar to those involved in invasion, including proteinases, motility factors and cellular adhesion molecules. For example, various genes have been implicated in the process of extravasation of breast-cancer CTCs into the lungs of preclinical models and it has been found that these genes are

also associated with lung metastasis in the clinic. Some of these genes are Fascin-1 and other members involved in invadopodia, epiregulin; WNT ligands which mediate cancer-cell motility [58,59], and ANGPTL4, VEGF, COX2, MMP1, osteonectin which are mediators of endothelial disjunction and vascular permeability [60-63]. It has also been reported that platelets can form clusters with CTCs and induce extravasation through secretion of TGF-β [64], or altering the endothelial cell-to-cell junctions by releasing adenine nucleotides [65]. The interaction between macrophages and CTCs also facilitates the migration of CTCs from capillary walls into the lung parenchyma [66].

F) Colonization

During colonization step, the tumor cells start to form clusters at secondary organ sites and this process is considered one of the most complex and rate-limiting in metastatic cascade. The tumor cells which survive upon infiltration of distant organs, known as disseminated tumour cells (DTCs), can reside in the bone marrow of cancer patients for long periods, however only a few of these patients develop overt metastasis [67]. In some tumor types such as melanoma and breast cancers, metastases can become clinically detectable decades after the resection of the primary tumor, indicating that the tumor cells can remain in a state of dormancy for long time. The capacity of DTCs to switch from dormancy to active proliferation may depend on cell-non-autonomous mechanisms, needed to convert the surrounding microenvironment into more favourable niche. For example, it has been proposed that the outgrowth of DTCs might also depend on the activation and mobilization of bone marrow-derived cells (BMDCs) and their subsequent recruitment to the metastatic organs. These processes may be triggered by systemic factors secreted by cancer cells, including osteopontin (OPN) or SDF-1 [68-69]. On the other hand, it has been hypothesized that the cancer cells in occult micrometastases may proliferate continuously without dramatic increase in their overall number, which is probably due to a high apoptotic rate. One possible explanation for this phenomenon could be the failure of the DTCs to induce neoangiogenesis [70]. For example, it has been reported that prosaposin (Psap) may inhibit metastatic colonization by promoting expression of the anti-angiogenic factors such as thrombospondin-1 in stromal cells [71]. On other hand, Angiopoietin 2 (Angpt2) has opposite effect and it is able to stimulate the metastatic colonization of breast and pancreatic carcinomas by promoting the capacity of infiltrating myeloid cells to support the vascularization of metastatic

lesions [72]. Figure 5 illustrates a scheme of the metastatic cascade, including all steps discussed in this chapter.

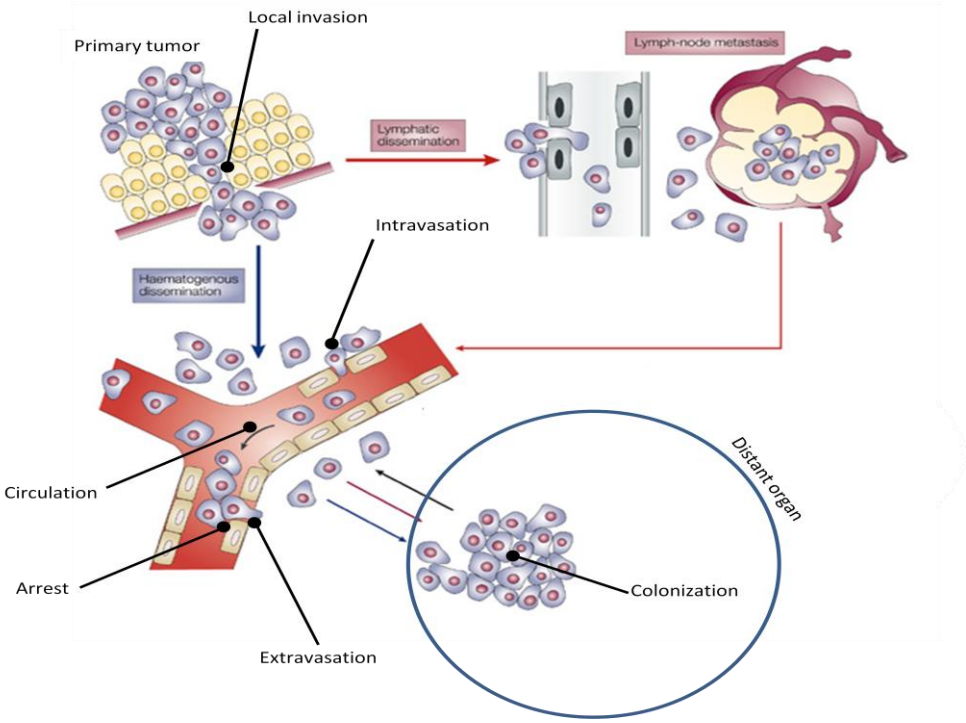

Figure 5. Scheme of the metastatic cascade. Metastasis initiating cells (MICs) disseminate either through blood circulation or through lymphatic system. In both scenarios, MICs detach from the primary tumor and migrate through the basement membrane. In the case of a haematogenous spread, MICs have to intravasate into circulatory system, survive in the blood circulation and extravasate from the vasculature endothelium to colonize the distant sites. The figure is adapted from Pantel and Brakenhoff, (2004) [73].

1.2.4. Metastasis organotropism.

Metastatic organotropism is the tendency of the cancer cells to establish metastatic tumors in specific organ sites. The patterns of metastatic distribution may depend on anatomic or mechanical characteristics. For example, the first capillary bed where CTCs become arrested is determined by patterns of blood circulatory system in the body [74]. The venous circulation usually leads to the right ventricle of the heart and to the lungs, except the venous system from the gut, which drains the blood first into the liver. For this reason, it is usually reported high metastatic incidence in liver

and lung organs [75]. In 1889, Stephen Paget spread the concept that the pattern of metastatic organ distribution is not accidental and metastatic cells establish overt metastasis only when the "seed" (tumor cells with metastatic capability) and the "soil" (organs or tissues providing favorable growth factors to seeds) are compatible, thus suggesting that the dissemination of metastatic cells is organ specific and not merely anatomic [76]. The mechanisms responsible for organ selectivity can be attributed to the capability of the tumor cells to recognize subendothelial basement membrane differences. For example several *In vitro* studies demonstrate organ-selective adhesion, invasion and growth [77-78]. There is a notion that metastatic tumor cells arrive in a premetastatic niche that was previously initiated in target organs by tumor-secreted systemic factors. It has been reported that BMDCs that express VEGFR1 and several integrins, selectively adhere to the future metastatic sites, where secretes different proteinases and chemokine factors and thus prepare a permissive niche for colonization by upcoming tumor cells [79].

Recently, it has been shown that tumor-derived exosomes, a small membrane-bound extracellular vesicles (size 30-100nm) carrying functional biomolecules (DNA, RNA and proteins) are able to determine organotropic metastasis. A recent study demonstrates that tumor-secreted exosomal integrins can determine organ-specific metastasis by fusing with host-specific resident cells to establish supportive metastatic environments through activation of Src phosphorylation and pro-inflammatory S100 expression [80]. In this study, it has been found that the exosomes expressing $ITGa_6\beta_4$ and $ITGa_6\beta_1$ integrins co-localized with S100A4-positive fibroblast cells and resident epithelial cells expressing pulmonary surfactant protein C in laminin-rich lung microenvironments, while the $ITGa_v\beta_5$-positive exosomes expressed by pancreatic cancer cells have been found to co-localize with $F4/80^+$ macrophages and to fuse with resident Kupffer cells in fibronectin-rich liver niches. The authors also demonstrated that inhibition of these exosomal specific integrins by short hairpin RNAs significantly reduced the exosome uptake and markedly decreased metastatic tumor burden in lung and liver mouse organs. In addition, the clinical data identified that the levels of $ITGa_6\beta_4$ are higher in exosomes isolated from circulating plasma of breast cancer patients with lung metastasis, as well as increased levels of exosomal $ITGa_v\beta_5$ were detected in pancreatic cancer patients diagnosed with liver metastasis in comparison to those without metastasis. Figure 6 summarizes the mechanisms responsible for metastasis organotropism.

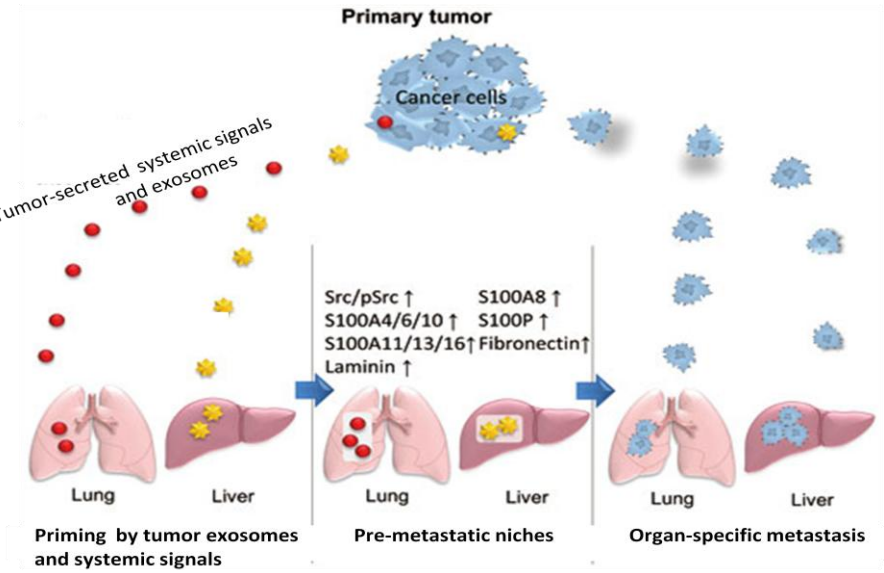

Figure 6. Metastasis organotropism triggered by tumor-derived systemic signals. Tumor-secreted systemic signals such as tumour-derived inflammatory cytokines, exosomes and extracellular-matrix-remodelling enzymes recruit bone-marrow-derived cells and precondition the microenvironment of distant organ for upcoming tumor cells. Different types of proteins and lipids transported by the tumor-derived exosomes can also fuse with resident cells of the future metastatic site and establish the pre-metastatic niche. The figure is adapted from Liu Y, Cao X. (2016) [81].

1.3. Experimental metastasis models.

Animal models are frequently utilized as a useful tool to recapitulate the entire metastatic cascade. The most commonly used strategy to model cancer metastasis is based on injecting mouse or human tumor cells directly into mouse circulation via the tail vein or left ventricle of the heart [82,83]. This model bypasses important steps such as invasion and intravasation, and therefore cannot recapitulate the whole multi-step metastatic process. Over the past decades, many Genetically Engineered Mouse Models (GEMM) models have been generated through incorporation of cancer-associated genetic mutations. These models accurately perpetuate the genetics and phenotype of several tumor types including pancreatic cancer. However, despite their multiple advantages, the GEMM models generally exhibit long tumor and metastatic latency or low metastatic incidence [84], thus making them less attractive model for studying metastatic disease.

Patient-derived xenografts (PDX) have become other popular models for studying cancer disease [85]. The PDX models generated by subcutaneous engraftment of patient tumors in nude mice, usually provide extensive local growth of primary tumor, but rarely metastasize to distant organs [86-87]. In contrast to subcutaneous transplants, the orthotopic transplantation is more frequently associated with distant metastasis [88] and multiple overt macrometastasis can be easily achieved, especially if the primary tumor graft is surgically removed [89]. The surgical resection of primary tumor can prolong survival and give sufficient time for metastatic cells to colonize the distant organs and form metastatic lesions, thus recapitulating the multiple sequential steps of the metastatic cascade. Nevertheless, the primary tumor removal is not an indispensible requirement for establishment of metastatic models of pancreatic cancer. For example, several studies reported successful metastatic spread of pancreatic xenograft tumors transplanted orthotopically in nude mouse model [90-91]. However, the metastatic rate in these models still remains unsatisfactory low, which is consistent with previous findings in breast xenograft models demonstrating that the immune status of the host mice strain can have a huge impact on establishment of distant metastasis [92]. Table 2 summarizes the preclinical models of spontaneous human metastasis described in the literature.

Table 2. Examples of preclinical models of spontaneous human metastasis.

Model	**Common sites of metastasis**	**reference**
Breast(213/LM2-4)	Lung	[89]
Breast(H2N/met2)	Lung and lymph nodes	[93]
Colon(KM12)	Lymph nodes and liver	[94]
Colon(Co-3,Col-3-JKC and Col-5-JCK)	Liver	[95]
Colon(LSLiM6)	Lymph nodes and liver	[96]

Gastric(St-4, St-40, H-111 and Sc-1HU)	Lymph nodes and liver	[95]
Melanoma (113/6-4L)	Lung	[97]
Melanoma(113/4-5B1 and 113/4-5B2)	Lung and central nervous system	[97]
Pancreatic(Panc-4)	Liver and peritoneum	[90]
Ovarian(RMG-1)	Peritoneum, lymph nodes and diaphragm	[98]

Table 2 is adapted from Francia G et al. (2011) [82].

1.4. Single-cell Sequencing technology.

The classical method in studying gene expression is to analyze the messenger RNA (mRNA) content of large pools of cells. However, tissue is composed of heterogeneous populations of cells where much variation takes place at the single-cell level. For example, tumor tissue is characterized by heterogeneous populations of multiple clonal expansions [99-101]. Therefore, analyzing a tumor tissue as a whole could mask important characteristics of the disease. Recently, various research groups have developed molecular techniques to overcome the challenges of sequencing small amounts of mRNA inside a single-cell.

Single-cell RNA-Seq became a powerful tool for studying the gene regulatory network at the single-cell level. This approach has been applied to single-cell studies including human preimplantation embryos, human embryonic stem cells, single-cells from dissected hippocampal tissue of mouse, and immune cells from mouse [102-103]. Commercial microfluidic approaches such as the Fluidigm C1 system have also been developed for analyzing up to 96 single-cell RNA profiles in parallel using nanoliter reaction volumes. In addition, this system allows the single-cell cDNA synthesis to take place in individual microfluidic chambers and show advantages over tube-based approaches, including improved mRNA capture efficiency and detection sensitivity.

1.4.1. Intratumoral heterogeneity during metastastic progression.

Several models of metastasis have been hypothesized, including late dissemination, early seeding, and self-seeding, but yet little is known about the molecular mechanisms driving the metastatic progression and dissemination of the primary tumor cells into distant organs. The major challenges in better understanding the metastatic disease are resolving the intratumoral heterogeneity and deciphering the genomic information of circulating tumor cells (CTCs), considered as the precursors of metastasis. The problem is that CTCs are presented at very low number in the blood, and generally only 1–50 cells can be enriched from 7.5-mL peripheral blood, which provides limited input material for genomic studies.

Several studies have attempted to decipher the transcriptional heterogeneity of CTCs at single-cell resolution. For example, in melanoma patients, scRNA-seq revealed three distinct gene signatures in CTCs, that are associated with metastasis [104]. In another study, scRNA-seq identified plakoglobin as a key regulator of CTC clusters in metastatic breast cancer patients and mouse xenograft models [105]. Using a orthotopic xenograft models, this study showed that CTC clusters exhibit increased metastatic potential compared to individual CTCs and inhibition of plakoglobin by short hairpin RNAs (shRNAs) markedly reduced the number of CTCs in the blood circulation, as well as the number of lung metastatic nodules. In another study, scRNA-seq was applied to study metastasis in GEMM models of pancreatic cancer and showed that the CTCs clustered separately from their primary tumors, showing low-proliferative signatures and are enriched for extracellular matrix genes [106]. In this study, the scRNA-seq data identified that SPARC was overexpressed in pancreatic CTCs and its knockdown by shRNAs resulted in suppression of cell migration and invasiveness in In-vitro wound scratch assay, as well as reduction of lung metastasis in orthotopic xenograft models. Therefore, this data demonstrate that CTCs of pancreatic cancer may have a very high level of heterogeneity, which is presumably related to their capacity of establishing distant metastases. However, since GEM KPC mice only produce disseminated micrometastatic foci, the authors were unable to directly compare the expression profile of CTCs with that of metastatic lesions and therefore the question whether pancreatic cancer metastasis is hierarchically organized phenomenon still remains unanswered.

II. OBJECTIVES.

The principal objective of this thesis is the development of metastatic PDX models of pancreatic cancer, which can serve as an efficient and reproducible *In-vivo* platform for modelling the whole multi-step metastatic process, which in turns can facilitate the discovery of novel molecular mechanisms involved in cancer dissemination, as well as development of more effective therapeutic strategies for metastatic pancreatic cancer. For this reason, we defined the following objectives:

1. Establishment of metastatic patient-derived tumor xenograft (PDX) model of pancreatic cancer to faithfully recapitulate the multi-step metastatic process.

2. Identification, purification and enrichment of the human tumor populations from primary tumor, blood and metastatic sites of metastatic PDX models.

3. Single-Cell RNA Sequencing of the human tumor populations enriched from the primary tumor, mouse blood and metastatic sites of PDX model with aim to:

   - decipher the transcriptional heterogeneity during metastatic disease.
   - identify potential anti-metastatic targets.

4. Pre-clinical evaluation of anti-metastatic effect of therapeutic agents that block the activity of the previously identified deregulated genes or pathways implicated in metastatic process.

5. Studying the role of tumor-derived exosomes in organotropic metastasis.

II. MATERIAL AND METHODS

3.1. Establishment of metastatic Patient-derived xenograft (PDX) models.

All experiments using mice were approved by CNIO-ISCIII Ethics Committee for Research and Animal Welfare (CEIyBA). Pancreatic cancer xenografts Panc265, Panc198, Panc020, Panc042, Panc047, Panc026, Panc219 from our tumor bank collection were used for the study. These xenografts have been generated from freshly biopsied pancreatic patient tumor samples and propagated subcutaneously (s.c) into successive mouse generations [107]. Freshly collected s.c grown tumors were cut with a sterile scalpel into small pieces of 1–2 mm3 and embedded in matrigel solution. NSG mice (purchased from Charles River, reproduced in the CNIO animal facility or provided by Inés Martín-Padura from CNIC) were anesthetized using Isoflurane gas anesthesia and administered with Buprenorphine dosed at 0.2 mg/kg. The left abdominal part was shaved and the skin was sterilized with 70% ethanol. Using a sterile surgical microscissors, small incision was made in the upper left abdomen, and the pancreas was exposed. Small tumor pieces from each xenograft model were implanted into the splenic lobe of the pancreas using 6-0mm absorbable sutures (B. Braun). Mice were monitored during the whole study and they were humanely sacrificed after appearance of several or all of the following symptoms: big tumor size, loss of body weight, lethargy, dyspnea and/or pain. The date of sacrifice was recorded and the organs: spleen, orthotopic primary graft, liver, lung, mesenteric lymph nodes, kidney and brain were collected and preserved in 10% formalin solution for subsequent histological studies. For calculation of tumor volume, the short and long diameter of each freshly resected orthotopic tumor graft was measured by caliber and the tumor volume was calculated according to the following formula:

Tumor volume = (short diameter^2 x long diameter)/2

3.2 Pancreatectomy procedure.

The NSG mice harboring Panc265 orthotopic xenograft were anesthetized using Isoflurane gas anesthesia and administered with Buprenorphine dosed at 0.2 mg/kg. The left abdominal was disinfected with 70% ethanol. Using a sterile surgical microscissors, small incision was made in the upper left abdomen, and the pancreas harboring pancreatic tumor was exposed. Then, the healthy pancreas proximal to the tumor was ligated with a 6-0mm sutures and using a bipolar

electrocautery system, the cauterization was performed close to the tumor graft. After the cauterization, part of the splenic lobe of the pancreas and the whole spleen were resected with a sterile microscissors. The abdominal cavity was carefully explored for evidence of abdominal hemorrhage, and the abdominal incision was closed with a 6-0mm absorbable suture. The general health status and body weight of each mice were monitored during the whole study.

3.3. Immunohistology.

3.3.1. Hematoxylin and Eosin staining.

The Comparative Pathology Unit at CNIO prepared the paraffin blocks from the mentioned above mouse tissues and generated 2.5-3 mm-thick sections, which were then deparaffinized, rehydrated and subjected to hematoxylin and eosin H&E staining.

3.3.2. Immunohistochemistry: Survivin and Vimentin staining.

Paraffin sections from some of the mentioned above tissues were subjected to deparaffinization and rehydration in graded ethanol washes. The CTCs isolated from metastatic PDX model were spun onto glass slides and fixed in 4% paraformaldehyde for 10 min at room temperature. Epitope retrieval was performed in an autoclave for 6 min (121°C) in sodium citrate buffer pH6 (Dako). Endogenous peroxidase activity was blocked by treatment with 3% hydrogen peroxide solution (Sigma Aldrich) for 10 min at room temperature. The slides were then blocked with 5% NMS for 1 hour in RT and incubated with a monoclonal rabbit anti-Survivin antibody (clone EP2880Y, Abcam, dilution 1/250 in PBS1% and 1% normal goat serum), overnight at 4 °C. The detection of Survivin antibody was performed using Vectastain ABC kit (Vector labs) and developed with 3,30-diamniobenzidine(DAB), according to the manufacturer's instructions. The slides were counterstained with hematoxylin, dehydrated in graded solutions of ethanol and mounted in DPX medium.

Comparative Pathology Unit at CNIO performed the immunohistochemistry staining for vimentin using the human specific ready to use antibody (clone V9, DAKO) according to standard procedures. The slides were digitalized with the Axio Scan Z1 and representative images were captured with the Zen Software and brithless and contrast were adjusted with Photoshop software.

3.4. Immunofluorescence:

3.4.1. Vimentin and GFAP staining.

Mouse brains were harvested and fixed with 4% paraformaldehyde (PFA) at 4 C. The PFA fixed brains were washed with PBS1x (3 times) and dehydrated in sucrose (15% and then 30%). Slicing of the brain was done by using a sliding microtome with freezing stage. 80-nm thick brain slices were blocked in 10% NRS, BSA 2%, Triton 0.25% in PBS for 2 hr at room temperature (RT, shaking). Primary antibodies were incubated overnight at 4C, shaking. After extensive washing in PBS-Triton 0.25% (6 times), the secondary antibody was added in the blocking solution and incubated for (2 hr, RT, shaking). After extensive washing in PBS-Triton 0.25% (3 times) and in PBS1x (3 times), nuclei were stained with Bis-benzamide 1:1000 for 5 min at RT, shaking. Primary antibodies: anti-human vimentin (clone V9, DAKO), anti-mouse GFAP (poly-clonal, DAKO). The slides were mounted in fluorescence mounting medium (DAKO). Images were acquired with Leica SP5 upright confocal microscope, and analyzed with ImageJ software. This methodology was elaborated in accordance to the protocol provided by Dr. Manuel Valiente from CNIO. Manuel Valiente's group performed the staining procedure. The representative images were acquired with the help of Dr. Manuel Valiente.

3.4.2. Survivin staining.

The CTCs isolated from metastatic PDX model were spun onto glass slides and fixed in 4% paraformaldehyde for 10 min at room temperature, followed by 3 washes in PBS1x for 5 min.
The cells were then permeabilized with 0.1% Triton X-100 diluted in PBS1x for 10 min. The slides were blocked in 5% NGS and 5% NMS sequentially for 1 hour at RT. Primary antibodies for Survivin (1/100 dilution) were sequentially incubated overnight at 4C. After extensive washing in PBS, the secondary antibodies: Alexa-Fluor anti-rabbit^{488}, anti-mouse^{555} (provided by Confocal Unit from CNIO) were diluted in PBS (1/200) and were then sequentially incubated for 1 hour at RT. After extensive washing in PBS, nuclei were stained with Hoechst (provided by Confocal Unit from CNIO) for 10 min at RT. The slides were mounted in fluorescence mounting medium (DAKO). Images were acquired with Leica SP5 upright confocal microscope, and prepared with Image J software.

3.5. In-situ Hybridization: Alu staining.

Alu positive control probe II is a cocktail of dinitrophenol (*DNP*)-labeled oligonucleotide probes, which hybridized to Alu repetitive sequences present within the primate genome [108]. Tissue samples were fixed in 10% neutral buffered formalin (4% formaldehyde in solution), paraffin-embedded and cut at 3 µm, mounted in superfrost®plus slides and dried overnight. For the whole technique an automated immunostaining platform was used (Ventana Discovery XT, Roche). Antigen retrieval was first performed with low pH buffer (RiboCC, Roche) and protease III (Roche). Slides were then incubated with the probe Alu positive control probe II (Ventana, Roche 05272041001). After the probe, stringency washes were necessary three times and the slides were incubated with an intermediate, Rabbit anti-DNP. Visualization systems were needed (OmniRabbit, Ventana, Roche) conjugated with horseradish peroxidase; immunohistochemical reaction was developed using Silver, as a chromogen (Silver kit, Ventana, Roche) and nuclei were counterstained with Carazzi's hematoxylin. Finally, the slides were dehydrated, cleared and mounted with a permanent mounting medium for microscopic evaluation. This protocol was elaboerated in accordance to the protocol provided by Histopathology Unit from CNIO. The Alu staining was performed by Histopathology Unit from CNIO.

3.6. Quantitative PCR: targeting human DNA (Alu-sequences) in blood of metastatic PDX models.

Fresh EDTA-blood was collected via a cardiac puncture from NSG mice implanted orthotopically with a highly metastatic Panc265 model. The blood from each animal was first centrifugated at 400g for 10 minutes and the plasma was separated from the cellular pellet. Next, the cellular pellets were resuspended in 2 ml of red blood cell lysis solution (Qiagen, Cat. No.79217) for 10 min at 37°C. The samples were then centrifuged for 7 min at 300 g, followed by two washing steps using 1 ml of sterile PBS1x. After the washing steps, the cellular pellets were resuspended in 200µl of sterile PBS1x and the DNA extraction from each sample was performed using DNeasy Blood & Tissue Kit (Qiagen, Cat. No. 69504) following the manufacturer's instructions . The DNA was then eluted in 100µl of nuclease-free water. Finally, the DNA concentrations were measured using a NanoDrop ND-1000 spectrophotometer.

Real-time PCR using TaqMan® was performed on Real-Time PCR System 7500 (Applied Biosystems), according to the manufacturer's instructions. Oligonucleotide primers for Alu

sequences are [For 5′-GTCAGGAGATCGAGACCATCCT-3′ (position 68–90) `/Rev 5′-AGTGGCGCAATCTCGGC- 3′ (position 244–227). The TaqMan® probe is 5′-6-FAM AGCTACTCGGGAGGCTGAGGCAGGA-TAMRA-3′ (position 167–192) [109]. The primers, probe and Taqman Universal PCR Master Mix were purchased from Applied Biosystems.

PCRs were carried out in 20 μL following the manufacturer's instructions. Each sample was then subjected to an initial denaturation of 95°C for 10 min, followed by 40 amplification cycles of denaturation at 95°C for 15 s and annealing/extension at 60°C for 1 min. DNA from murine blood and water were used as negative controls.

Data from the PCR experiments were exported from PCR system 7500 software (Applied Biosystems) into a Microsoft® Excel® spreadsheet where the mean value and standard deviation were calculated for each point on the standard curve. Using the Excel trendline option, a line of best fit was plotted with Y-error bars equal to the standard deviation. The Excel chart wizard was used to construct bar graphs with Y-bars equal to one standard deviation.

3.7. Tissue dissociation.

All solid mouse tissues were dissociated using a human tumor dissociation kit (Miltenyi Biotec) and a gentleMACS dissociator (Miltenyi Biotec) according to the manufacturer's instructions. The dissociated single-cell suspension was then passed through a 40-μm cell strainer (BD Biosciences) and resuspended in MACS cell sorting buffer (Miltenyi Biotec) to determine the cell number and viability using trypan blue dye, prior to further applications.

For blood collection, tumor-bearing mice were bled using a 1 ml syringe via a cardiac puncture and collected in EDTA containing tubes. The blood was then diluted 1:1 with PBS1x, and carefully layered upon 1.5 volume of Ficoll-Paque Plus (*VWR International Eurolab)* and centrifuged for 30 to 40 minutes at 400g, without brake, at room temperature. The mononuclear cell layer was then collected, washed in PBS1x, counted and prepared for further application.

3.8. Flow cytometry.

Antibodies for the human antigen HLA-ABC (clone G46-2.6, BD Pharmingen) and for mouse antigen H2kD (clone SF1-1.1.1, eBioscience) were purchased commercially. All antibodies were validated in this study directly. Antibody staining was performed in 1%PBS. After 20min at 4 °C, stained cells were washed of excess unbound antibodies. Forward-scatter height versus forward-

scatter width (FSC-H versus FSC-W) and side-scatter area versus side-scatter width (SSC-A versus SSC-W) were used to exclude cell debris and aggregates. Dead cells were eliminated by excluding DAPI (4',6-diamidino-2-phenylindole) positive cells. Data were acquired on a BD FACSCanto and analyzed using FlowJo software. The flow cytometry analyses were performed in Flow Cytometry Unit from CNIO.

3.9. Isolation of human tumor cells from metastatic PDX models.

Human tumor cells from the mouse peripheral tissues were purified by autoMACS Pro Separator using MS columns (Miltenyi Biotec) in accordance with the manufacturer's instructions. Before loading, the single-cell suspension was filtered through a 40-μm cell strainer (BD Biosciences). Human tumor cells were enriched by two-step process: first incubating with a PE-conjugated primary antibody for the human antigen HLA-ABC (clone G46-2.6, BD Pharmingen), followed by incubation with Anti-PE MicroBeads UltraPure (Miltenyi Biotec). The enriched human tumor cells were imaged using a confocal microscope (Leica SP5-MP).

3.10. Single-cell RNA sequencing and processing.

Tumor cells enriched from primary tumor, mouse blood and liver of PDX metastatic model were individually separated on the C1™ Single-Cell Auto Prep System (Fluidigm, South San Francisco, CA,USA)and cDNA amplification was generated using the SMARTer®Ultra™ Low RNA kit for the Fluidigm C1™ System (Clontech, Mountain View, CA, USA). In total, 137 cells were captured on three C1 array chips for mRNA sequencing (17–25 μmFluidigm). In total 84 samples passed the quality criteria. cDNA quantity and quality was measured with a 2100 Bioanalyzer (Agilent). Libraries were generated from 300 pg of amplified cDNA using the Nextera XT DNA Sample Prep Kit (Illumina) and sequenced on the HiSeq 2500 sequencer (Illumina) to generate 50 bases single reads at a depth of 7.5–13.2 million reads. After single-cell sequencing, any putative murine cell was discarded by FastQ Screen software (v. 0.4.4) [110], which is able to detect mRNA sample reads that belongs to the human or to the mouse transcriptomes. The mRNA reads derived from human single cells were aligned on the human genome reference (hg19 assembly, UCSC) using the TopHat2 algorithm (v. 2.0.10) [111], retrieving the best hit with the default parameters, but allowing a maximum of five multi-hits with the same alignment score. The gene-level expressions was quantified as the sum of all reads mapping on the exons for each gene

towards the gene annotation for the human genome (hg19, UCSC) using HTSeq-count (v. 0.5.4p5) [112]. The genomics experiments were performed by Genomics Unit from CNIC. Part of this methodology was elaborated by Genomics Unit from CNIC.

3.11. Computational and statistical analysis of single-cell gene expression data.

Statistical analysis.

Genes with no expression data in all the cells from the study, which are either not expressed or dropped-out as an artifact of the single-cell RNA sequencing, were filtered out for further analysis. The R function *prcomp* was used to perform a principal component analysis (PCA) on the log2-transformed single-cell gene expression profiles (read counts per million).

The differential gene expression test based on read counts from single-cell RNAseq was carried out using SCDE (bioconductor R package, v. 1.99.4) [113], with the recommended parameters by the authors. The single-cell error/regression model was fit using all individual cells included in the study, and grouping by cell subpopulation at the first cross-comparison to extract the subset of genes with consistent expression within the subpopulation. Genome-wide tests for expression differences between the three cell subpopulations were performed by pairs, with the default parameters (1000 bootstrap randomizations). After adjusting p-values for multiple testing (Benjamini & Hochberg method) [114], genes with false discovery rate (FDR) < 0.05 were considered statistically significant. For PCA and differential gene expression analysis were only included DAPI-/HLA-ABC PE+ cells.

A pre-ranked gene list by the Z-score of the expression difference between circulating tumour cells and primary tumour cells obtained by SCDE was used to perform Gene Set Enrichment Analysis using the GSEA Java Software (Broad Institute, v. 2.2.1) [115], with the default parameters (weighted Enrichment Score formula, 1000 permutations). Several gene set collections were tested to find biological insights: KEGG and Hallmark gene set collections from MSigDB (Broad Institute, v. 5.1), kinase substrates from Kinase Enrichment Analysis Library (KEA2015, downloaded from http://amp.pharm.mssm.edu/Enrichr/enrich). Additionally, custom gene sets for the selected drugs and their target genes were generated from the LINCS L1000 data set (described elsewhere), and used to further investigate drug candidates from the connectivity map analysis.

Gene sets with false discovery rate (FDR) < 0.05 were considered statistically significant [114].

Computational anti-metastatic drug prescription.

The *in-silico* anti-metastatic treatment prescription was carried out based on the Connectivity Map analysis, described in Lamb J. *et al.* 2006 [116]. Briefly, the connection of the gene expression signature of the biological transition of primary tumour cells to circulating tumour cells was interrogated against a comprehensive collection of gene expression signatures that represent cellular states of cell lines upon the transcriptional response to different types of perturbations (gene knock-down, gene over-expression and drug treatments). For this, The Library of Network-Based Cellular Signatures (LINCS) L1000 data set (Broad Institute LINCS Center for Transcriptomics (1U54HL127366) [117]) provides a large-scale catalogue of transcriptional responses to pharmacological and genetic perturbations of a large panel of cell lines. The CLUE data portal analysis (http://www.clue.io, Broad Institute) was used for a broad search looking for opposing drug connections amongst the LINCS L1000 catalogue, using the top 100 most significantly up- and down-deregulated genes (by the z-score of the expression difference) from the differential gene expression between circulating tumour cells and primary tumour cells. To further investigate selected connections (drugs and target genes), consensus perturbation signatures of cell lines were generated from the LINCS level 3 data (quantile log2 normalized gene expression profiles) using limma (v. 3.24.15) [118], by comparing the differential gene expression between treated and untreated control experiments for a given perturbation, and using an additive linear model to block for cell line/batch effects across experiments (experiments that were done experimentally in different L1000 plates). Gene sets derived from the selected signatures were defined using the top 100 most up- and down-expressed by ranking the moderated-t statistic of the differential gene expression test. The computational analysis were performed by Bioinformatics Unit from CNIO. This methodology was elaborated by Bioinformatics Unit from CNIO.

3.12. *In vivo* treatment experiments.

3.12.1. Single cell-driven *In-vivo* treatment experiments.

YM155(purchased from Selleckchem) was dissolved and diluted in saline, Danusertib(purchased from Medchem express) was dissolved in an *in situ* salt prepared as previously described [119]

and diluted in 5% dextrose, Abraxane was dissolved and diluted in saline, Pac-1(purchased from Medchem express) was dissolved in DMSO and diluted in saline prior to administration. For the single cell-driven *In-vivo* efficacy studies, the following drug treatment regimens were established: YM155 (2 mg/kg/d, i.v.) [120]; Abraxane (50mg/kg once a week, i.v.); PAC-1 (5 mg/kg/d, i.v) [121]; Danusertib (PHA-739358) (15 mg/kg/d, i.p.) [119]; PAC-1+Abraxane; YM155+Abraxane; Danusertib+Abraxane, 6-8 mice per group. The drug treatment course was initiated 1 week after implantation of Panc265 model. For early *In-vivo* treatment study with a highly metastatic Panc265 model, the treatment course with YM155 and Abraxane was initiated 2 and 3 days after tumor implantation , respectively. For *In-vivo* efficacy study with Panc198 metastatic model, the treatment course with YM155 and Abraxane was initiated 2 weeks after tumor implantation. The mice were treated during 4 weeks with all compounds and 3 weeks with Abraxane, monitored daily for signs of toxicity, and were weighed thrice a week. Animals that developed adverse effects (for example, 20% weight loss) were humanely euthanized and excluded from the study. After treatment period, small number of mice of Danusertib and/or YM155 treatment group were euthanized at the time of ethical endpoint sacrifice of control group and the rest mice were subsequently monitored and sacrificed when they manifested the mentioned above signs of sickness. For evaluation of metastatic tumor burden in Panc265 metastatic model, mouse livers and lungs of control and treatment groups (Danusertib and/or YM155) were subjected to Alu-staining and the percentage of Alu-positive cells was determined by Axio Vision. Kaplan–Meier survival plots were prepared using GraphPad software and median survival times were determined for all experimental groups.

3.12.2. Withaferin-A treatment experiment:

Withaferin-A (WFA) (purchased from Enzolifesciences) was dissolved in DMSO and dilute in saline prior to administration. Panc265 bearing mice were randomly assigned to two treatment groups (6 mice per group): (1) Control; (2) WFA (2 mg/kg/d, i.p.). The drug treatment course was initiated 1 week post-implantation. Mice were treated during 28 days, monitored daily for signs of toxicity, and were weighed thrice a week. After treatment period, all mice were subsequently monitored and sacrificed when they showed the mentioned above signs of sickness. Histological sections of mouse liver and lung were examined microscopically for presence of metastases in all

animals of each group. Kaplan–Meier survival plots were prepared and median survival times were determined for all experimental groups.

3.13. Proteomic analyses of the exosomes derived from metastatic PDX models.

Sample Preparation.

The exosomes from primary tumors and metastatic organs of each PDX model were purified and prepared by Hector Peinado's group at CNIO. Exosomes from PDAC, lung and liver explants were quantified using the Qubit platform (Life Technologies). The equivalent to 15 ug of each sample was loaded onto unit filters and digested according to the FASP protocol[1] with some changes. Samples were made up to 250 uL with 8M urea 0.1M Tris-HCl pH=8 solution (UT buffer). Then the proteins were reduced with 15 mM TCEP for 30 min at RT and alkylated with 15mM CAA for 30 min in the dark. After several washes with UT buffer, proteins were doubly digested with LysC (Wako) overnight at RT and with Trypsin (Promega) for 5 h at 37ºC at a ratio 1:50 (enzyme: substrate) in 0.1M Tris-HCl. Resulting peptides were further desalted and concentrated using homemade reversed phase micro-columns filled with Poros Oligo R3 beads (Life Technologies), containing a C18 Emporedisk (3M) at the bottom of the tip. The samples were dried using the Speed-Vac and dissolved in 30 µL of loading buffer (0.2% FA).

LC-MS/MS analysis.

Peptides were separated by reversed-phase chromatography using a nanoLC Ultra system (Eksigent), directly coupled with a LTQ-OrbitrapVelos instrument (Thermo Fisher Scientific) via nanoelectrospray source (ProxeonBiosystem). Peptides were loaded onto the column (Dr. Maisch, ReproSil-Pur C18-AQ GmbH 2.4µm, 500x0.075 mm), with a previous trapping column step (NS-MP-10 BioSphere C18 5 µm 120Å 360/100 µm, L=20 mm, Nanoseparations), during 10 min with a flow rate of 2.5 µl/min of loading buffer (0.1% FA). Elution from the column was made with a 120 min linear gradient (buffer A: 4% ACN, 0.1%FA; buffer B: 100% ACN, 0.1%FA) at 250 nL/min. The peptides were directly electrosprayed into the mass spectrometer using a PicoTip emitter (360/20 OD/ID µm tip ID 10 µm, New Objective) a 1.4 kV spray voltage with a heated capillary temperature of 325°C and S-Lens of 60%. Mass spectra were acquired in a data-

dependent manner, with an automatic switch between MS and MS/MS scans using a top 20 method with a threshold signal of 800 counts. MS spectra were acquired with a resolution of 60000 (FWHM) at 400 m/z in the Orbitrap, scanning a mass range between 350 and 1500 m/z. Peptide fragmentation was performed using collision induced dissociation (CID/CAD) and fragment ions were detected in the linear ion trap. The normalized collision energy was set to 35%, the Q value to 0.25 and the activation time to 10 ms. The maximum ion injection times for the survey scan and the MS/MS scans were 500 ms and 100 ms respectively and the ion target values were set to 1E6 and 5000, respectively for each scan mode. Samples were randomly injected and analysed in duplicates. A quality control was run every 6 samples to check system performance.

Data analysis.

Raw files were analyzed either by Proteome Discoverer (version 1.4.1.2) or by MaxQuant[2](v1.5.3.30) against a forward-reverse concatenated database. The database included human and mouse proteins (UniProtKB/Swiss-Prot20,187 and UniProtKB/Swiss-Prot/TrEMBL 43,539 sequences, respectively) and common contaminants. Human accession numbers were taggedin order to differentiate protein matches from each organism, when possible. Carbamidomethylation of cysteineswas considered as fixed modificationwhereas oxidation of methionines was set as variable modifications in both SequestHT and Andromeda search engine (v2.2). SequestHT, in conjunction with Percolator provided the list of proteins for Proteome Discoverer. Minimal peptide length was set to 6 amino acids and a maximum of two missed-cleavages were allowed. Peptides were filtered at 1% FDR. For protein assessment in MaxQuant, at least one unique peptide provided by Andromeda search engine[3] with a FDR = 1% was required for both identification and quantification. Other parameters were set as default. Afterwards, the "proteingroup"filewasuploadedinPerseus[4] (v1.5.5.2). After removing proteins annotated as contaminants, only identified by site and/or reversed, the missing values of the matrix were imputed as a normal distribution assuming low intensity values. Then, a Welch t-test analysis (p value 0.05, FDR 0.01) was performed on proteins present in 70% of the samples of at least one of the 2 groups. Only significant proteins with a fold-change above 1.5 (log2) were considered as regulated. Protein classification enrichment analysis (molecular function, biological process and protein class) was performed by PANTHER software, using the entire list of identified proteins as the reference data set to analyse the regulated proteins. This methodology was provided by

Proteomics Unit from CNIO. The proteomics experiments and analysis were performed by Proteomics Unit from CNIO.

3.14. Statistical analyses.

An unpaired two-tailed t test was applied to calculate the statistical significance of Alu-positive cells between control and drug treated groups; to calculate the statistical significance of tumor weights between control and YM155 treated group; to calculate the statistical significance of the human DNA level in the mouse blood at different time points using a Graphpad software.

A log-rank test (Mantel-Cox) was applied to determine the statistical differences in the survival curves of the animal experimental groups. Differences were considered statistically significant at P value < 0.05. Statistical significance is indicated by * ($p < 0.05$), ** ($p < 0.001$) and *** ($p < 0.0001$).

IV. RESULTS.

4.1. Metastatic PDX models of pancreatic cancer.

4.1.1. Choice of a recipient mouse strain for modeling the metastatic disease.

A first decisive choice for establishment of an In-vivo metastasis model was the one of the recipient mouse strain. Several immunocompromised strains have been developed during the past years. Three immunocompromised mouse strains (Nude, SCID and NOD/SCID/IL2g (NSG) mice) were studied and compared for their suitability as a models for experimental metastasis. Nude mice are homozygous for the nude spontaneous mutation (*Foxn1*^{nu}, formerly *Hfh11*^{nu}). They are characterized by abnormal hair growth and defective development of the thymic epithelium. These mice lack T cells and suffer from a lack of cell-mediated immunity. Homozygous nude mice show partial defect in B cell development. In contrast, the SCID mice possess a genetic autosomal recessive mutation (SCID). This mice strain show a severe combined immunodeficiency affecting both B and T lymphocytes. They have normal natural killer (NK) cells, macrophages, and granulocytes. On the other hand, NSG mice are double homozygous for the severe combined immunodeficiency (SCID) mutation and for the allelic mutation of the common gamma chain of the interleukin-2 receptor (IL-2RG) [122]. These mice are functionally incompetent for B, T and NK cells, and are deficient in cytokine signaling.

In order to determine which of these immunocompromised strains would be better recipients for the experimental metastasis assay, various PDAC xenografts were implanted orthotopically and the metastatic incidence of each xenograft model was compared between the three mouse strains. High metastatic incidence was observed in NSG mice strains, however no metastatic lesions were detected in Nude and Scid mice (Figure7, Table3), indicating that NSG mice are more permissive recipients for establishment of *In-vivo* metastasis models. In contrast to NSG mice strain, both Nude and Scid mice have functional NK cell, macrophages and dendritic cell, suggesting that the immune status of host mice strain could have an important impact on tumor dissemination and establishment of distal metastasis.

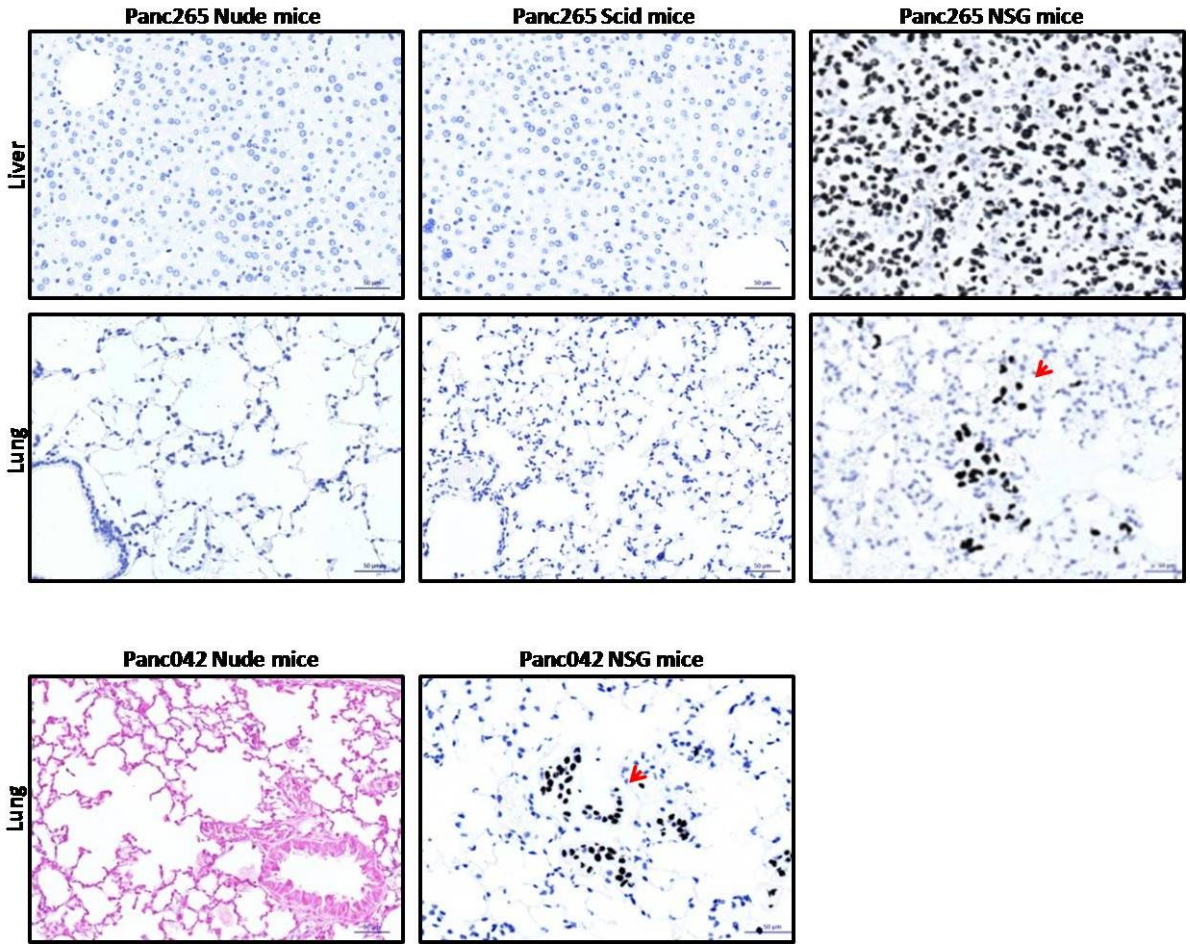

Table 3.

Number (percentage) of mice affected with metastasis			
Mice strain	**PDX model**	**Liver**	**Lung**
Nude	Panc265	0/5 (0)	0/5(0)
	Panc042	0/5(0)	0/5 (0)
Scid	Panc265	0/5(0)	0/5(0)
NSG	Panc265	5/5(100)	5/5(100)
	Panc042	0/5(0)	5/5(100)

Figure 7. **Choice of a Xenograft recipient for modeling the metastatic disease.** Representative photomicrographs of Alu *In-situ* hybridization (Alu ISH) of liver and lung tissues obtained from metastatic Panc265 and Panc042 model implanted orthotopically in Nude, Scid and NSG mice. The red arrows indicate the Alu-positive human tumor cells in mouse lungs. The silver staining corresponds to human nuclei, in which the Alu probe hybridizes (scale bar 50µm). The lung slide

of Panc042 model was counterstained with eosin staining. **(Table 3)** - Summary table of metastatic incidence in PDX models.

4.1.2. Development of Metastatic PDX model of pancreatic cancer.

In order to develop an *in-vivo* metastatic model that recapitulates the metastatic disease, we implanted several pancreatic cancer xenografts from our tumor bank (Panc265, Panc198, Panc020, Panc026, Panc042, Panc047, Panc219) orthotopically into severely immunocompromised NSG mice. Upon orthotopic transplantation, Panc265 xenograft model exhibits aggressive metastatic behavior and results in massive liver and lung metastasis in all mice with median survival rate of 25 days (Figure8A, 8D, Table 4). Sporadic brain micrometastasis on single-cell level has been also detected in Panc265 metastatic model by *In-situ* hybridization for primate ALU sequences (Figure8B). Moreover, Immunofluorescence staining using human-specific antibody against the vimentin protein (expressed by the tumor cells, discussed below) detected small cluster of human metastatic cells in brain parenchyma, surrounded by GFAP-positive reactive astrocytes (Figure8B), which activation is considered as a hallmark of brain metastasis[123]. At late stages of tumor progression, Panc265 bearing mice displayed signs of lethargy, significant lost of body weight and respiratory insufficiency.

Panc198 is the second metastatic model, which was able to establish liver and lung metastasis in all mice with median survival rate of 54.5 days (Figure8A, 8D, Table 4). The other fifth metastatic models Panc020, Panc026, Panc042, Panc047 and Panc219 gave rise only to lung micrometastasis in all implanted mice with different survival rates (Figure8C, 8D, Table 4). The mice of these models were often sacrificed due to primary tumor size and respiratory insufficiency. The presence of human tumor cells in host liver and lung was detected by *In-situ* hybridization to primate ALU sequences (Figure8A, 8C). In total, we generated seven metastatic PDX models with high metastatic incidence, model-specific dissemination pattern and distinct survival rates. For subsequent studies, we mainly focused on Panc265 model, since it showed the most aggressive phenotype with the shortest survival rate.

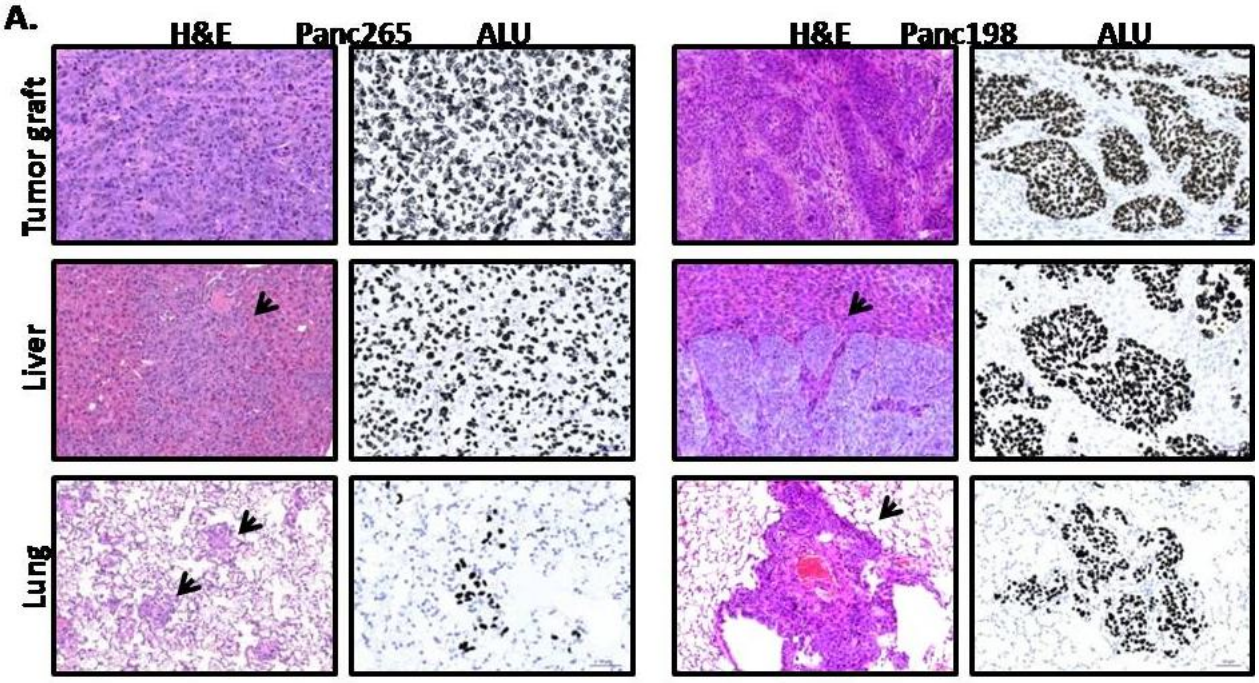
A.
H&E
Panc265
ALU
H&E
Panc198
ALU
Tumor graft
Liver
Lung

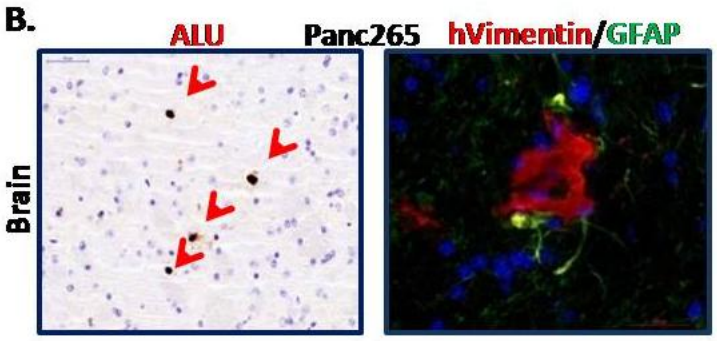
B.
ALU
Panc265
hVimentin/GFAP
Brain

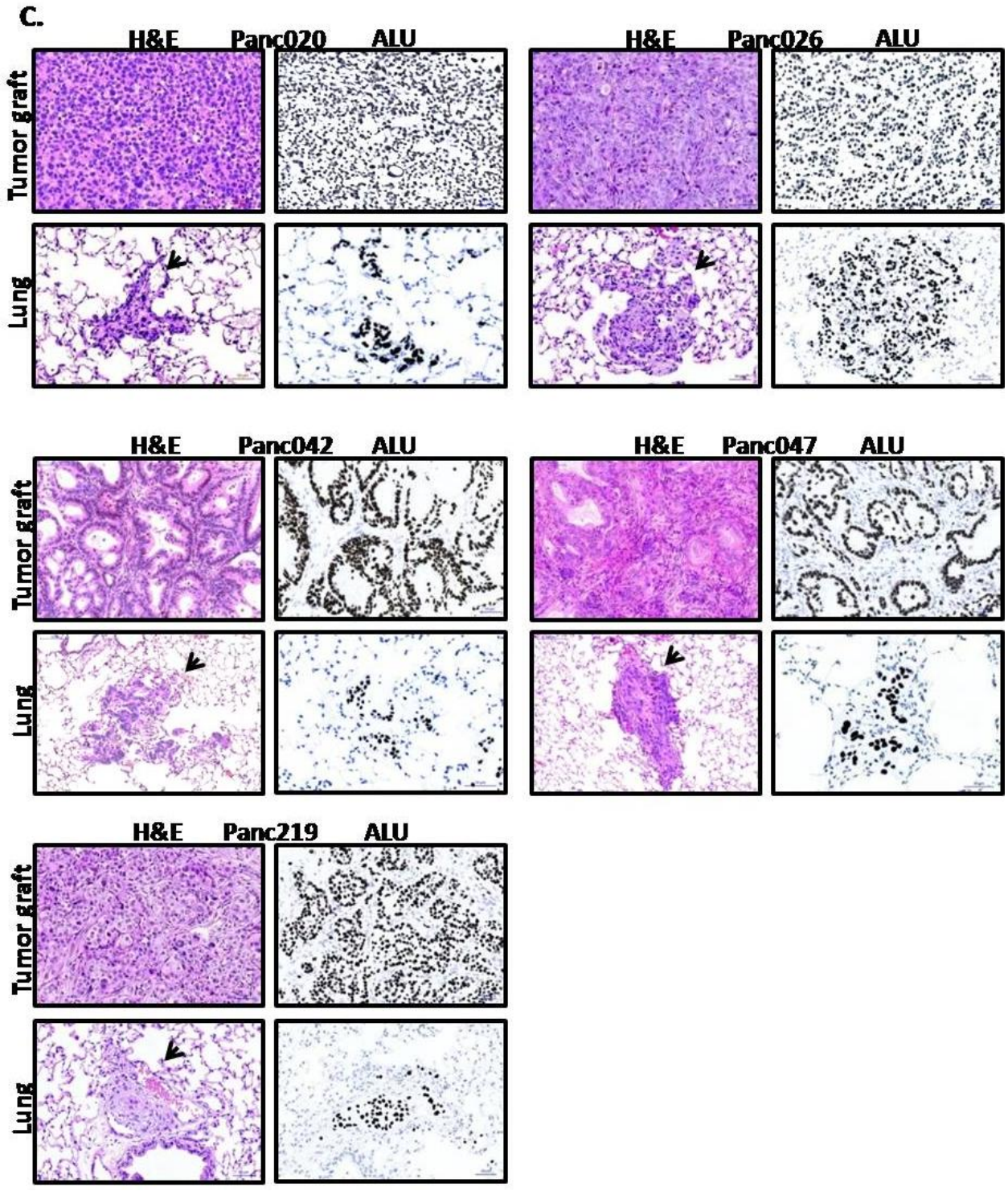
C.
H&E
Panc020
ALU
H&E
Panc026
ALU
Tumor graft
Lung
H&E
Panc042
ALU
H&E
Panc047
ALU
Tumor graft
Lung
H&E
Panc219
ALU
Tumor graft
Lung

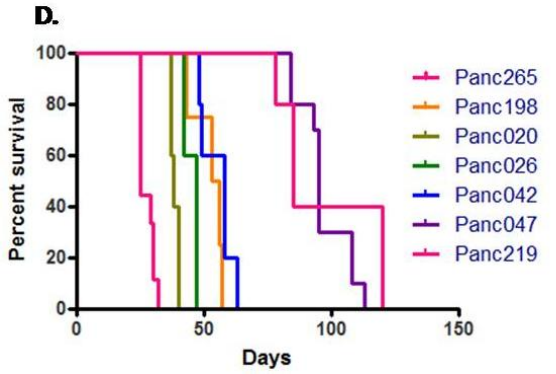

Table 4.

Number (percentage) of mice affected with metastasis			
PDX model	Survival days	Liver	Lung
Panc265	25	9/9 (100)	9/9(100)
Panc198	54.5	8/8(100)	8/8 (100)
Panc020	38	-	5/5 (100)
Panc026	47	-	5/5(100)
Panc042	58	-	9/10(90)
Panc047	95	-	9/10(90)
Panc219	85	1/5(20)	5/5(100)

Figure 8. **Development of metastatic PDX models of pancreatic cancer. (8A)** – Left vertical panels - Representative photomicrographs of Hematoxylin and Eosin (H&E) staining of tumor, liver and lung tissues derived from metastatic PDX models (Panc265, Panc198). The black arrows indicate the metastatic lesions in mouse livers and/or lungs. Right vertical panels – Representative photomicrographs of Alu ISH of a tumor graft, liver and lung sections - the silver staining corresponds to human nuclei, in which the Alu probe hybridizes (scale bar 50µm) **(8B) –** Left panel - Representative photomicrographs of Alu ISH of a brain section derived from a highly metastatic Panc265 model. Right panel - Representative immunoflourescence image of human vimentin (red) and mouse GFAP (green). **(8C)** - Left vertical panels - Representative photomicrographs of Hematoxylin and Eosin (H&E) staining of tumor, liver and lung tissues derived from metastatic PDX models (Panc020, Panc026, Panc042, Panc047, Panc219). The black arrows indicate the metastatic lesions in mouse livers and/or lungs. Right vertical panels – Representative photomicrographs of Alu ISH of a tumor graft, liver and lung sections (scale bar 50µm). **(8D)** - Kaplan-Meier plot of metastatic PDX models. **(Table 4)** - Summary table of metastatic incidence in PDX models.

4.1.3. Human vimentin expression predicts the occurrence of metastasis in PDX orthotopic models of pancreatic cancer.

4.1.3.1. Assesment of vimentin protein expression in metastatic and non-metastatic PDX models of pancreatic cancer.

In this study, we evaluated the human vimentin expression in a series of PDX models of PDAC with metastatic and non-metastatic *In-vivo* capacity. Interestingly, 6 out of 7 metastatic PDX models were positive for human vimentin marker (Figure 9A). More interestingly, the metastatic

lessions of these six metastatic PDX models also contain vimentin-positive tumor cells (Figure 9A). The models with higher vimentin expression are characterized by poor histological differentiation, aggressive metastatic phenotype and shorter survival rate (Figure 9 A, B, C), which is in agreement with the previously reported findings showing that vimentin expression is associated with poor prognosis[124-132]. Moreover, the vimentin expression pattern in two PDX models is consistently similar to the pattern of their corresponding human tumor specimens (Figure 9B), which is consistent with previous reports that the PDX models preserve essential properties of the original tumors. We also evaluated the vimentin expression in a series of non-metastatic PDX models and found that 2 out of 4 non-metastatic models were vimentin negative and one model with low vimentin expression (Figure9C, Table5). Only Panc059 non-metastatic model was characterized by high vimentin expression, fast-growing tumors and short survival rate (Figure 9B,D). Together these results suggest that (1) - Vimentin could serve as a predictive marker for In-vivo metastatic potential of PDAC xenograft tumors; (2) - It could play an important role in pancreatic cancer metastasis.

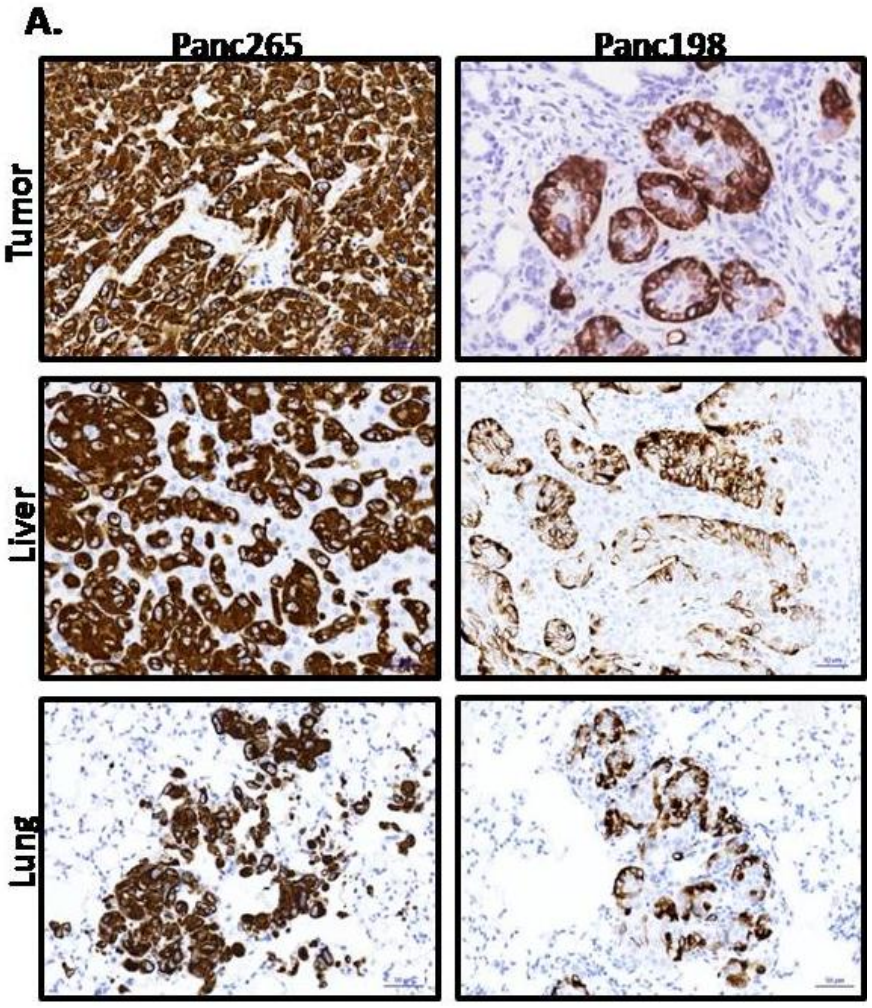
A.
Panc265
Panc198
Tumor
Liver
Lung

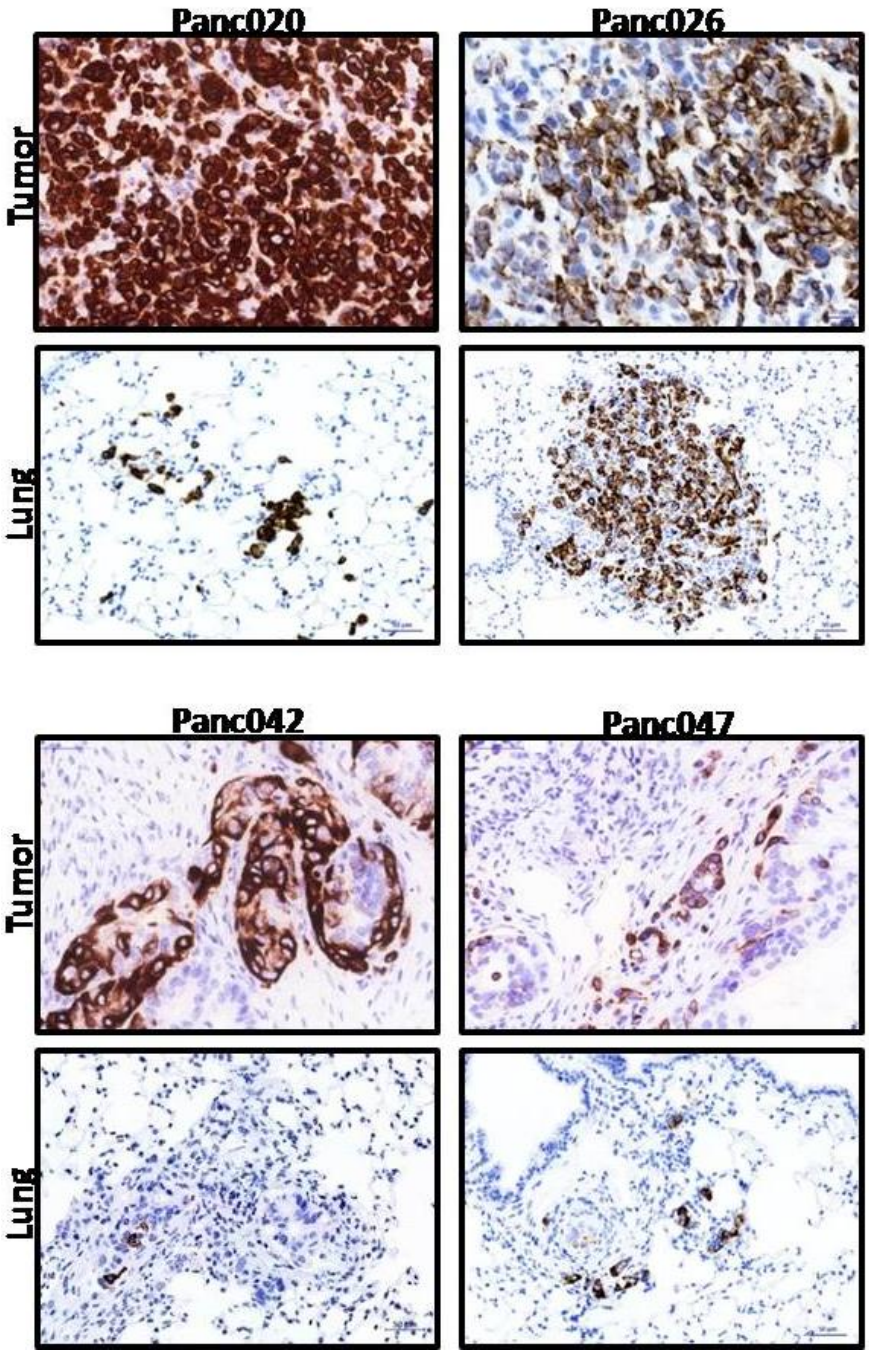
Panc020
Panc026
Tumor
Lung
Panc042
Panc047
Tumor
Lung

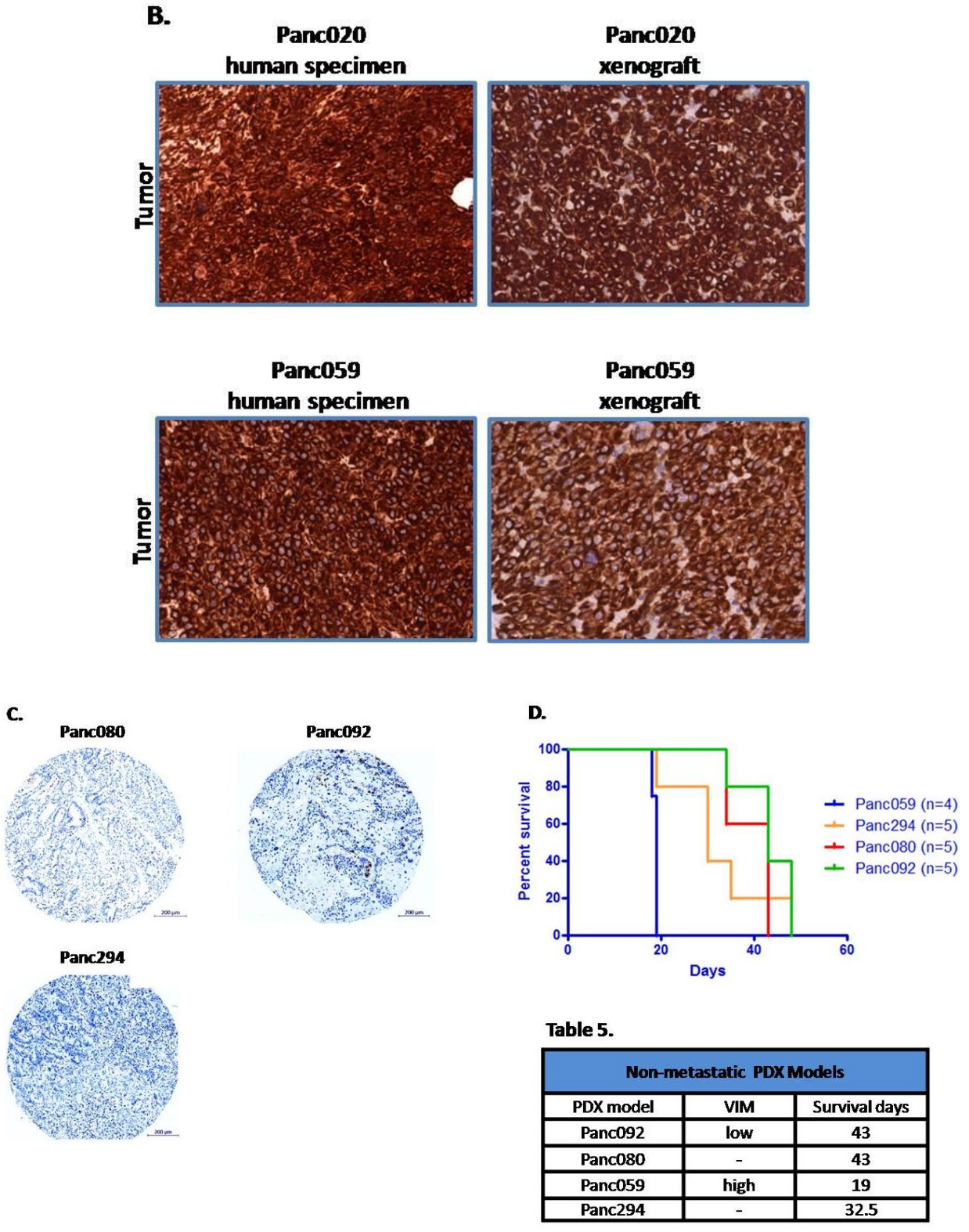

Table 5.

Non-metastatic PDX Models		
PDX model	VIM	Survival days
Panc092	low	43
Panc080	-	43
Panc059	high	19
Panc294	-	32.5

Figure 9. Evaluation of Vimentin expression in metastatic PDX models of pancreatic cancer. **(9A)** – Representative images of immunohistochemistry (IHC) staining for vimentin in tumor,

liver and lung tissues of metastatic PDX models (scale bar 50µm). **(9B)** – Representative images of IHC staining for vimentin in human pancreatic tumor specimens (Panc020 and Panc059) and their corresponding xenograft models. **(9C)** – Representative images of IHC staining for vimentin in tumor xenografts of non-metastatic PDX models (scale bar 200µm). **(9D)** - Kaplan-Meier plot of non-metastatic PDX models. **(Table 5)** - Summary table of vimentin expression and survival days of non-metastatic PDX models. Survival data were analyzed using GraphPad Prism 6 software.

4.1.3.2. In-vivo efficacy study with Withaferin-A in a highly metastatic Panc265 model.

To investigate whether vimentin could be an anti-metastatic target, we carried out an In-vivo efficacy study with the highly aggressive Panc265 metastatic model, evaluating the effect of Withaferin-A (a natural product shown to decrease vimentin protein expression in MDA-MB-231 xenografts and MMTV-*neu* tumor *in vivo*) [133] on metastasis formation and survival. Mice bearing orthotopically engrafted tumors were divided in two groups and treated with vehicle and WFA. The results demonstrated that WFA showed no significant increase in survival compared to vehicle treated mice (Figure10A). Furthermore, the H&E stained sections of mouse liver and lung organs of each treatment group were carefully examined and it was observed that 100% of vehicle and WFA treated animals had massive metastatic lesions in the liver and lung organs (Table 6). To assess whether WFA had an effect on decreasing the expression of vimentin at protein level, the tumors and distal organs of WFA treated mice were stained for human vimentin. The results showed abundant vimentin expression in primary tumor, liver and lung metastatic lesions, equal to that of control group (Figure10B). This study demonstrated that WFA compound was inefficient to reduce the metastatic tumor burden and to increase the survival of the animals, therefore new strategies are needed to prove whether vimentin plays a pivotal role in pancreatic cancer spreading.

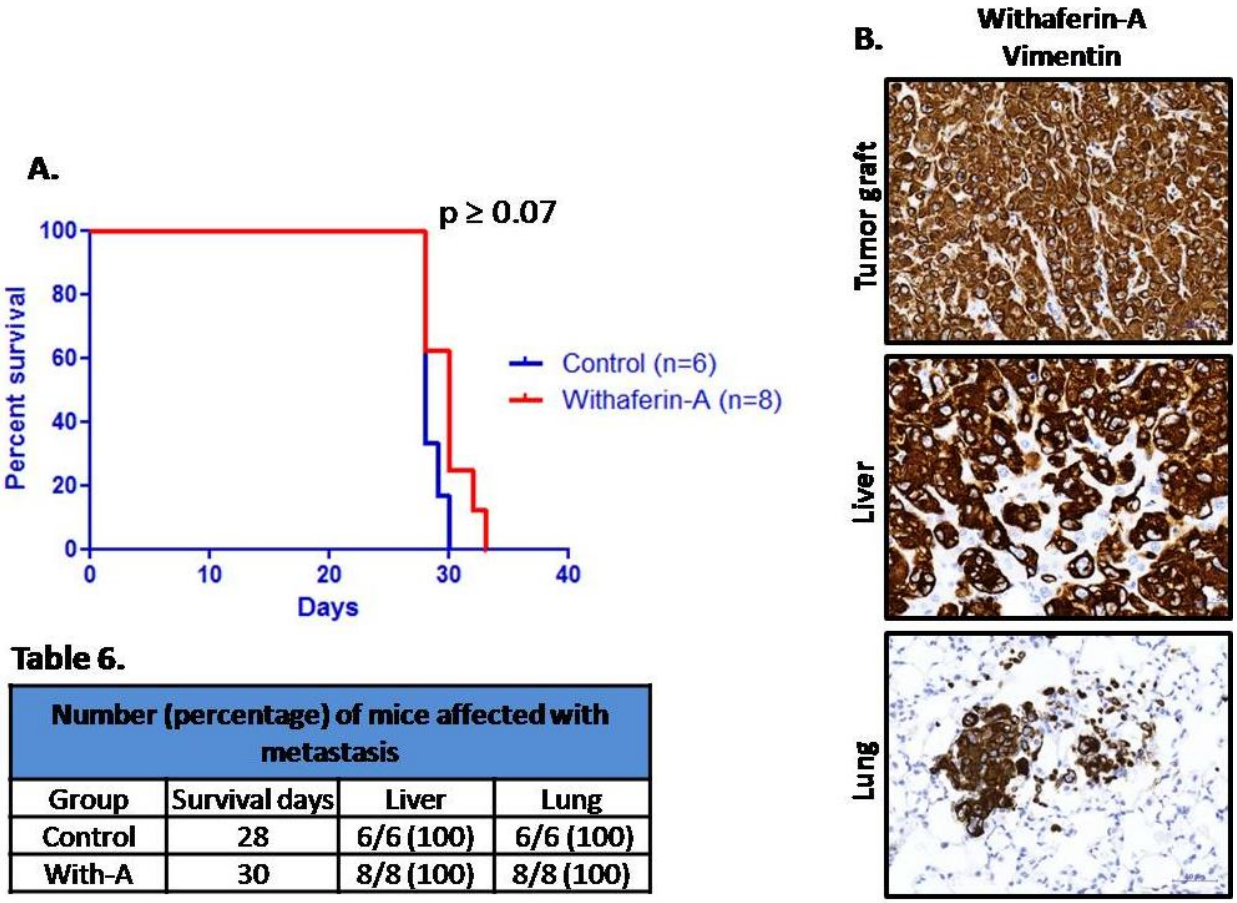

Table 6.

Number (percentage) of mice affected with metastasis			
Group	Survival days	Liver	Lung
Control	28	6/6 (100)	6/6 (100)
With-A	30	8/8 (100)	8/8 (100)

Figure 10. Efficacy study of Withaferin-A in Panc265 metastatic model. (10A) - Kaplan–Meier survival curves of control and drug treated groups. **(Table 6)** - Summary table of metastatic incidence in PDX models. **(10B) -** Representative images of IHC staining for Vimentin in tumor graft, liver and lung derived from treated group (scale bar 50μm). Survival data were analyzed using GraphPad Prism 6 software. P-values for survival differences were calculated using the log-rank (Mantel-Cox) test.

4.1.4. Evaluation of metastatic progression in a highly metastatic Panc265 model.

In order to monitor the primary growth, metastatic tumor burden and CTCs kinetics, we performed a time-course experiment of a highly metastatic Panc265 model. Groups of three mice were sacrificed periodically starting as early as 1 week after tumor implantation and primary tumor, metastatic organs and blood were collected at each time point. Alu-positive human cells in

mouse liver and lung organs have been detected as early as 2nd week post-tumor implantation and their number increased exponentially at later time points (Figure 11A,B). Using a RT-PCR specific for human Alu sequences, a significant increase in human DNA level in mouse blood was detected at 3rd week after tumor implantation and its level increased exponentially at 4th week time point (Figure 11C).

The results from this study demonstrated that the increased levels of human DNA in mouse blood at 3rd and 4th week correlated quite nicely with the primary tumor growth kinetics (Figure 11D) and with the increase of Alu-positive metastatic cells in mouse liver and lung organs (Figure 11B). However, there is still room for improvement in CTCs detection at early points of disease progression. One possible explanation for the failure to detect the human CTCs-derived DNA at 1st and 2nd week could be the application of Red blood cell (RBC) lyses solution prior to DNA extraction from the mouse blood samples. In subsequent studies, we observed that the usage of hypotonic solutions to remove the RBC resulted in significant lost of the human CTCs. This observation is in agreement with previous studies, reporting that hemolysis of RBC is associated with deleterious hypotonic damage and loss of CTCs [134-136].

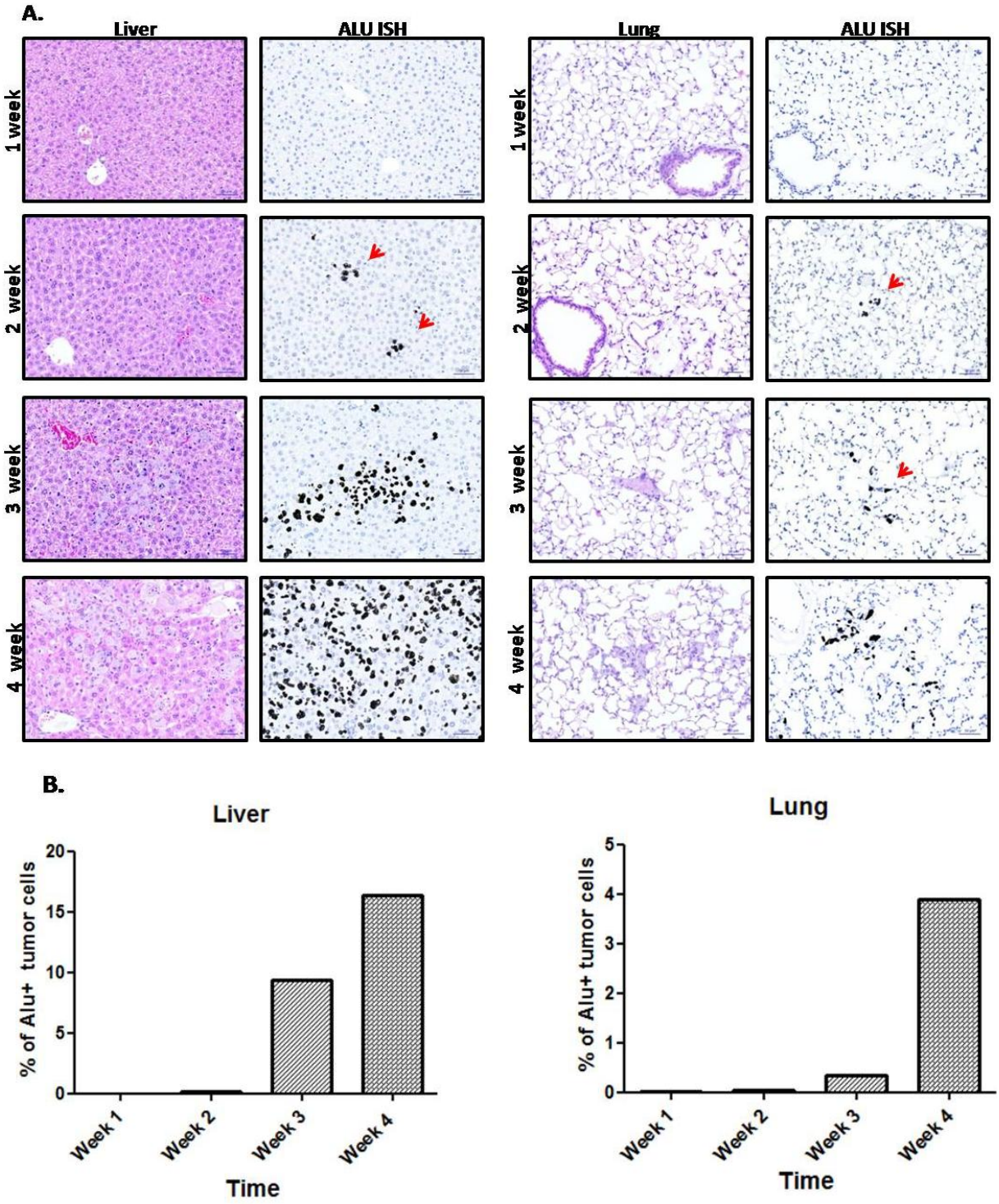
A.
Liver
ALU ISH
Lung
ALU ISH
1 week
2 week
3 week
4 week
B.
Liver
% of Alu+ tumor cells
20
15
10
5
0
Week 1
Week 2
Week 3
Week 4
Time
Lung
% of Alu+ tumor cells
5
4
3
2
1
0
Week 1
Week 2
Week 3
Week 4
Time

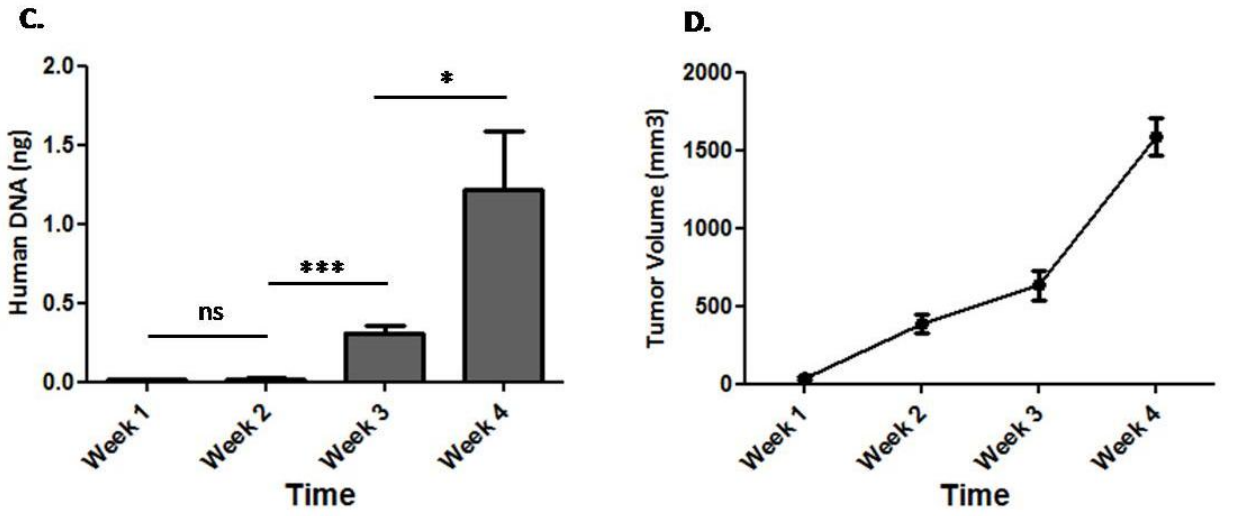

Figure 11. Time-course experiment of a highly metastatic PDX model. **(11A) –** 1st and 3rd vertical panel – Representative Photomicrographs of H&E staining of liver and lung sections derived from a highly metastatic Panc265 model from 1st to 4th week after tumor implantation, respectively. 2nd and 4th vertical panel – Alu ISH of liver and lung sections obtained from 1st to 4th week after tumor implantation, respectively (scale bar 50µm). The red arrows indicate the Alu-positive human tumor cells in mouse lungs. **(11B)** - Percentage of Alu+ positive human tumor cells relative to the total cell number in mouse livers and lungs resected from 1st to 4th week. **(11C)** – RT-qPCR quantification of human DNA in blood of PDX metastatic model at different time points. **(11D) -** The growth curve graph shows the primary tumor volume from 1st to 4th week. * ($p < 0.05$), *** ($p < 0.0001$).

4.1.5. Identification and isolation of human tumor populations from metastatic PDX models.

To identify the human tumor cells from metastatic PDX models, we checked the expression of MHC class I (HLA-ABC) antigen in two of our metastatic PDX models (Panc265, Panc198). This surface antigen is expressed on the surface of all nucleated cells and it is commonly used marker for identifying human cells in PDX models [137-138]. By Flow Cytometry, we identified that HLA-ABC is expressed by 83-86% of the tumor cells dissociated from Panc265 and Panc198 xenograft models with negletable background in control mouse peripheral tissues (Figure12A,B,C). For identification of infiltrating mouse cells in xenograft tumors, we used H-2kD marker (mouse MHC class I), which is expressed on the surface of all mouse nucleated cells.

To isolate viable human tumor cells from the mouse organs of metastatic PDX models, we performed magnetic-activated cell sorting (MACS) assay, where we applied a two-step process using a human specific HLA-ABC antibody to recognize the human tumor cells and anti-flourochrome magnetic beads, which specifically recognize the flourochrome of primary antibody. By this approach, we were able to capture and purify the majority of primary tumor cells, CTCs and metastatic cells from the mouse organs of metastatic PDX model (Figure12D).

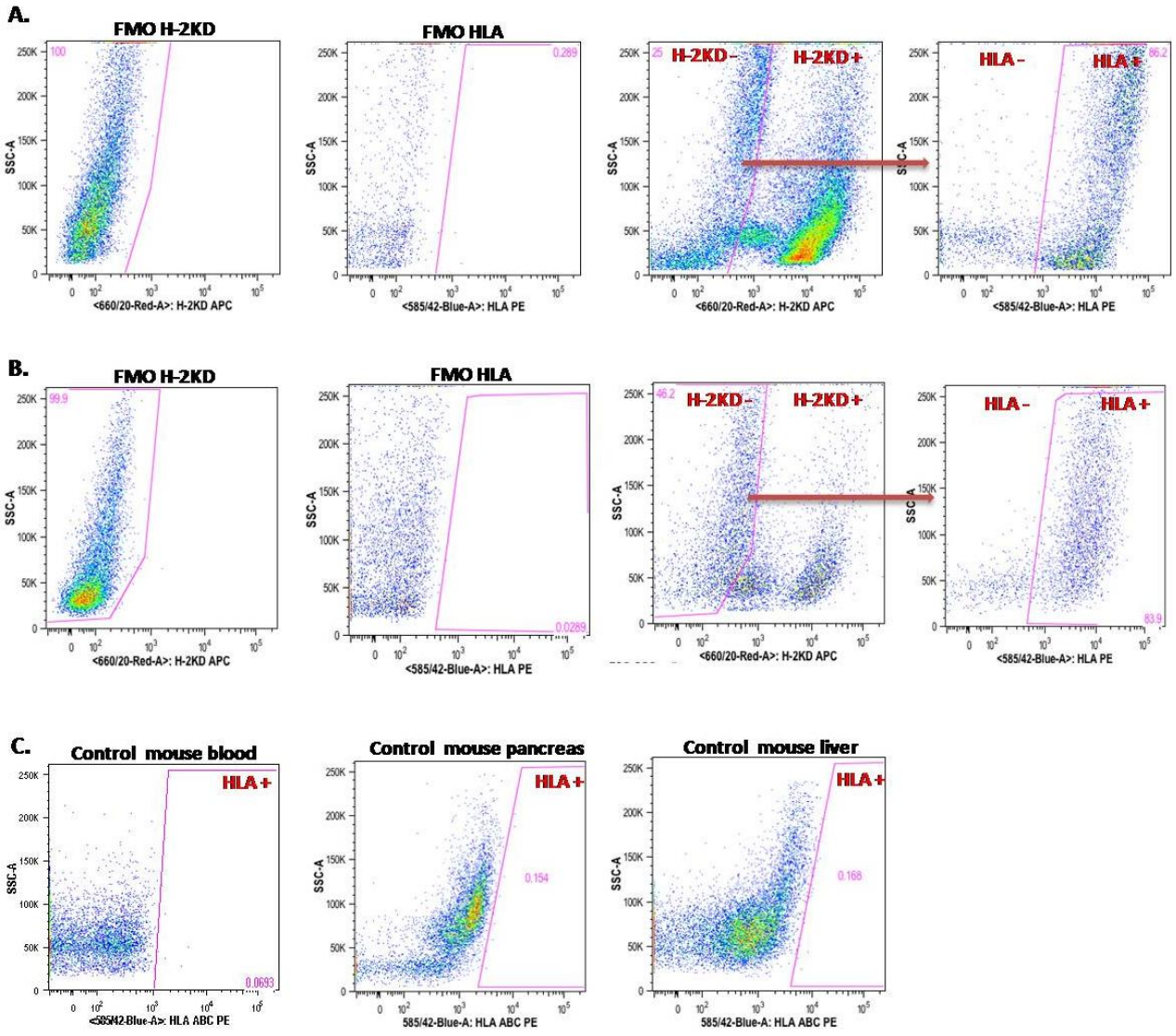

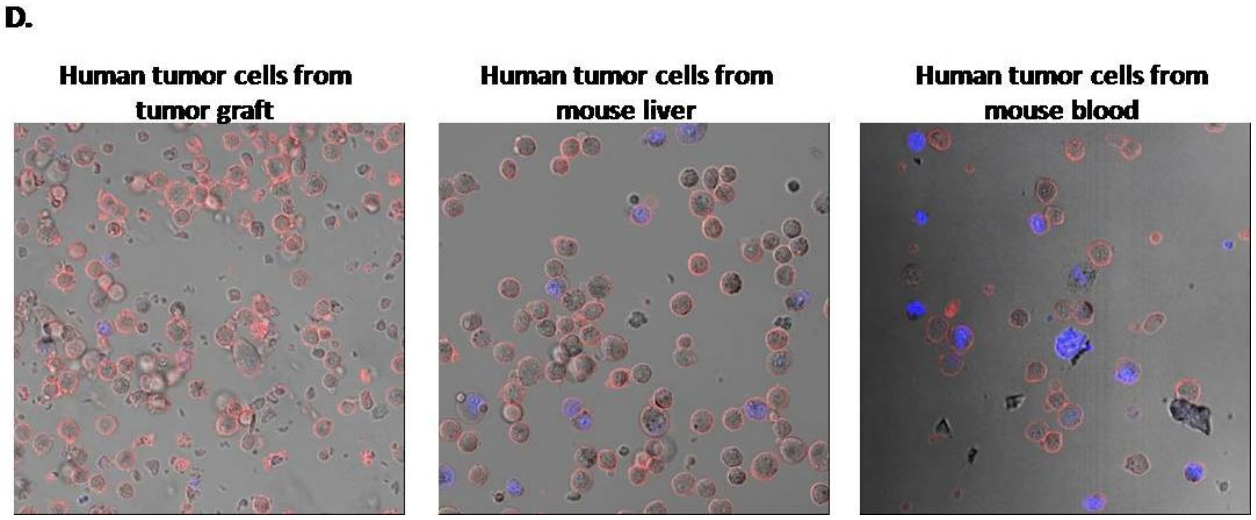

Figure 12. Identification of human metastatic cells in metastatic PDX models.

(12A) - FACS plots show fluorescence-minus-one (FMO) controls of H-2kD and HLA-ABC and the percentage of human HLA-ABC and mouse H-2kD cells in dissociated tumors of Panc265 model (left to right, respectively). **(12B) -** FACS plots show fluorescence-minus-one (FMO) controls of H-2kD and HLA-ABC and the percentage of human HLA-ABC and mouse H-2kD cells in dissociated tumors of Panc198 model (left to right, respectively). **(12C) -** FACS plots show the percentage of HLA-ABC cells in pancreas, liver and lung dissociated tissues derived from naive mice. **(12D) -** Representative photomicrographs of HLA-ABC positive human tumor cells isolated by magnetic separation from tumor graft, liver and blood of a highly metastatic PDX model.

4.1.6. Tumorigenic and metastatic capacity of CTCs derived from metastatic PDX model.

To evaluate whether the CTCs derived from metastatic PDX model possess tumorigenic capacity, we isolated the human CTCs utilizing anti-human HLA-ABC antibody from the blood of a highly metastatic Panc265 model and subcutaneously injected 10000 and 5000 cells in one of the flanks of a NSG mice. Remarkably, we detected measurable tumors in 7 out of 8 transplants within a month after implantation and all of them produced large tumors reaching a volume of 1300 mm^3 (Figure 13A-B, Table 7). The histopathology and immunohistochemistry (IHC) of CTC-derived tumors and their corresponding parental primary tumor was also evaluated. We observed similar morphological pattern between primary and CTCs derived tumors, with neoplastic cells

characterized by moderate to severe nuclear pleomorphism with large bizarre nuclei and aberrant mitosis. CTC-derived tumors also display high expression of vimentin, consistent with the expression pattern of parental tumor (Figure 13D).

To determine whether CTC-derived tumors also exhibit metastatic potential, we examined the livers and lungs of the tumor-bearing animals. Although no macrometastases were observed on visual inspection, subsequent histological examination of liver and lung sections revealed micrometastatic clusters of tumor cells in pulmonary parenchyma in all implanted mice and one sporadic liver micrometastasis (Figure 13C, Table 8). The human origin of CTC-derived tumors and their corresponding metastasis was confirmed by Alu staining (Figure 13C). Altogether, these findings support the hypothesis that CTCs population contain cells with tumor-initiating and metastasis-initiating properties [139-140].

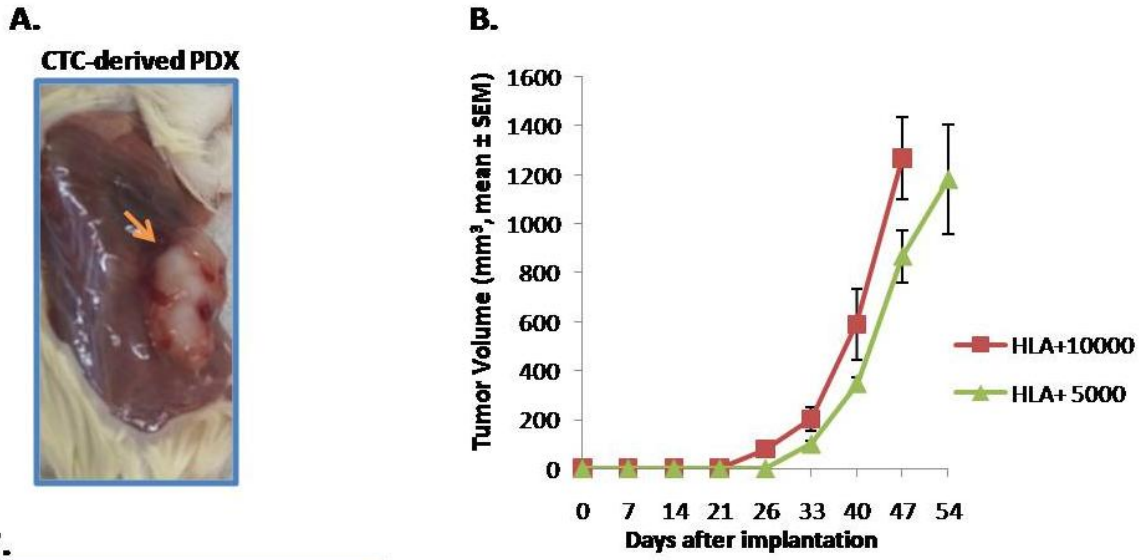

Table 7.

Tumor take after CTCs implantation	
No of cell injected	No of tumors
10000	4/4(100%)
5000	3/4(75%)

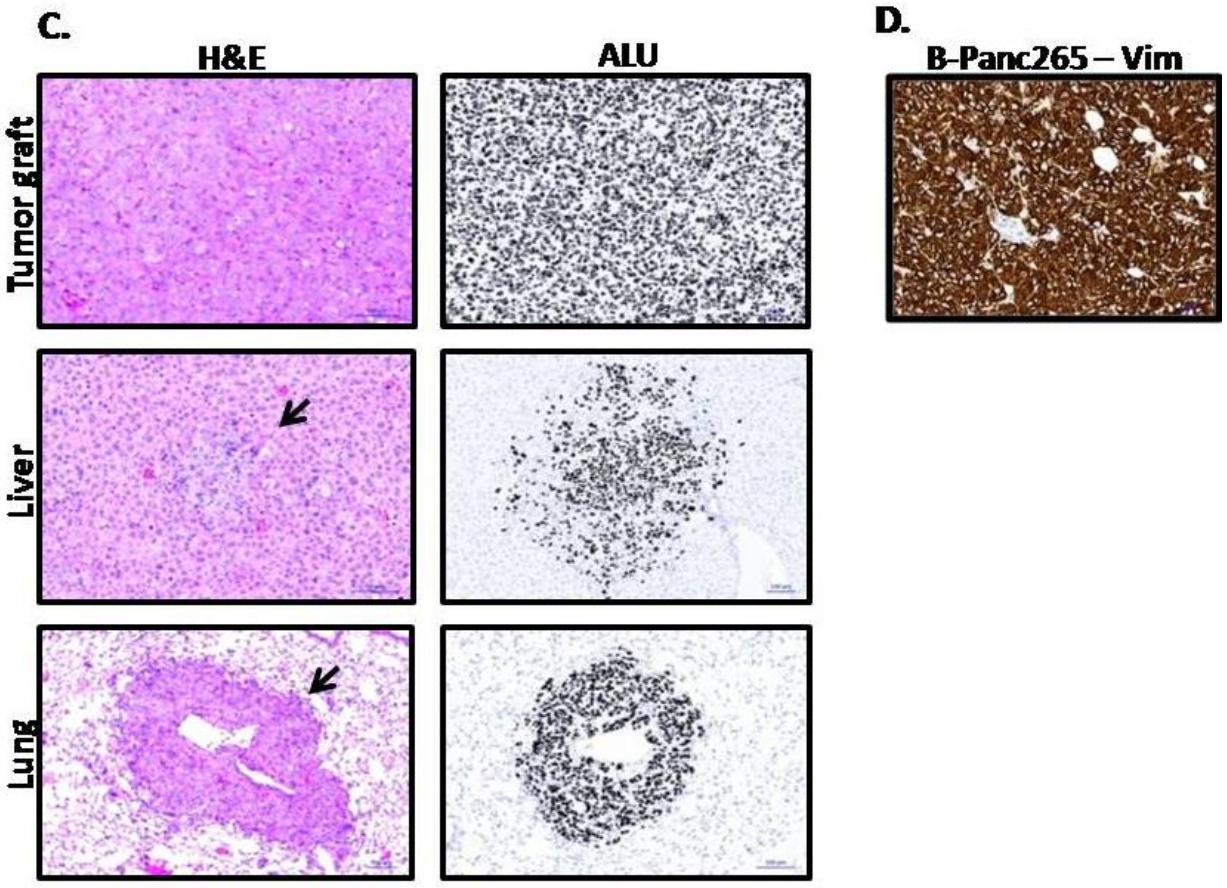

Table 8.

Number (percentage) of mice affected with metastasis	
Liver	Lung
1/7 (14%)	7/7(100%)

Figure 13. Human pancreatic CTCs possess tumor-initiating and metastatic capacity. (13A) - Representative photographs of mice carrying a subcutaneous CTC-derived tumor. The orange arrow indicate the CTC-derived tumor graft. **(Table 7) -** Summary table of tumor take rate after CTCs implantation. **(13B) -** Tumor volume over time after implantation with CTCs ($5x10^3$ and $1x10^4$ cells) isolated from Panc265 metastatic PDX model. **(13C)** – Left vertical panel- H&E staining of tumor, liver and lung tissues obtained from mice bearing CTCs derived tumors. The black arrows indicate the metastatic lesions in mouse liver and lung. Right vertical panel- Alu ISH of tumor graft and metastatic lesions in mouse liver and lung (scale bar 50μm). **(Table 8) -**

Summary table of metastatic incidence in CTCs bearing mice. **(13D) -** Representative images of immunohistochemistry (IHC) staining for vimentin in tumor graft of CTC derived tumor.

4.2. Single-cell RNA sequencing of the human pancreatic tumor populations involved in metastatic disease.

To investigate the transcriptional heterogeneity during the metastatic progression, we performed single cell RNA-seq to profile individual pancreatic tumor cells isolated from primary tumor graft, mouse blood and liver of one of our highly metastatic Panc265 model. An automated microfluidic-based platform (Fluidigm) was used to capture and lyse individual human PDX tumor cells, followed by reverse transcription of mRNA and amplification of complementary DNA. We successfully sequenced 37 human primary tumor cells, 23 metastatic tumor cells and 10 CTCs to a depth of 7.5–13.2 million reads, of which 86.4%–89.5% uniquely aligned to the human reference genome, which is comparable to the mapping rates of other single cell RNA-seq data (Figure 14A, Table 9). The average number of expressed genes detected across single cell RNA seq analysis was above 8000 genes in primary and liver metastasis tumor cells and above 3000 genes in CTCs (Figure 14B), thus suggesting that CTCs display a degree of transcriptional repression compared to primary and metastatic cells.

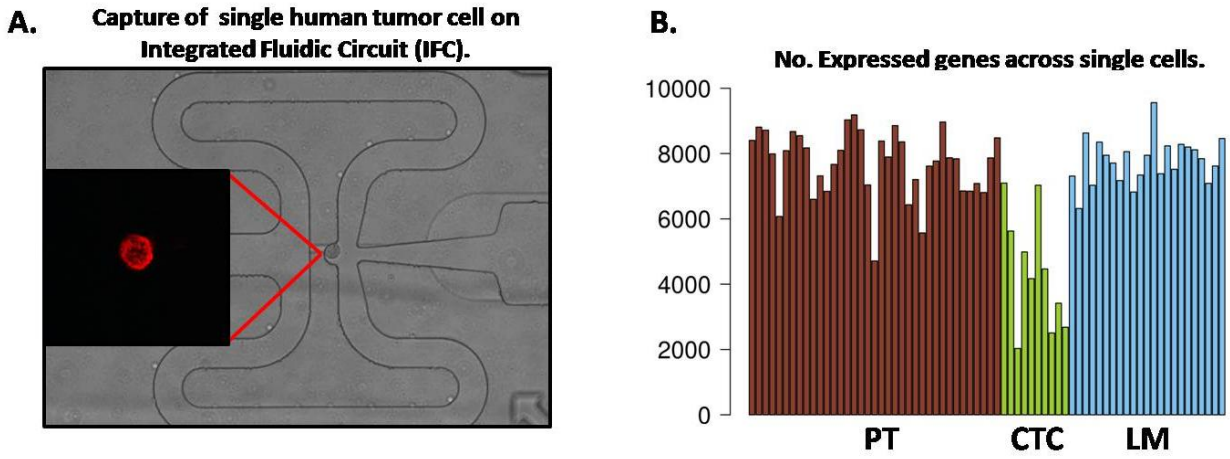

Table 9. Single-cell RNAseq:

		Primary tumour	CTCs	Liver Metastasis
Samples in study	Secuenced	45	13	32
	Discarded	8	3	9
	Final	37	10	23
Sequencing run	Avg raw reads (M)	12.7	17	14.2
	Avg mapping	89.50%	86.40%	87.60%
	Read counts (M)	7.5	13.2	9.5

Figure 14. Single-cell RNA-seq of tumor cells isolated from a highly metastatic PDX model. (14A) – Photomicrograph of single tumor cell captured on Integrated Fluidic Circuit (IFC) (10x). **(Table9) –** Summary table of single-cell RNA seq performance including the number of sequenced cells, average read counts and mapping **(14B) -** Represantative graph of number of expressed genes across single-cell analysis.

4.2.1 Deciphering the transcriptional intra-tumoral heterogeneity during metastatic progression.

In collaboration with Bioinformatics Unit from CNIO, we compared the gene expression profiles of all sequenced human tumor cells and the differential gene expression analysis revealed a small number of genes that were differentially expressed (FDR<0.05) between primary tumor, CTCs and liver metastasis cells (Table S2, S3, S4). To further investigate the gene expression signatures of the human PDX cells, we applied principal component analysis (PCA), which is the most widely used method for reduction of dimensionality of the data, and it has been effectively used in a

number of single-cell genomics studies. Remarkably, PCA clusters all sequenced human tumor cells into three distinctive main clusters: CTCs, primary and metastatic tumor cells (Figure 15). The first principal component separates the CTCs from primary and liver metastatic cells. The second principal component separates primary tumor cells from liver metastasis cells. Together, these results demonstrate that single-cell RNA-seq enables the identification of three biological groups with a high degree of intratumor heterogeneity, mostly pronounced in the CTCs.

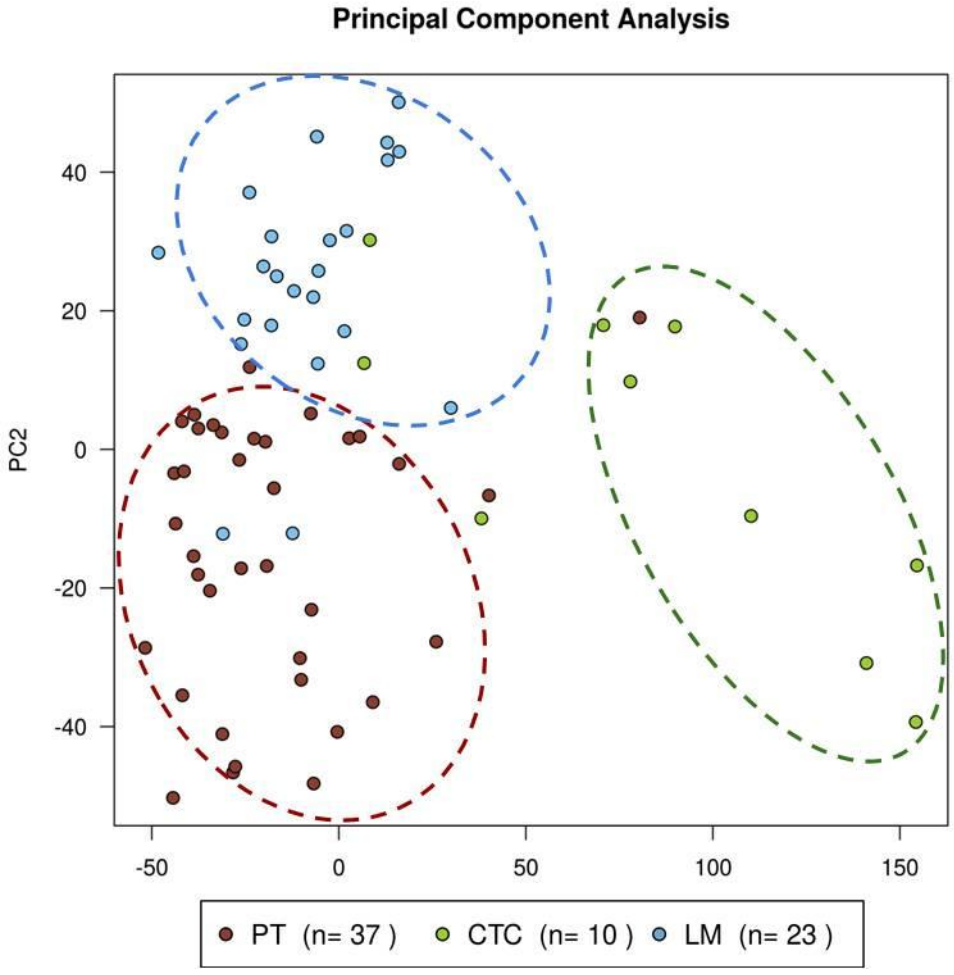

Figure 15. Principal component analysis (PCA) of single cells based on the two first principal components. PCA of primary tumor, liver metastasis and CTCs at single cell level. of single cell level. Brown: Primary tumour cells (n=37), light blue: liver metastasis cells (n=23), light green: Circulating tumour cells (n=10).

To further characterize the aspects of this transcriptional heterogeneity, we employed a recently published approach, called PAGODA [141], that resolves the transcriptional diversity at single-cell level. This method identified that ECM interaction and focal adhesion, cell cycle and ribosome biogenesis are the main pathways differentially expressed among the single-cell populations (Figure 16). The first pattern separates the primary tumor cells from the CTCs and metastatic cells, based on increased expression of fibronectin1 (*FN1*), integrin subunit beta 5 (*ITGB5*), collagen type I alpha 1 chain (*COL1A1*) among others known markers of ECM interaction. The second major aspect is driven by a gene set associated with cell cycle, which is highly expressed in metastatic cells and subpopulation of primary tumor cells. To further dissect the cell cycle states, we employed a computational analysis [142] using annotated signatures for each phase of the cell cycle (G1, S, G2/M). Interestingly, the primary tumor and metastatic cells were similarly distributed between the cell cycle phases with higher frequency of cells in G1 and G2/M phase (Figure17). In contrast, the vast majority of CTCs were primarily allocated to G1 phase. Therefore, these results show that the primary tumor and metastatic group are composed of a large proportion of actively cycling cells, while the CTC group might be characterized by quiescent or slow-cycling cells with prolonged interphase. The third pattern reflects Ribosome signature, which is most pronounced in CTCs with high expression of ribosomal protein L38 (*RPL38*), ribosomal protein *S16* (*RPS16*), ribosomal protein S29 (*RPS29*) among others common markers (Figure 16).

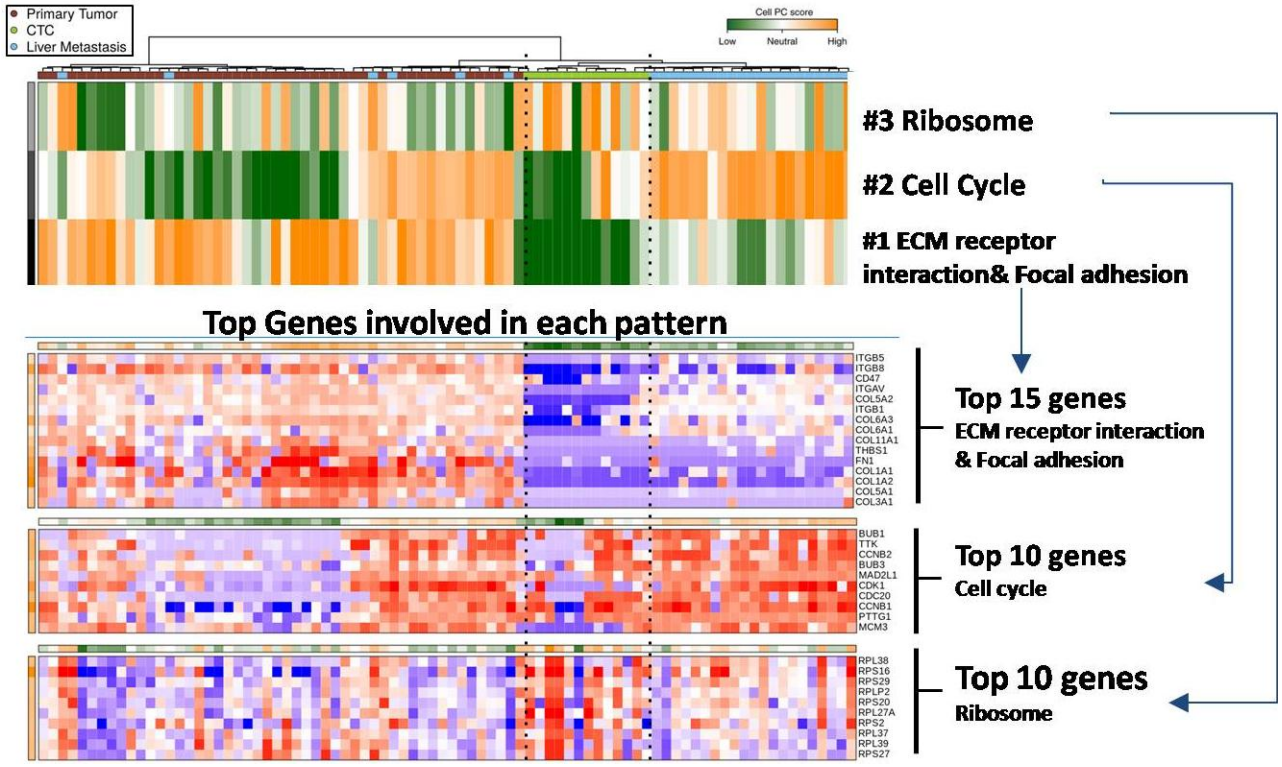

Figure 16. Deciphering the most important patterns of transcriptional heterogeneity.

Heatmap of significant gene set patterns of transcriptional heterogeneity obtained by Pathway and Gene Set Overdispersion Analysis (PAGODA method; $P < 0.05$) using KEGG pathways. Significant patterns: 1=ECM receptor interaction and Focal adhesion. 2=Cell cycle. The dendrogram shows overall clustering of individual cells using biological pathways, brown= primary tumor cells, lightblue= Liver metastasis, lightgreen = CTCs.

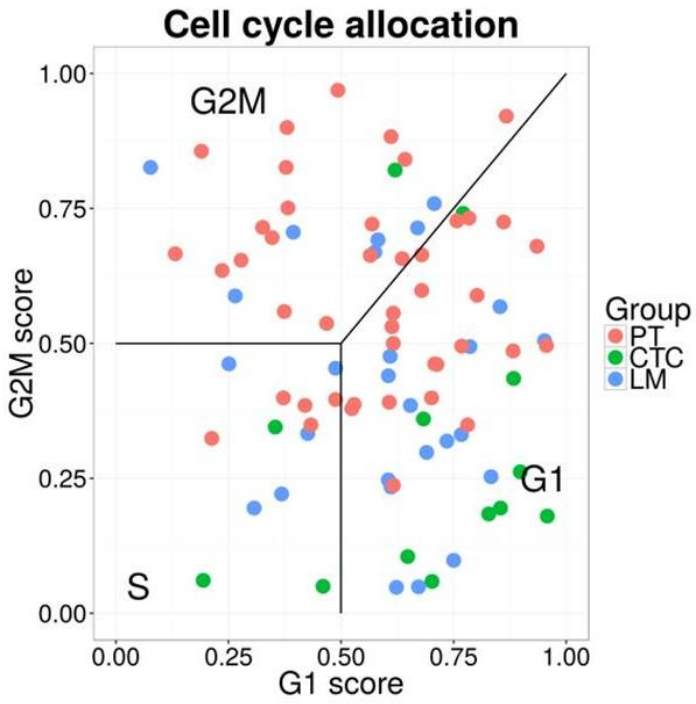

Figure 17. Cell cycle allocation of the human tumor populations isolated from metastatic PDX model.

(17) - Cell-cycle phase distribution of human tumor populations isolated from metastatic PDX model.

4.2.2. Identification of potential anti-metastatic targets for pancreatic cancer.

Next goal of the thesis was to identify potential anti-metastatic targets such as metastasis-associated genes or pathways, which are deregulated in the CTCs (precursors of metastatic disease) with aim to find and test new therapeutic strategy that could inhibit pancreatic metastasis. In order to find potential anti-metastatic candidates, we decided to interrogate the gene expression profile of the human CTCs isolated from one of the metastatic PDX models. Interestingly, we found that the gene baculoviral IAP repeat containing 5 (*BIRC5*), also known as Survivin, is significantly up-regulated in CTCs (a 3.2 log2 fold change, FDR=0.02) in comparison to primary tumor profile (Table S1). *BIRC5* is cancer-related gene, which belongs to the inhibitor of apoptosis family (IAP) and to chromosomal passenger complex involved in regulating chromomal segregation and cytokinesis during mitosis.

To identify other potential anti-metastatic therapeutic targets, we also employed a connectivity mapping approach, which uses gene-expression profiling to connect genes, disease and drugs.

This method is a powerful tool to identify potential therapeutic drugs that are able to alter the gene expression signature of particular biological conditions [116]. Interestingly, drug connectivity map analysis using the gene expression signatures of primary tumor cells and CTCs showed that aurora kinase A (*AURKA*), aurora kinase B (*AURKB*) and polo like kinase 1 (*PLK1*) knock-down signatures had opposite connections and their kinase substrates were over-expressed in CTCs compared to primary tumor cells (Figure 18A, Table 10). Moreover, the top opposite drug signatures are enriched on various aurora kinase inhibitors including Danusartib (Table 11). This approach also revealed an enrichment of anti-apoptotic state in CTCs and the top most opposite drug compound was PAC-1 (promoter of caspase signaling) (Table 11).

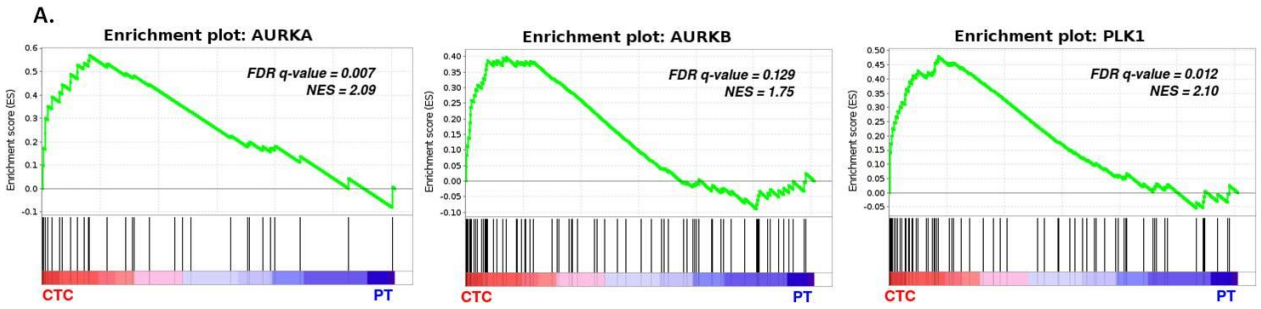

Table 10.

Gene set name	Direction	Size	ES	NES	NOM p-val	FDR q-val
AURKB_KNOCK-DOWN_DN	Up-regulated	100	0.61	2.84	0.000	0.000
AURKA_KNOCK-DOWN_DN	Up-regulated	100	0.57	2.65	0.000	0.000
PLK1_KNOCK-DOWN_DN	Up-regulated	95	0.32	1.45	0.012	0.013
AURKB_KNOCK-DOWN_UP	down-regulated	78	-0.41	-1.43	0.022	0.036
AURKA_KNOCK-DOWN_UP	down-regulated	69	-0.42	-1.40	0.037	0.044
PLK1_KNOCK-DOWN_UP	down-regulated	70	-0.38	-1.28	0.102	0.131

Table 11.

Name	Perturbation	CMap Score	Description
PAC-1	Drug compound	-97,15	-
PAC-1	Drug compound	-97,08	Caspase activator
danusertib	Drug compound	-55,66	Aurora kinase inhibitor

Figure 18. Identification of potential anti-metastatic targets for pancreatic cancer.

(18A) - Enrichment of kinase substrates of *AURKA*, *AURKB* and *PLK1* towards up-regulation in CTCs. (**Table 10) -** Opposite connection of *AURKA*, *AURKB* and *PLK1* knock-down signatures

(source: LINCS L1000) in the gene expression signature from the biological state of CTCs vs. primary tumour cells. **(Table 11) -** Connectivity map statistics on the selected drug compounds for further drug efficacy studies. ES:Enrichment score; NES: Normalized Enrichment Score; NOM p-val: Nominal p-value. FDR q-val: False Discovery Rate.

4.2.3. *In-vivo* validation of single cell-driven therapeutic strategy.

To validate whether targeting the previously identified candidates could have an *In-vivo* anti-metastatic effect, we chose to test the following compounds: YM155 (small-molecule transcriptional repressor of Survivin, currently undergoing phase II clinical trials in patients with various types of cancer), Danusertib (a small molecule pan-aurora kinase inhibitor, currently in phase II clinical trials for treatment of patients with solid tumors) and Pac-1 (a small molecule that activates procaspase-3 to caspase-3, resulting in apoptosis of cancer cells, currently in phase 1 clinical trials for the treatment of patients with advanced malignancies). Danusertib and Pac-1 are the top opposite drug signatures compounds identified by connectivity mapping analysis.

To evaluate the *In-vivo* effect of selected treatment regimens on metastasis formation and survival, mice implanted with a highly metastatic Panc265 model were randomized to the following experimental groups: (1) Control; (2) YM155; (*3*) PAC-1; (*4*) Danusertib; (*5*) PAC-1+Abraxane (Abx); (6) YM155+Abx; (7) Danusertib+Abx; (doses and schedule are described in material and methods). The Abraxane arm was included in order to control the primary tumor growth and to evaluate whether the combo treatment will result in improvement in median survival compared with monotherapy regimens. One week post-implantation, the experimental groups were subjected to a 4-week treatment course. The results showed that upon completion of the treatment, Pac-1 monotherapy failed to demonstrate a significant increase in survival of the mice compared to control group. However, YM155 and Danusertib monotherapy significantly improved the median survival of treated animals compared to control animals (Figure 19A, Table 12). Pac-1 + ABX treatment resulted in a median survival of 40 days, but there was no significant difference in comparison to the median survival of YM155 and Danusertib single agent (Figure 19A, Table 12). Both YM155 + ABX and Danusertib + ABX showed a slightly significant improvement in median survival compared with YM155, Danusertib and Pac-1+ABX treatment groups (Figure 19A, Table

12). At the survival endpoint, the tumor-bearing mice of all treated groups displayed the usual signs of sickness (described in methods) caused by the progression of metastatic disease.

Next, we evaluated the metastatic tumor burden of YM155 and Danusertib treated animals sacrificed at the survival endpoint of control group. The results showed that while Danusertib treatment failed to reduced significantly the metastatic tumor burden, treatment with YM155 significantly decreased the percentage of the human metastatic cells in the liver and lung organs of drug treated group compared to control animals (Figure 19B,C).

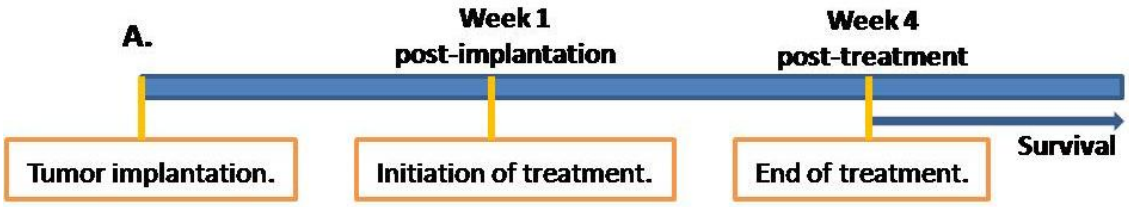

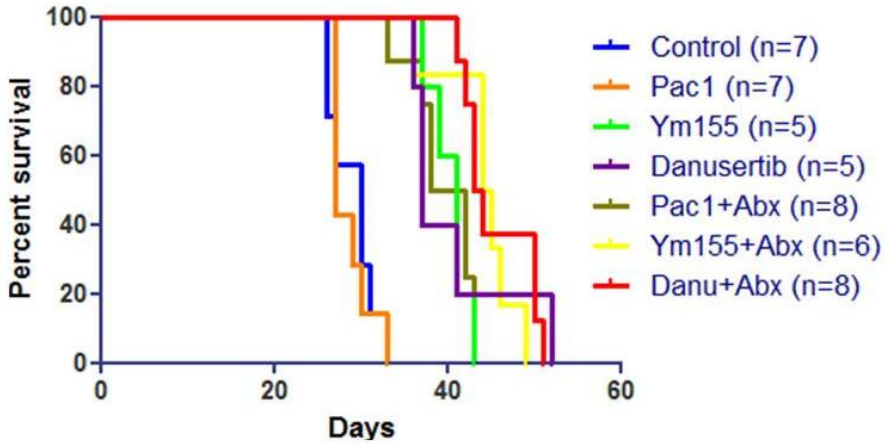

Table 12. **p value Mantel-Cox test:**

Groups	Median survival (days)	Control	Pac-1	Ym155	Danusertib	Pac1+Abx	Ym155+Abx
Control	30						
Pac-1	27	0.82 ns					
Ym155	41	0.001	0.0007				
Danusertib	37	0.001	0.0007	0.59 ns			
Pac1+Abx	40	0.0001	0.0001	0.87 ns	0.51 ns		
Ym155+Abx	44.5	0.0004	0.0003	0.01	0.01	0.007	
Danu+Abx	43.5	0.0001	0.0001	0.01	0.008	0.01	0.5 ns

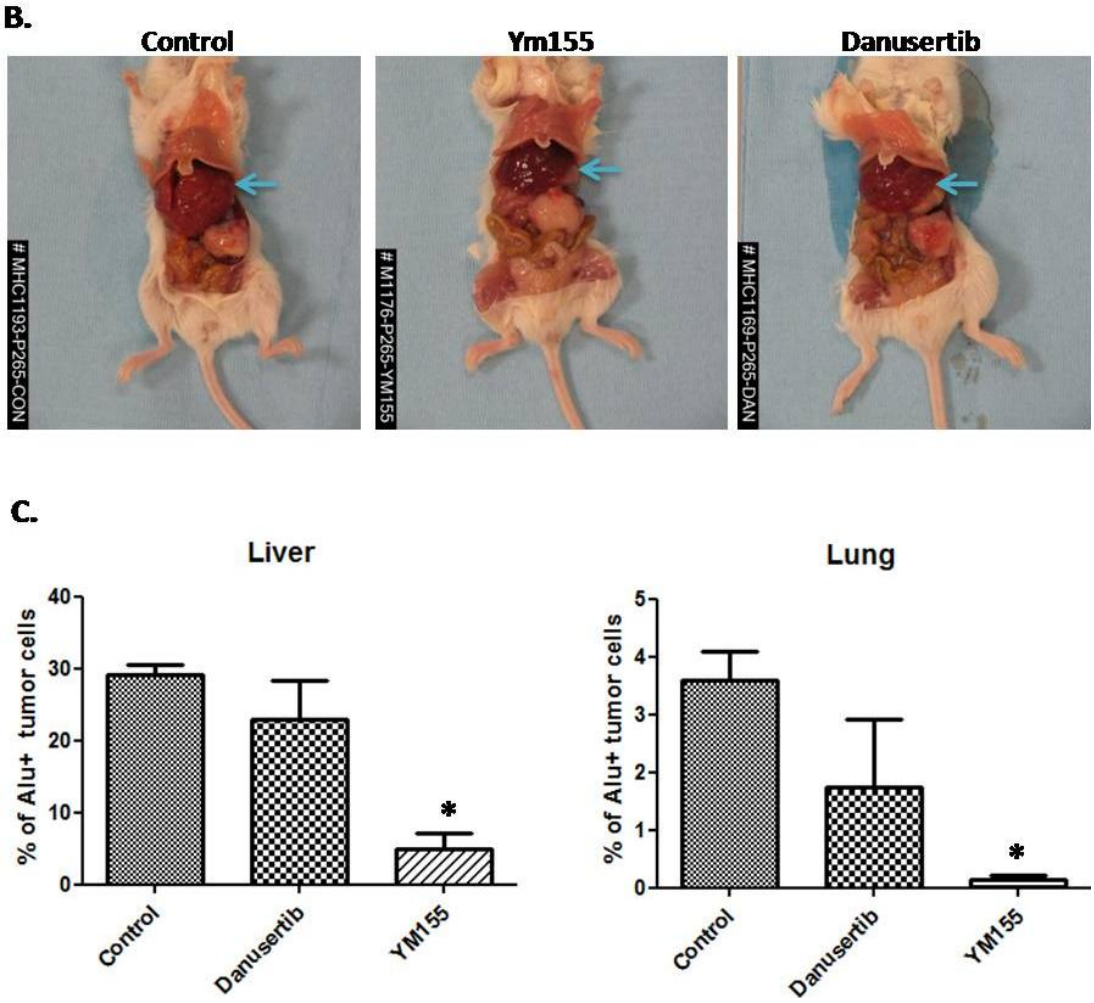

Figure 19. In-vivo validation of single cell-driven therapeutic strategy. (19A) – Treatment course in PDX mice harbouring a highly metastatic Panc265 model (top). Kaplan–Meier survival curves of control and drug treated groups. **(Table 12)** - The table shows the median survival days and statistical significance of the experimental groups. Survival data were analysed using GraphPad Prism 6 software. P-values for survival differences were calculated using the log-rank (Mantel-Cox) test. **(19B)** - Representative photographs of Conrol, Danusertib and YM155 treated mice after 4-week treatment course. The blue arrows indicate the livers of control and treated groups. The liver of control group displays hepatomegaly with macroscopic tumor lesions. **(19C)** - Percentage of Alu+ positive human cells relative to the total cell number in mouse livers and lungs of control and drug treated groups after 4-week treatment course.

4.3. Survivin: A therapeutic target for metastatic pancreatic cancer.

4.3.1. Assessment of Survivin protein expression in PDX metastatic models.

Since the treatment with the Survivin suppressor (YM155) exerted the best anti-metastatic activity, we focused on its further characterization. First, the protein expression of Survivin was assessed in Panc265 metastatic model used in scRNA sequencing experiment. Interestingly, IHC analysis revealed nuclear expression of Survivin protein in primary tumor cells, CTCs, liver and lung metastatic cells (Figure 20A,B). Most of the tumor cells positive for Survivin are undergoing mitosis, mostly in metaphase and anaphase (histological observation). Moreover, immunofluorescence (IF) nicely confirmed its nuclear localization in CTCs isolated from the highly metastatic Panc265 model (Figure 20B). The protein expression of Survivin was also evaluated in the other metastatic models and the IHC showed nuclear expression of the protein in the primary and metastatic lesions of all PDX models, thus suggesting that Survivin may play an essential role in tumor cell division during the metastasis progression of pancreatic cancer.

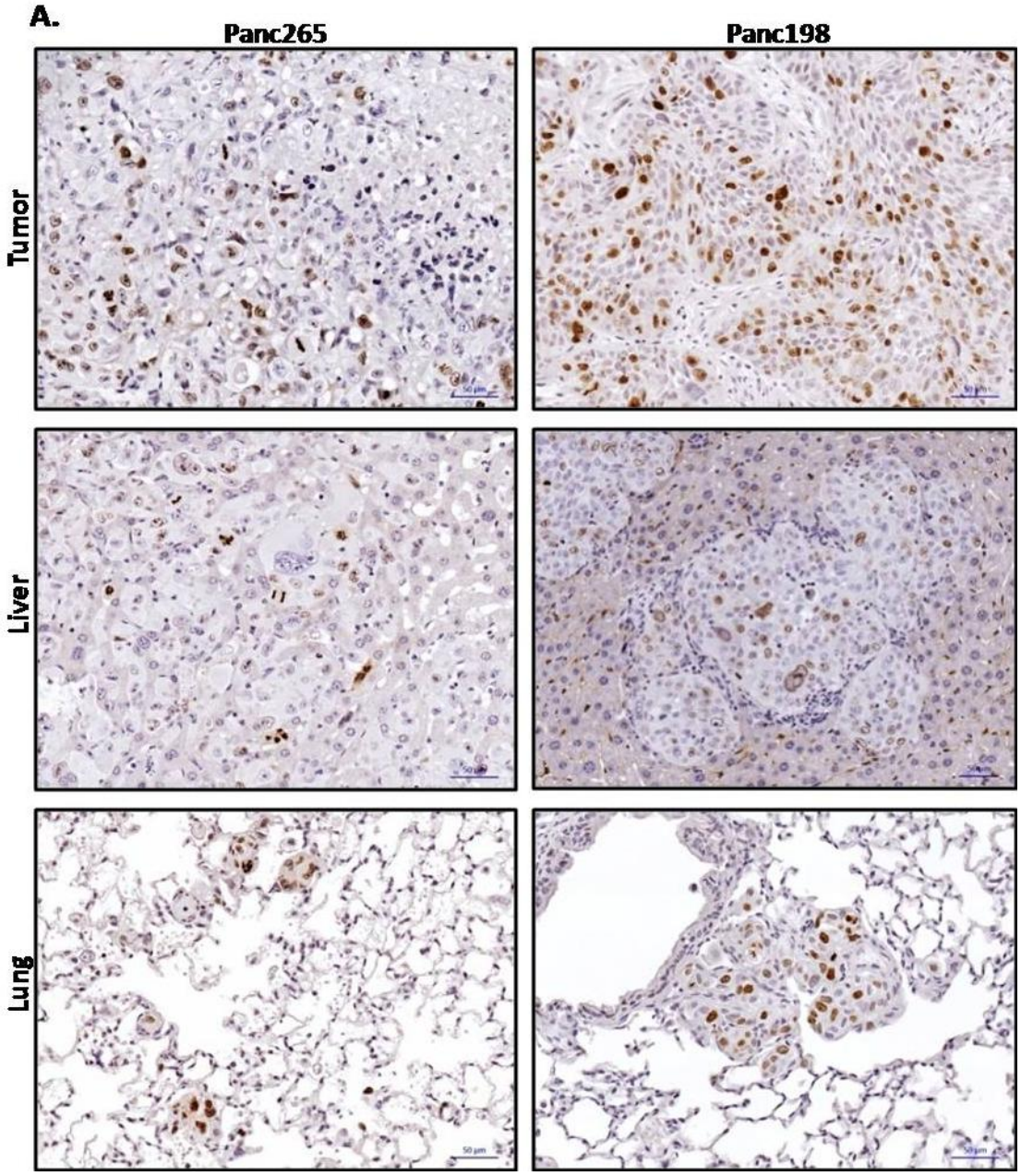
A.
Panc265
Panc198
Tumor
Liver
Lung

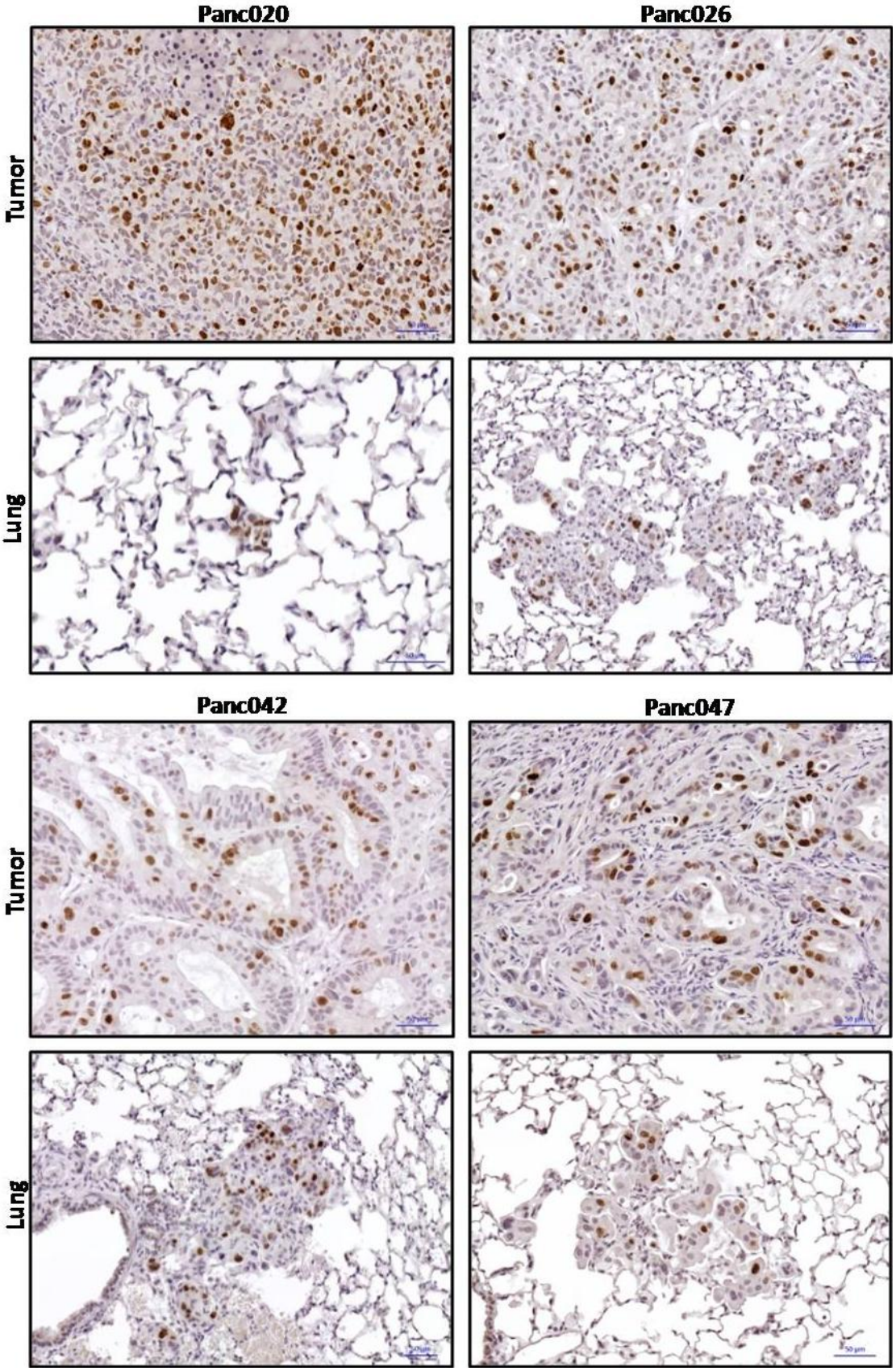
Panc020
Panc026
Tumor
Lung
Panc042
Panc047
Tumor
Lung

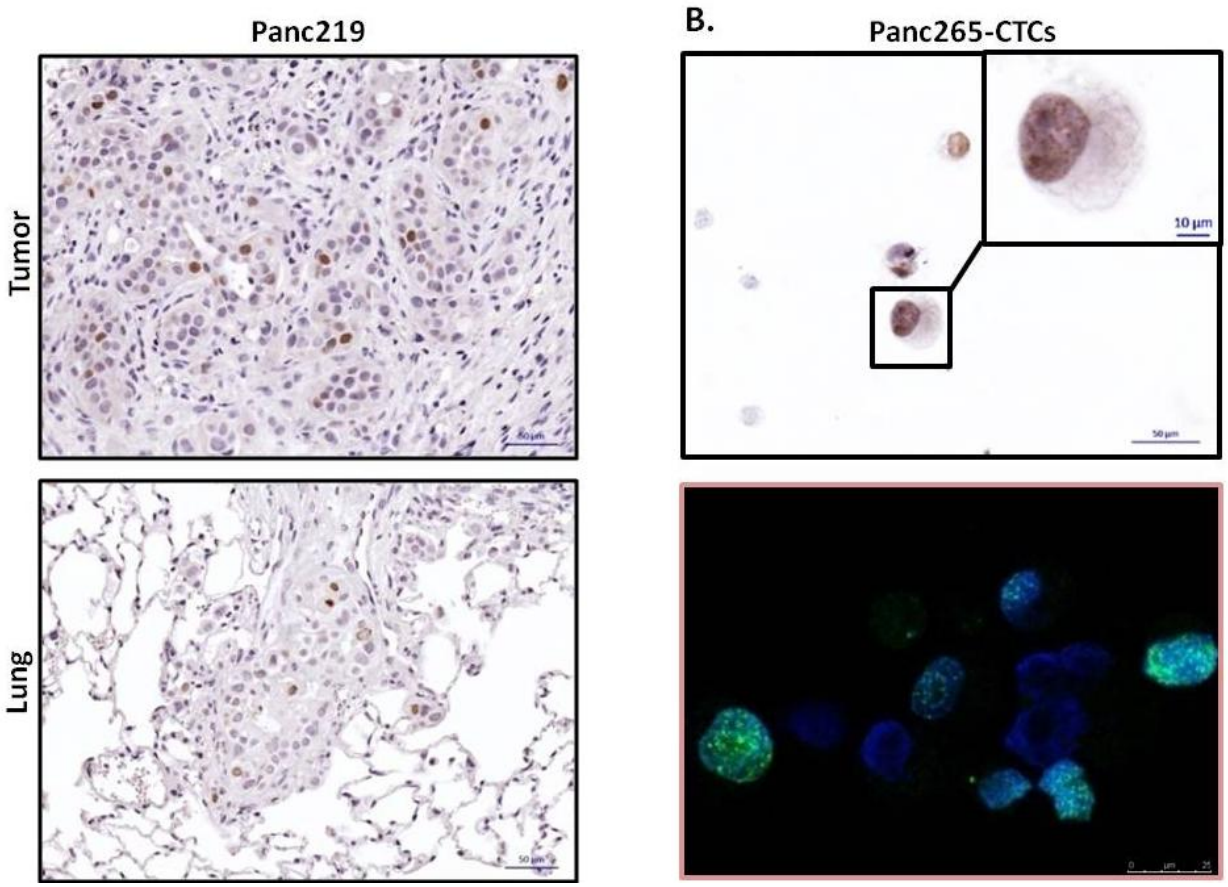

Figure 20. Evaluation of Survivin protein expression in metastatic PDX models of pancreatic cancer. (20A) – Representative images of immunohistochemistry (IHC) staining for Survivin in tumor, liver and lung tissues of metastatic PDX models (scale bar 50µm). **(20B)** – Top panel - Representative images of IHC staining for Survivin in human pancreatic CTCs isolated from highly metastatic PDX model (scale bar 50µm and 10µm). Bottom panel - Representative Immunoflourescence image of human Survivin (green) and Dapi (blue) in human pancreatic CTCs (scale bar 25µm).

4.3.2. Early *In-vivo* efficacy study with YM155 and Abraxane in a highly metastatic Panc265 model.

Panc265 metastatic model exhibits the most aggressive phenotype with the shortest survival rate and early dissemination. This led us to test whether earlier initiation of YM155 theatment could result in improvement of median survival compared to previous study. Mice harboring a highly metastatic Panc265 orthotopic model were divided into four experimental groups: (1) Control; (2)

YM155; (3) ABX; (4) YM155+ABX. Two days after tumor implantation the groups were subjected to 4-week treatment course. After cessation of the treatment, the median survival of the groups was evaluated and the results showed that YM155 monotherapy significantly prolonged the median survival to 56 days in comparison to control group. (Figure 21A, Table13). ABX monotherapy show no statistically significant improvement in median survival compared with YM155 treatment (Figure21A, Table13). Remarkable, the median survival of the animals in YM155 + ABX combination was statistically superior to that of ABX and YM155 alone (Figure21A, Table13), suggesting possible synergistic interaction between ABX and YM155.
In addition, one mouse treated with ABX and two mouse treated with YM155+ABX combo achieved a complete response (eradication of primary tumor) with no detectable metastasis. At the survival endpoint, the tumor-bearing mice of all treated groups displayed the usual signs of sickness (described in methods) caused by the progression of metastatic disease.

The metastatic tumor burden of YM155 treated mice sacrificed at the same time point as the control animals, was also examined. Strikingly, earlier initiation of the YM155 treatment totally blocked the tumor dissemination with no detectable macro and micrometastasis in liver and lung organs compared with control group (Figure21B, Table 14). Moreover, the weight of the tumor grafts of YM155 treated group was significantly smaller than that of the control group (Figure 21C).

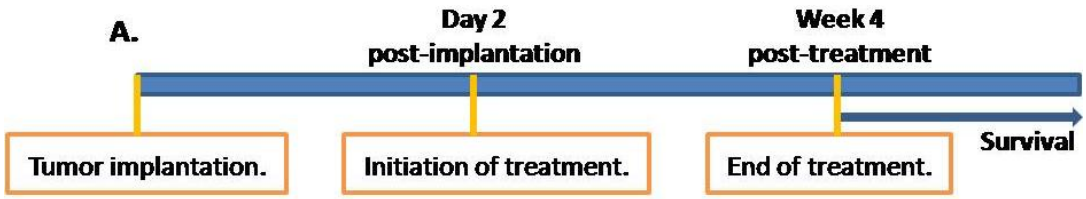

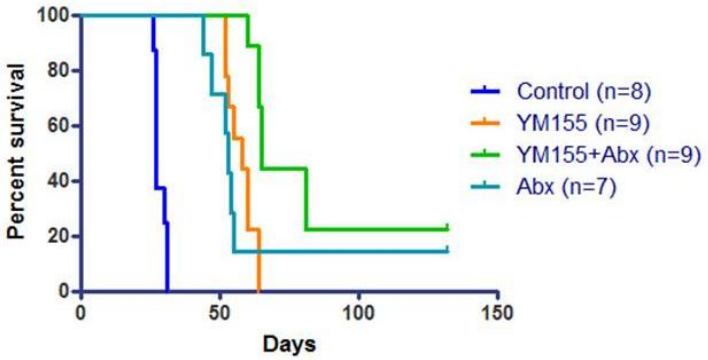

Table 13. P value Mantel-Cox test

Groups	Median survival (days)	Control	Ym155	ABX
Control	27			
Ym155	58	<0.0001		
ABX	53	0.0001	0.42 ns	
Ym155+Abx	65	<0.0001	0.0005	0.02

B.

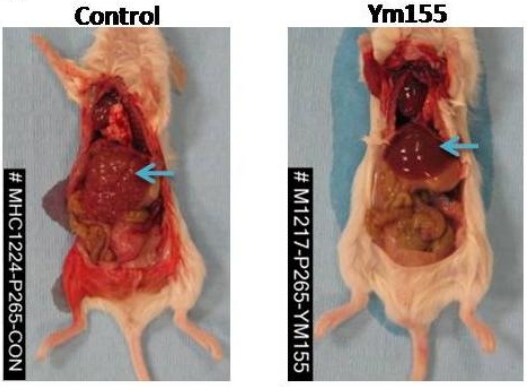

Table 14.

Number (percentage) of mice affected with metastasis		
Group	Liver	Lung
Control	5/5(100)	5/5 (100)
YM155	0/5(0)	0/5 (0)

C.

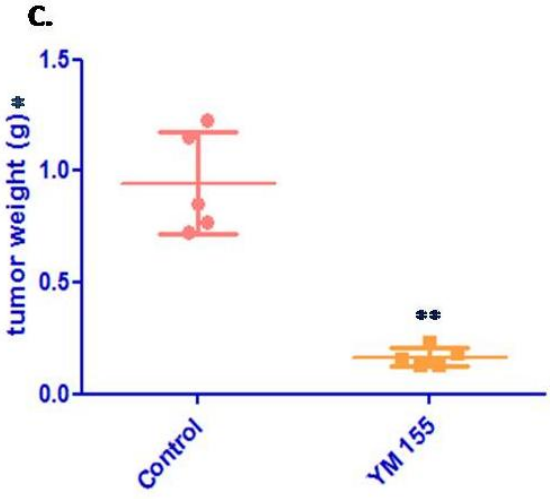

Figure 21. Early *In-vivo* efficacy study of YM155 and ABX in a highly metastatic Panc265 model.

(21A) - Treatment course in PDX mice harbouring a highly metastatic Panc265 model (top). Kaplan–Meir survival curves of control and drug treated groups. **(Table13)** - The table shows the median survival days and statistical significance of the experimental groups. Survival data were analyzed using GraphPad Prism 6 software. P-values for survival differences were calculated using the log-rank (Mantel-Cox) test. **(21B)** -Representative photographs of Control and YM155 treated mice and their corresponding liver and lung organs after 4-week treatment course. The blue arrows indicate the livers of control and treated groups. The liver of control group displays hepatomegaly with macroscopic tumor lesions, whereas the liver of YM155 groups has normal size. **(Table 14)** - Summary table of metastatic incidence in control and YM155 treated groups **(21C)** - Weights of the tumors including the mouse pancreas resected from control and YM155 treated group. Bar represents that the weight of the tumors including the mouse pancreas of YM155 group is smaller than of control group. * Tumor including the mouse pancreas. **P < 0.001 versus control group.

4.3.3. Primary tumor resection of a highly metastatic Panc265 model in combination with YM155 and Abraxane therapy.

To mimic the clinical therapeutic setting for pancreatic cancer, we performed resection of primary tumor combined with YM155 and Abraxane combo treatment in a highly metastatic Panc265 model. In this study we established the following three experimental groups (1) Control; (2) YM155; (3) YM155+ABX. One week after implantation the YM155 treatment course was initiated and 11 days post-implantation all mice underwent partial pancreatectomy that was performed by an electrocautery system. The treatment course was reinitiated 3 days after the surgery including the Abraxane regimen (Figure 22A,B)

Interestingly, the median survival of the control mice subjected to partial pancreatectomy was 35 days. During the necropsy, it was observed macroscopic local tumor invasion to the adjacent organs such as peritoneum and remaining lobes of the pancreas, as well as distal overt metastasis to the liver and lung organs, thus representing equal metastatic pattern to that of Panc265 orthotopic model (Figure22C). Remarkable, after cessation of the treatment course YM155 and

YM155+ABX treatment resulted in extending the median survival to 60 and 67 days respectively and it was statistically significant in comparison to control group (Figure 22D, Table 15). However, the combo regimen was unable to statistically improve the median survival compared to monotherapy treatment (Figure 22D, Table 15). At the survival endpoint, the tumor-bearing mice of all groups displayed the usual signs of sickness (described in methods) caused by the progression of metastatic disease.

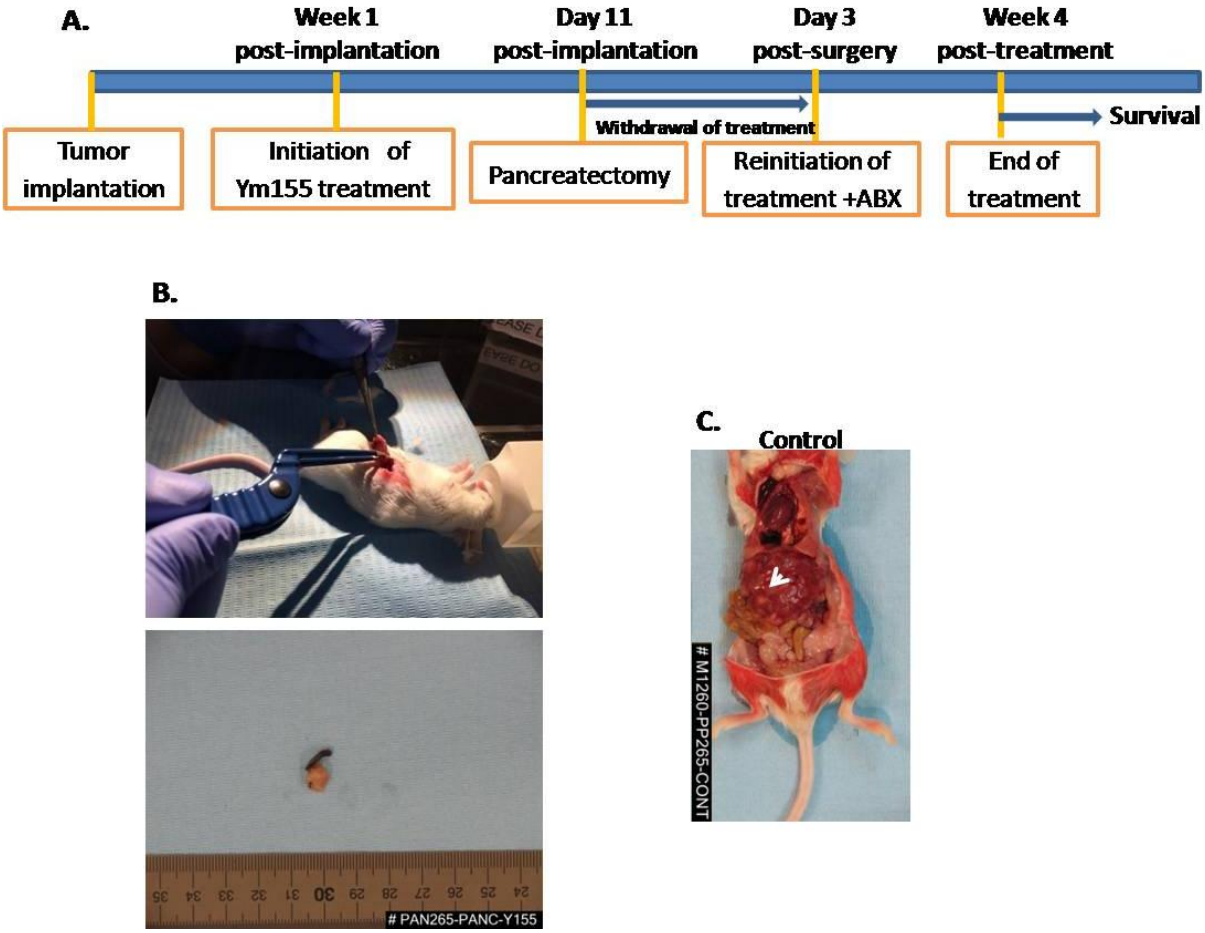

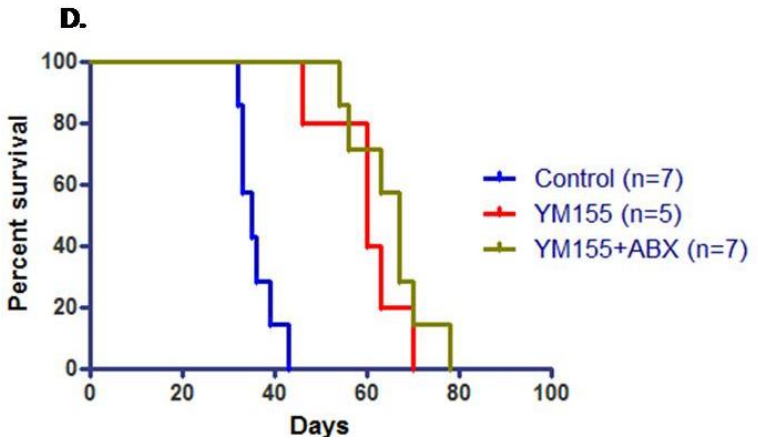

Table 15. P value Mantel-Cox test

Groups	Median survival (days)	Control	Ym155
Control	35		
Ym155	60	0,0010	
Ym155+Abx	67	0,0001	0,3545

Figure 22. In-vivo efficacy study of YM155 and ABX in a highly metastatic Panc265 model subjected to partial pancreatectomy.

(22A) – Treatment course in PDX mice implanted with a highly metastatic Panc265 model and subjected to partial pancreatectomy for removal of primary tumor graft. **(22B) -** Representative photographs of the pancreatectomy procedure using a bipolar electrocautery. The top picture shows mice under anestesia and the heated electrode is applied to the exposed pancreas implanted with Panc265 xenograft model. The bottom picture shows a representative photographs of the resected pancreas and spleen. **(22C) –** Representative photographs of control group mice sacrificed upon reaching a human endpoint criteria. The white arrow shows the macroscopic metastatic nodules in the liver. **(22D) –** Kaplan–Meir survival curves of control and drug treated groups. **(Table 15) -** The table shows the median survival days and statistical significance of the experimental groups. Survival data were analyzed using GraphPad Prism 6 software. P-values for survival differences were calculated using the log-rank (Mantel-Cox) test.

4.2.4. In-vivo efficacy study with YM155 and Abraxane in Panc198 metastatic model.

Next, we tested whether YM155 treatment could have similar anti-metastatic activity in other metastatic PDX models. For this reason, we established four experimental groups using Panc198 metastatic models: (1) Control; (2) YM155; (3) ABX; (4) YM155+ABX. Two weeks after tumor implantation the experimental groups were subjected to 4-week treatment course. The results showed that YM155 monotherapy significantly prolonged the median survival to 62 days in comparison to control group (54.5 days) (Figure 23A, Table16). ABX monotherapy showed a significant advantage compared to YM155 alone by prolonging the survival to 68 days (Figure 23A, Table16). Interestingly, the combination of YM155+ABX showed a median survival of 77 days and it was superior to YM155 and ABX single agents (Figure 23A, Table16). At the survival endpoint, the tumor-bearing mice of all groups displayed the usual signs of sickness (described in methods) caused by the progression of primary tumor and/or metastatic disease.

To evaluate wheter YM155 treatment exerted any effect on metastatic tumor burden, we sacrificed small set of animals from YM155 treated group at the same time point as the control group. Interestengly, microscopic examination of the distant organs confirmed the presence of several big metastatic nodules in livers and lungs of the control mice (Figure 23B). In contrast, the YM155 treated mice had much fewer and smaller metastatic lesions in liver and lung parenchyma. Altogether this data suggests that the survival benefit of YM155 treatment could be due to the reduction of metastatic tumor burden. However, further studies are needed to precicely explain the beneficial effects of this drug in metastatic PDX models of pancreatic cancer.

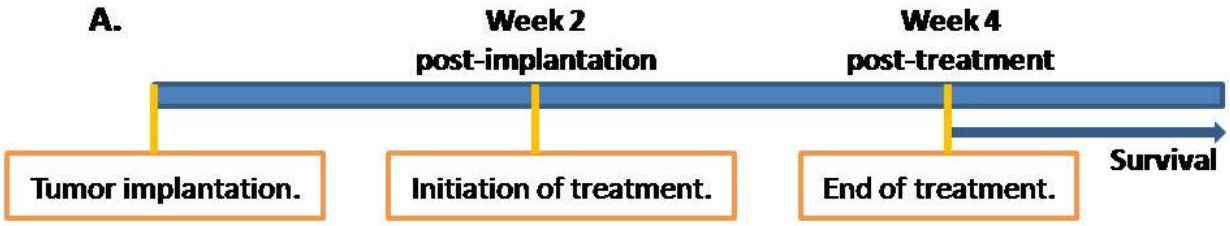

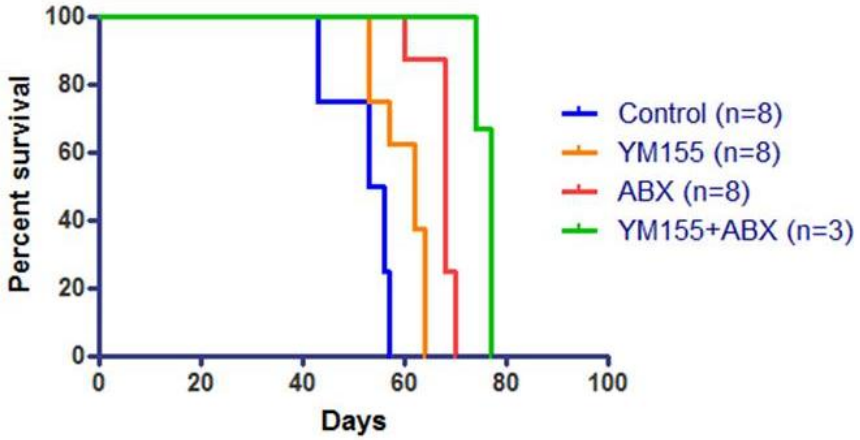

Table 16. **P value Mantel-Cox test**

Groups	Median survival (days)	Control	Ym155	ABX
Control	54.5			
Ym155	62	0.009		
ABX	68	<0.0001	0.001	
Ym155+Abx	77	0.007	0.008	0.005

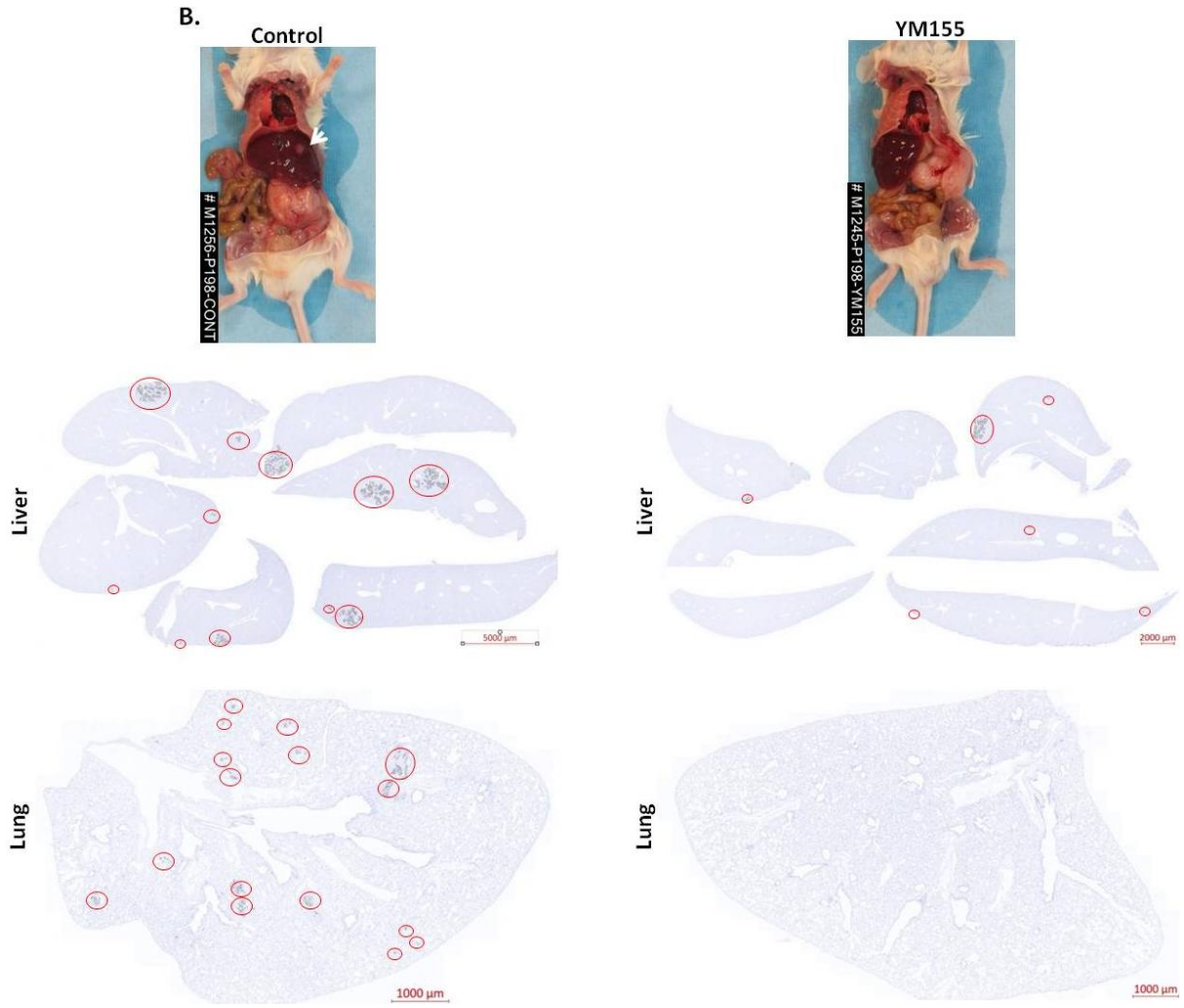

Figure 23. In-vivo efficacy study of YM155 and Abraxane in Panc198 metastatic model.

(23A) – Treatment course in PDX mice harbouring a metastatic Panc198 model (top). Kaplan–Meir survival curves of control and drug treated groups. **(Table 16) -** The table shows the median survival days and statistical significance of the experimental groups. Survival data were analyzed using GraphPad Prism 6 software. P-values for survival differences were calculated using the log-rank (Mantel-Cox) test. **(23B)** - Representative photographs of control and YM155 treated mice implanted with Panc198 model (top). The white arrow shows the macroscopic metastatic nodules in the control liver. Representative photomicrographs of liver and lung tissues resected from control and YM155 treated mice (bottom). The metastatic lesions composed of human tumor cells are detected by Alu staining and indicated by red circles. (scale bar 1000-5000µm).

4.4. The role of tumor-derived exosomes in organotropic metastasis.

4.4.1. Isolation and proteomics analysis of tumor-derived exosomes from Metastatic PDX models.

The metastatic models established in this thesis are characterized by specific dissemination pattern. Two of these models have a propensity to metastasize to the liver and lung organs, whereas the other five models disseminate only to the lungs. We wondered whether this metastasis organotropism could be determined by molecules present on tumor-derived exosomes. To test this hypothesis, we profiled the exosomal proteome of five metastatic models (Panc265, Panc198, Panc020, Panc042, Panc047). After reaching the humane end point criteria, the orthotopic tumor-bearing animals from each model were sacrificed and in collaboration with Hector Peinado´s group we purified the exosomes of primary tumor and metastatic organs (liver and/or lung) (Figure24A,B).

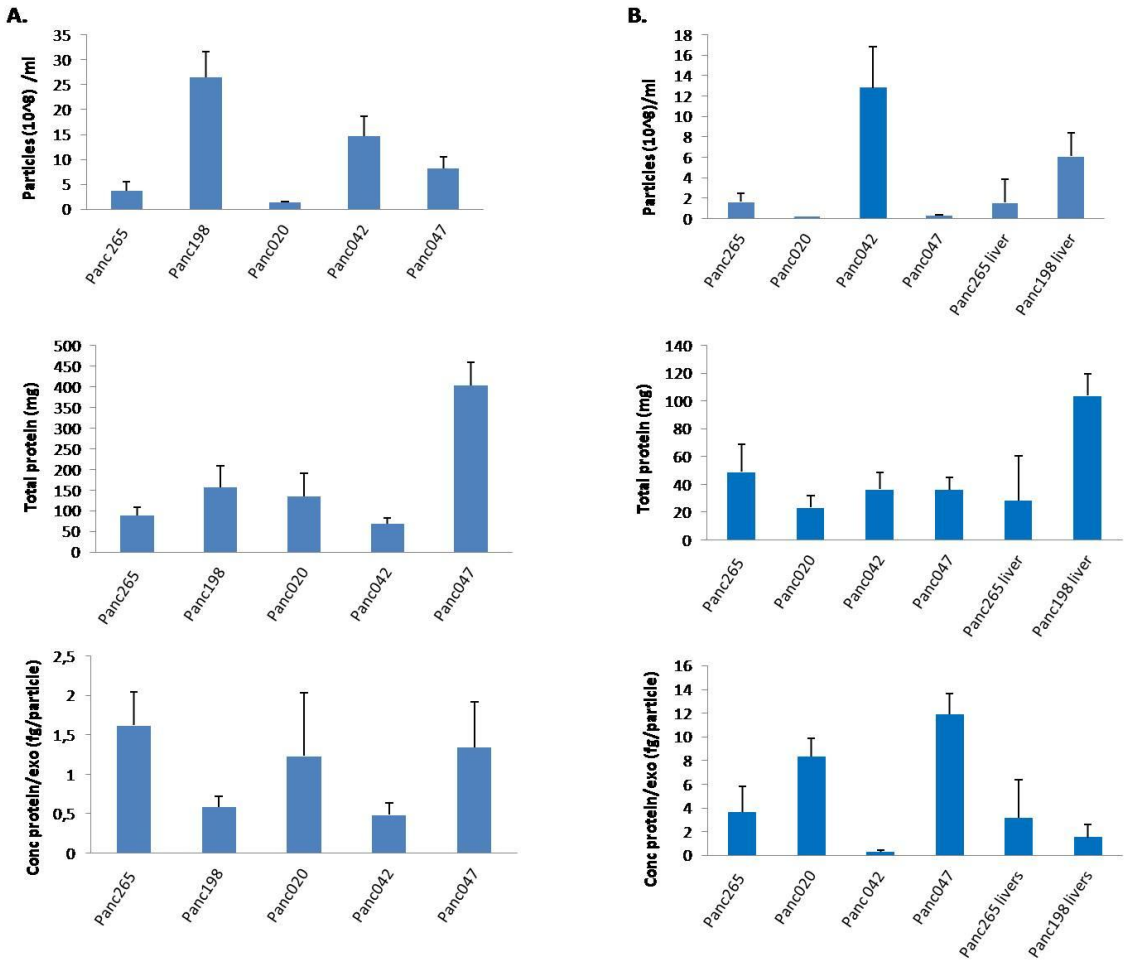

Figure 24. Exosomes release from metastatic PDX models. (A) Left vertical panels represents the number of exosomes particles purified from the primary tumors of metastatic PDX models, total protein extracted from the isolated exosomes and the exosome concentration presented as μg exosomal protein per exosome particle (up to down, respectively). Right vertical panels represents the number of exosomes particles purified from liver and lung organs, total protein extracted from the isolated exosomes and the exosome concentration presented as μg exosomal protein per exosome particle (up to down, respectively).

Next, the protein extract of the exosomes was subjected to further proteomics analysis. The label free mass spectrometry of primary tumor, liver and lung exosomes identified 5456 proteins of which 1901 were human specific and 3555 were murine (Figure 25). Then, we compared the exosome proteome of metastatic models that colonize to the liver and lung (hereafter, they are abbreviated as “Aggressive”) versus the metastatic models that metastasize primarily to the lung (hereafter, they are abbreviated as “Less-Aggressive”). The main goal of this comparison was to establish proteome signatures that can cluster the models based on their aggressiveness and/or their metastatic pattern. This comparison identified 181 differentially abundant human proteins between aggressive and less-aggressive primary tumor exosomes, and 11 human proteins between aggressive and less-aggressive lung exosomes. However, the unsupervised hierarchical clustering of these differentially abundant human proteins derived from the primary tumors and metastatic sites failed to separate the aggressive from less-aggressive models (Figure 26-27).

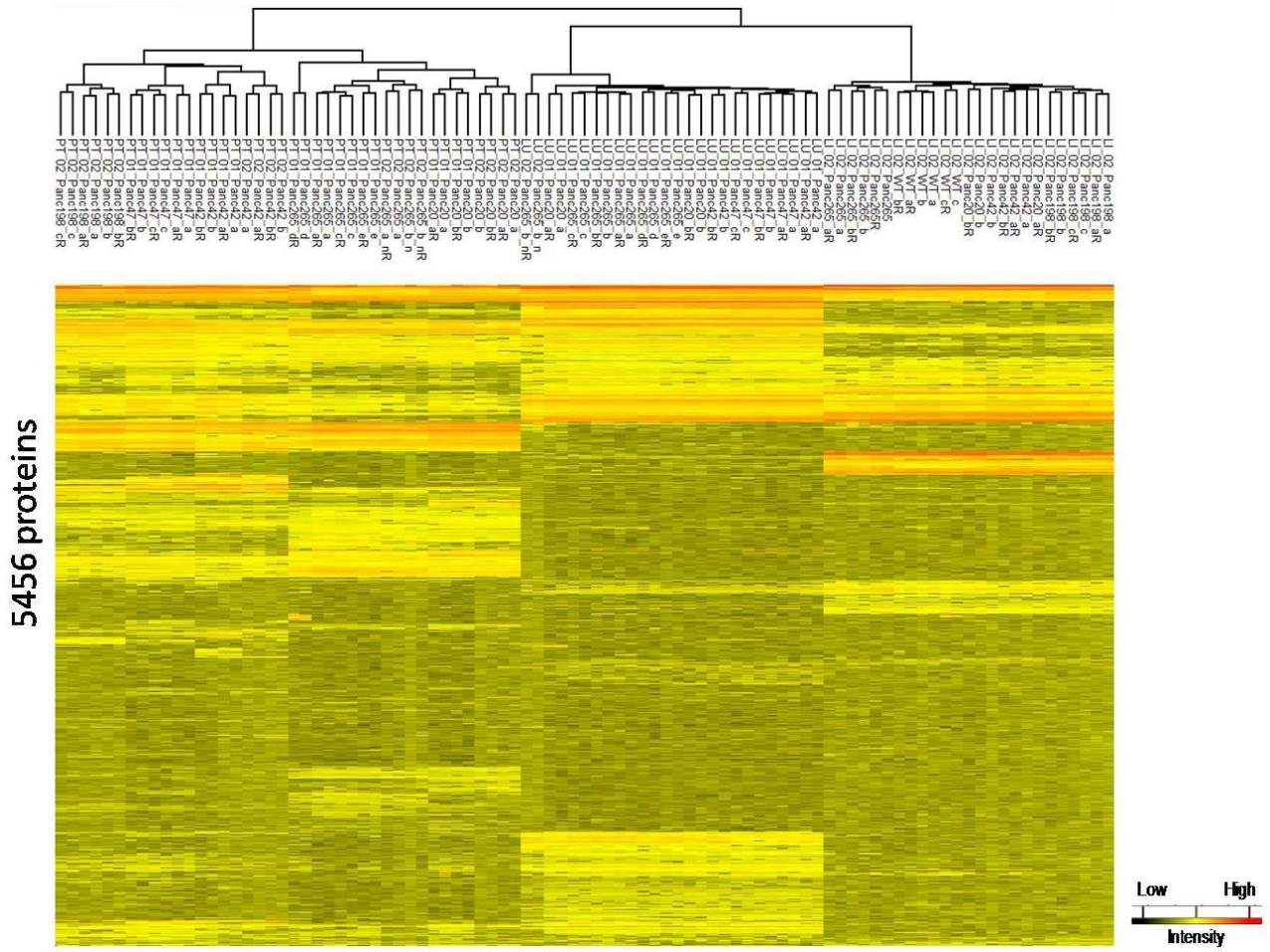

Figure 25. Unsupervised hierarchical clustering of exosomal secretome profiles. Hierarchical clustering of exosomal secretome profiles (n = 5456 human/mouse proteins with ≥1 peptides) of primary tumor grafts and metastatic organs collected from metastatic PDX models. Three biological replicates with two technical replicates of each metastatic model are included and each of the secretomes are shown. The entire protein list was used. Columns represent samples; rows are proteins. Relative protein abundance is colored-coded with red corresponding to a relatively high abundance, black corresponding to a relatively low abundance.

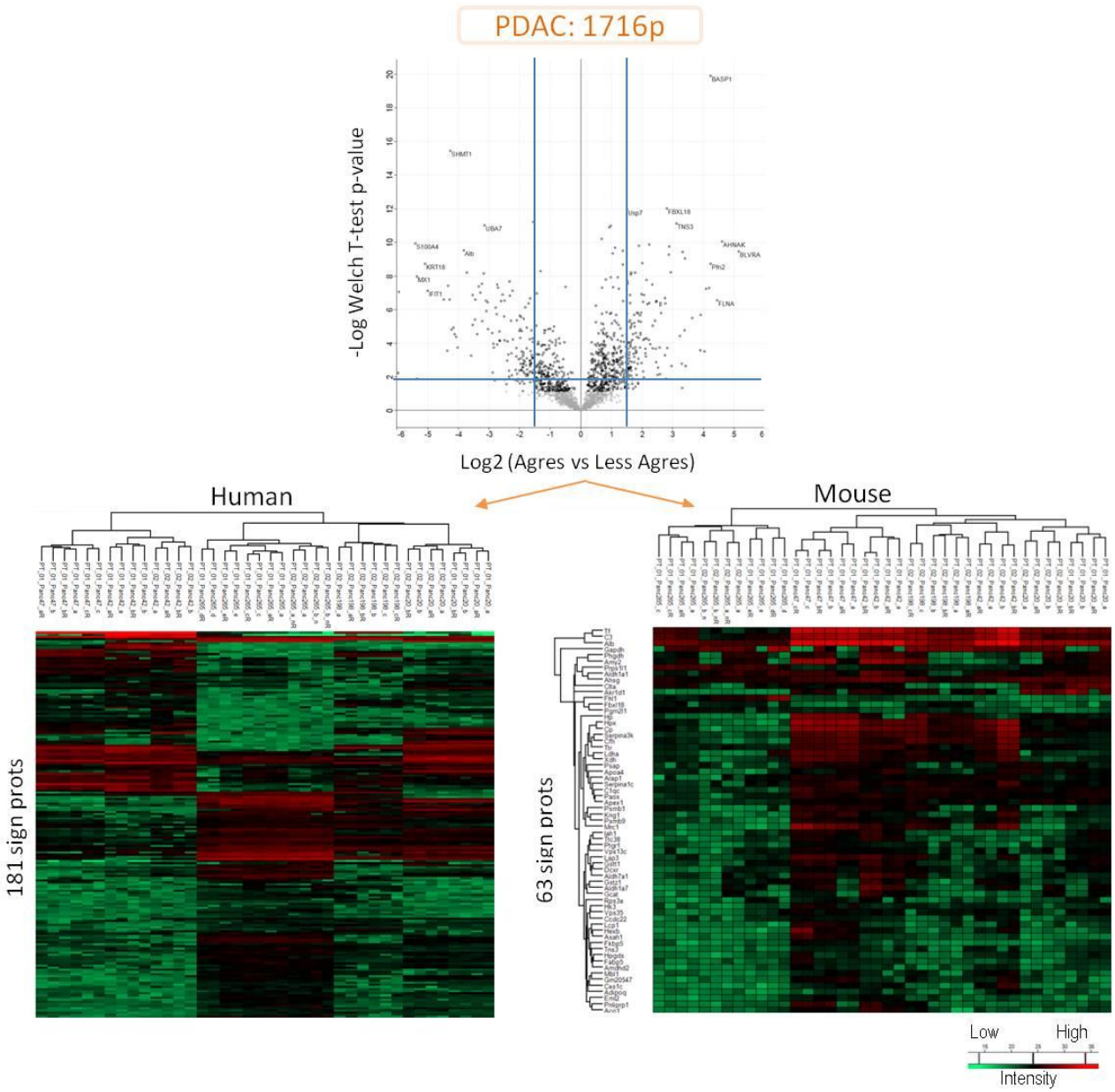

Figure 26. Significantly abundant exosomal proteins in primary tumor grafts of metastatic PDX models. Volcano plot show the log2 fold change above 1.5 (p value 0.05, FDR 0.01) in exosomal proteins of primary tumor grafts (aggressive vs less-aggressive models) Welch t-test analysis was performed on proteins (1716 proteins) present in 70% of the samples of at least one of the 2 groups. Bottom-left - Hierarchical clustering of 181 differentially abundant human exosomal proteins showed a separation of the aggressive models from most of less-aggressive models (except Panc20). Bottom-right - Hierarchical clustering of 63 differentially abundant mouse exosomal proteins.

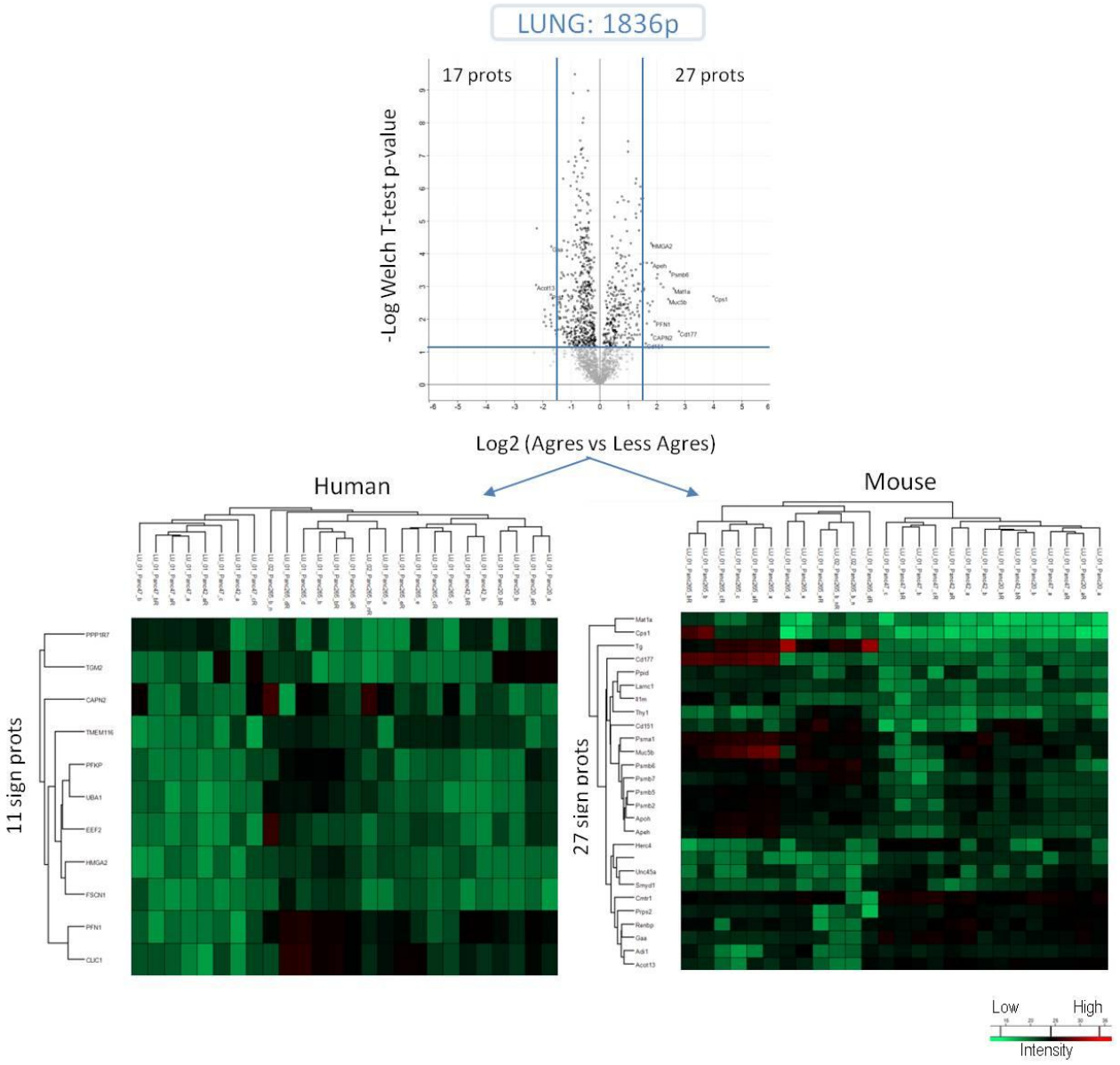

Figure 27. Significantly abundant proteins in lungs of metastatic PDX models. Volcano plots show the log 2 fold change above 1.5 (p value 0.05, FDR 0.01) in exosomal proteins of lung tissues (aggressive vs less-aggressive models) Welch t-test analysis was performed on proteins (1836 proteins) present in 70% of the samples of at least one of the 2 groups. Bottom-left - Hierarchical clustering of 11 differentially abundant human proteins showed a separation of the aggressive models from most of less-aggressive models (except Panc20). Bottom-right - Hierarchical clustering of 27 differentially abundant mouse proteins.

4.4.2. Identification of organ-specific exosomal protein signatures.

To establish the "organ-specific" exosomal protein signatures, we compared the exosomal protein profiles of all organs to each other. 634 significantly abundant human proteins were identified between primary tumor- and liver-derived exosomes, 648 human proteins between primary tumor- and lung-derived exosomes and 21 proteins between liver- and lung-derived exosomes. Remarkable, the unsupervised hierarchical clustering nicely separated the three biological groups (primary tumor, liver and lung of each PDX model) from each other, based on their distinct exosomal protein signatures (Figure 28-30).

Next, we interrogated these differentially abundant protein signatures with aim to identify potential candidate proteins associated with the metastatic disease and organotropic metastasis. Interestingly, we identified that the human protein $ITGa_6$ was abundantly expressed in primary tumor exosomes and it was identified by at least 1 peptide in at least 70% of the lung-derived exosomes (Figure 31, Table S4). S100A11 is another protein that was identified to be abundantly expressed in primary tumor- and lung-tropic exosomes compared to liver-derived proteome profile (Figure 31, Table S4). These two protein candidates have been found to be abundantly expressed in the exosomes of multiple cancer types including pancreatic cancer, which suggest that they may have a role in metastatic disease. However, additional studies are needed to elucidate their contribution to organotropic metastasis in pancreatic cancer.

Moreover, Vimentin is another protein that was present in at least 70% of the lung-derived exosomes and it was abundantly expressed in primary tumor exosomes (Figure 31, Table S4). However, despite the overwhelming amount of literature describing the role of Vimentin in essential steps of metastatic cascade such as EMT process during tumor invasion (see chapter 1.2.3), the precise role of this intermediate filament protein in organotropic metastasis have not been officially documented.

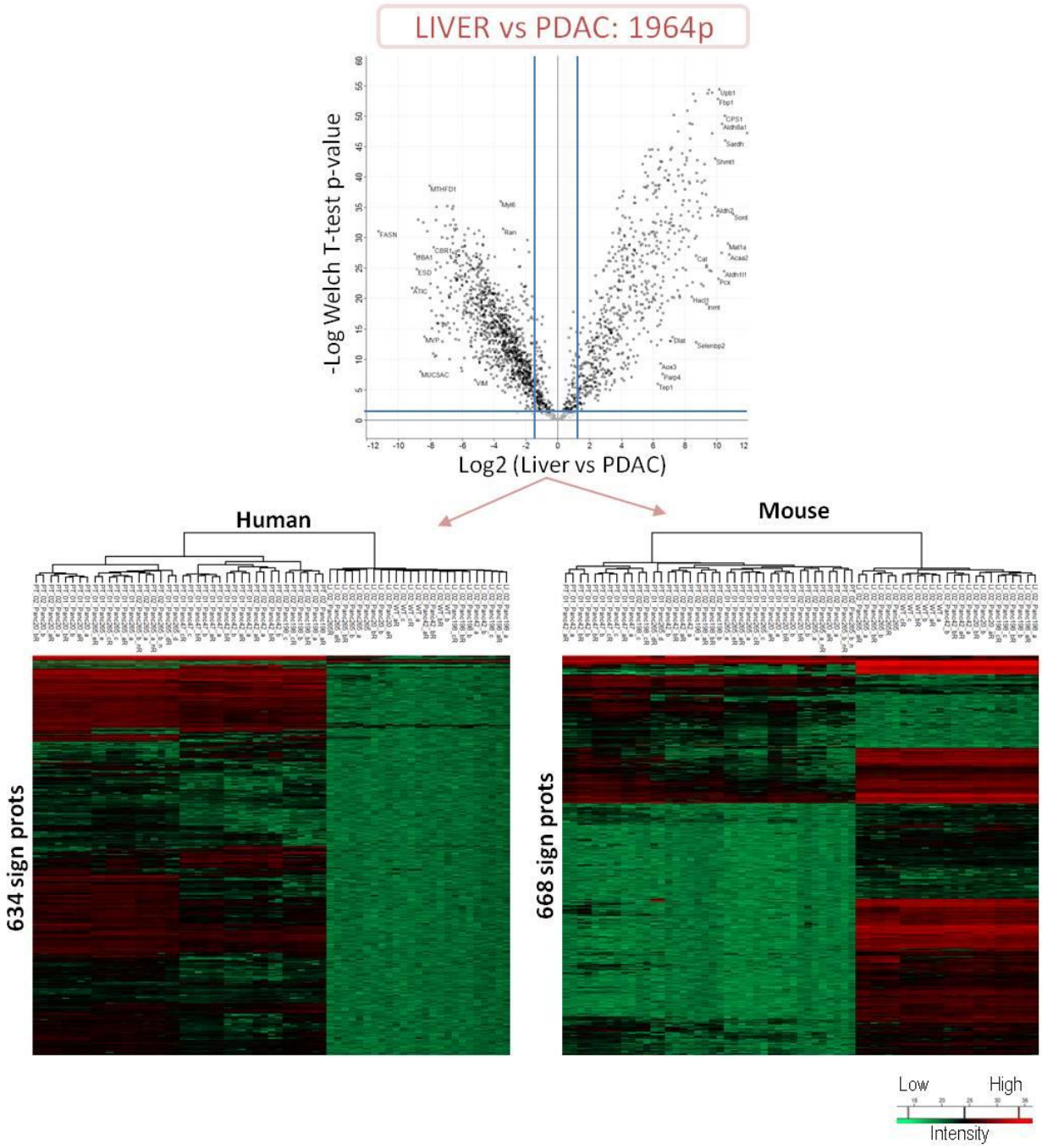

Figure 28. Significantly abundant proteins in Livers vs PDAC of metastatic PDX models. Volcano plots show the log 2 fold change above 1.5 (p value 0.05, FDR 0.01) in exosomal proteins in PDAC vs Livers. Welch t-test analysis was performed on proteins (1964 proteins) present in 70% of the samples of at least one of the 2 groups. Bottom-left - Hierarchical clustering of 634 differentially abundant human proteins showed a separation of the primary tumour profiles

from liver profiles. Bottom-right - Hierarchical clustering of 668 differentially abundant mouse proteins.

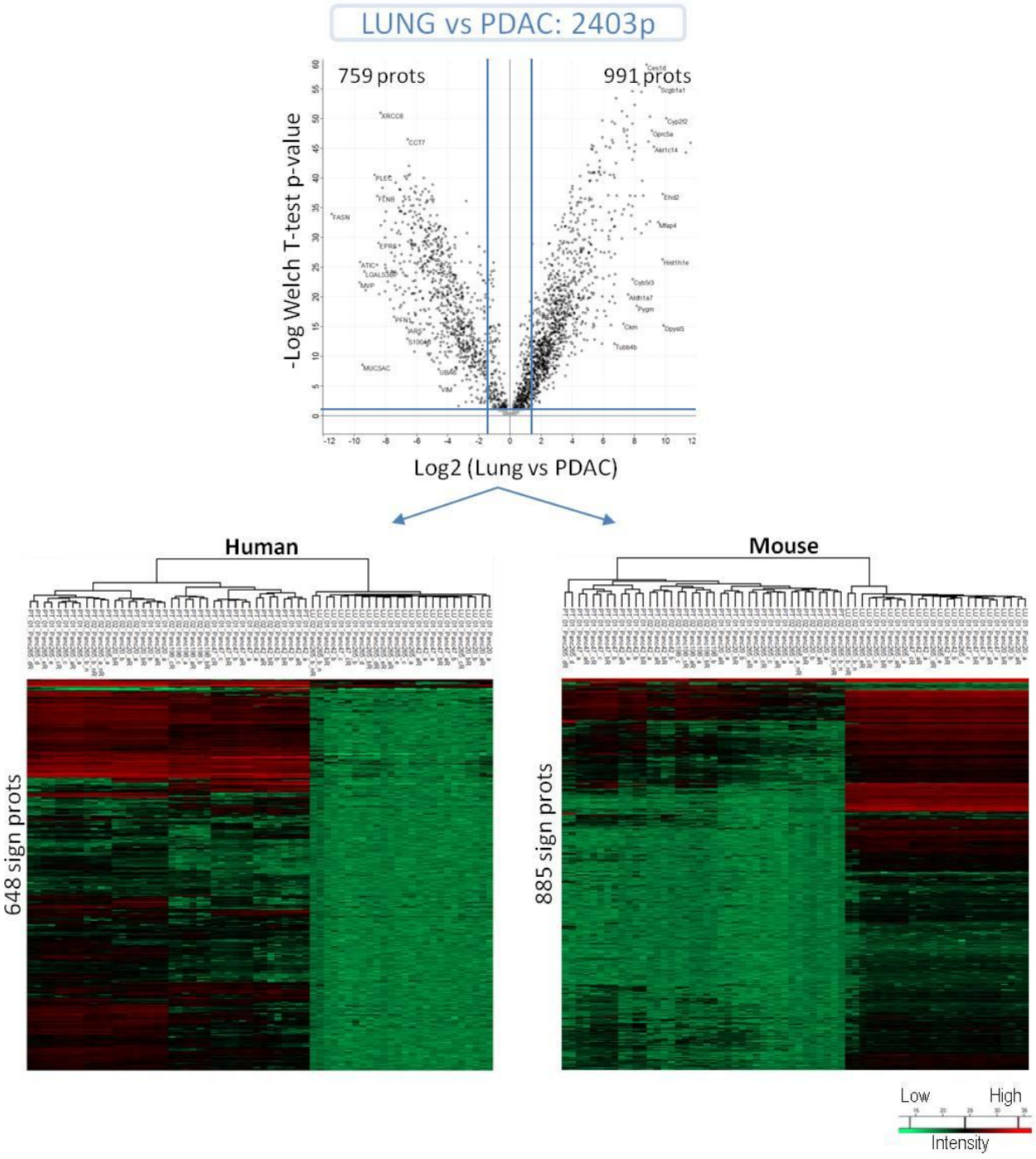

Figure 29. Significantly abundant proteins in Lung vs PDAC of metastatic PDX models. Volcano plots show the log 2 fold change above 1.5 (p value 0.05, FDR 0.01) in exosomal

proteins in PDAC vs Livers. Welch t-test analysis was performed on proteins (2403 proteins) present in 70% of the samples of at least one of the 2 groups. Bottom-left - Hierarchical clustering of 648 differentially abundant human proteins showed a separation of the primary tumour profiles from lung profiles. Bottom-right - Hierarchical clustering of 885 differentially abundant mouse proteins**.**

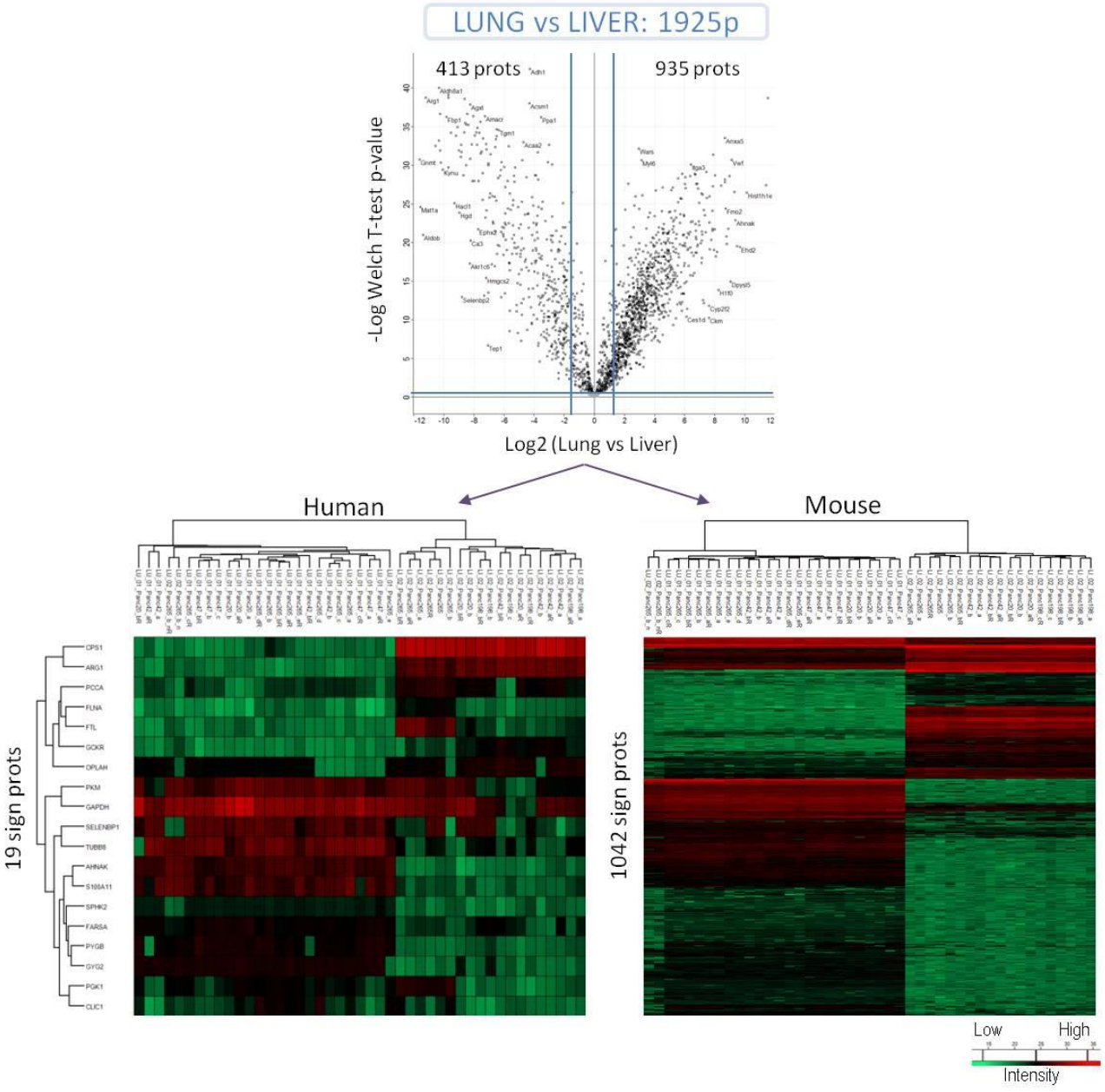

Figure 30. Significantly abundant proteins in Lung vs Liver of metastatic PDX models. Volcano plots show the log 2 fold change above 1.5 (p value 0.05, FDR 0.01) in exosomal proteins in Lungs vs Livers. Welch t-test analysis was performed on proteins (1925 proteins)

present in 70% of the samples of at least one of the 2 groups. Bottom-left - Hierarchical clustering of 19 differentially abundant human proteins showed a separation of the primary tumour proteome profiles from liver proteome profiles. Bottom-right - Hierarchical clustering of 1042 differentially abundant mouse proteins**.**

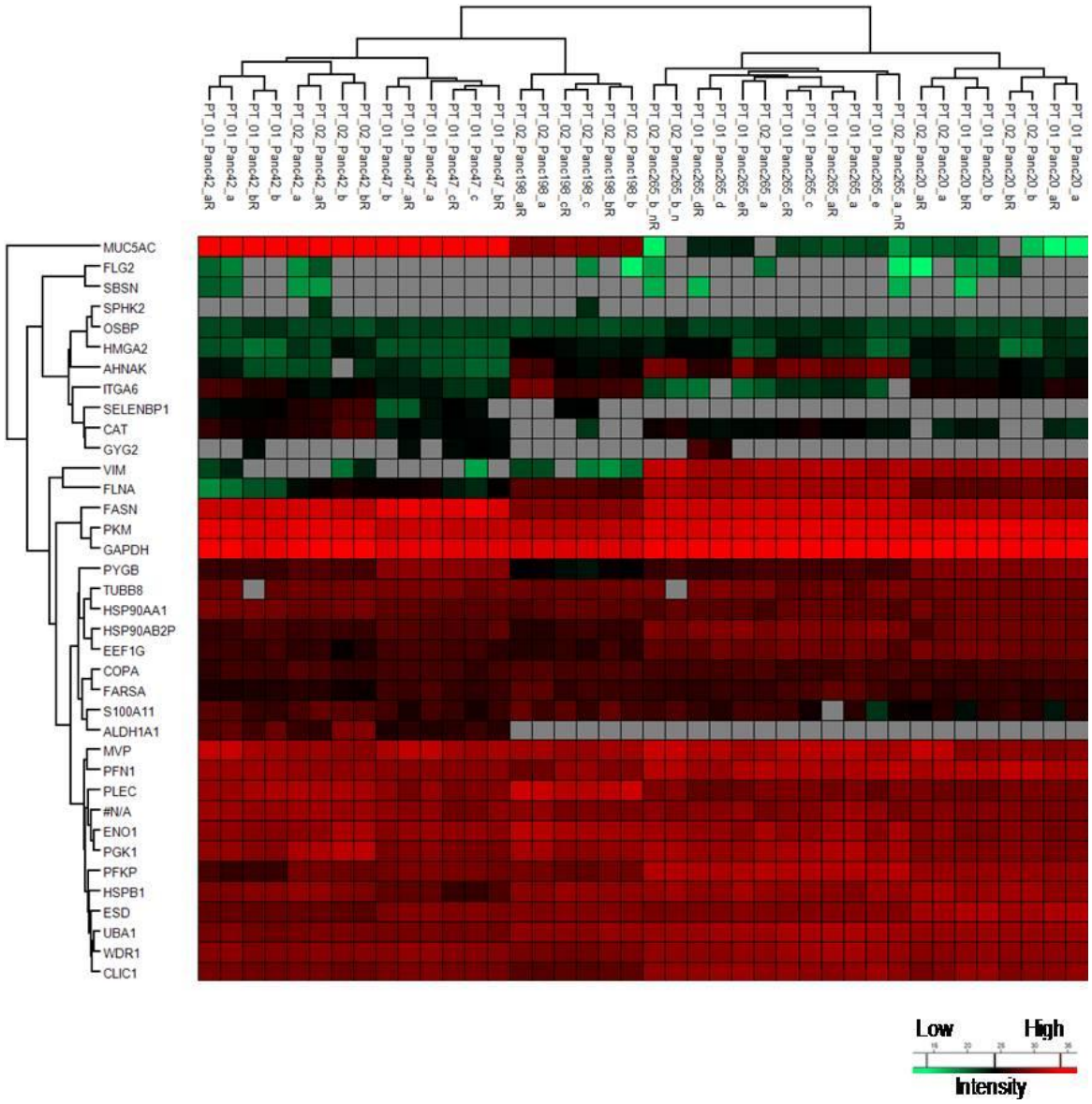

Figure 31. Human proteins present in at least 70% of lung-tropic exosome samples.

Hierarchical clustering of the human proteins present in at least 70% of the lung-tropic exosome samples (n = 37 human proteins with ≥1 unique peptide). Columns represent samples; rows are proteins. Relative protein abundance is colored-coded with red corresponding to a relatively high abundance, black corresponding to a relatively low abundance.

V. DISCUSSION.

5.1. Metastatic PDX models of pancreatic cancer.

5.1.1. PDX orthotopic models of pancreatic cancer: An efficient and reproducible *In-vivo* system for modeling the metastatic disease.

Unfortunately, the vast majority of the pancreatic cancer patients are diagnosed in late stage with presence of distal metastasis. This short window between diagnosis and disease progression for advanced pancreatic cancer extremely limits the study of metastatic disease in clinical settings. Over the past decades, animal models have been commonly used as an *In-vivo* tool for modelling the metastatic process of multiple cancer types. For successful modelling pancreatic cancer metastasis, several *In-vivo* models have been used including injection of murine or human cancer cell lines directly in mouse circulation, development of GEMM of pancreatic cancer and establishment of PDX models by orthotopic transplantation of intact human pancreatic specimens in nude immunodeficient mice. However, the main drawbacks of these models are: 1) direct injection of cancer cells in mouse circulation bypasses some initial steps of metastasis such as invasion and intravasation, and therefore cannot perpetuate the entire process; 2) The GEMM of pancreatic cancer generally exhibit long tumor and metastatic latency, as well as the metastatic incidence in these models remains relatively low; 3) The orthotopic transplantation of patient pancreatic tumors in nude mice results in low metastatic rate [90-91]. Altogether, this leads to an urgent demand for development of more efficient metastatic pancreatic models.

For this reason, one of the first goals of this thesis was to improve the current available experimental metastasis models by development of an efficient, fast and reproducible In-vivo platform, which accurately recapitulates the entire multi-step metastatic process of pancreatic cancer. Indeed, the seven metastatic PDX models generated in this study were able to established distal metastasis with a high reproducibility rate. Moreover, each model is characterized with different survival rate and model-specific dissemination pattern. Contrary to the metastatic PDX models of pancreatic cancer described in the literature, the models in this thesis were generated in a highly immunodeficient mouse background (NSG mice), which allowed this high metastatic

incidence. This observation is in agreement with other study showing that reduction of host immunity correlates with higher metastatic rate [143].

However, as discussed above, the critical aspect for development of these metastatic PDX models is the need to use immunodeficient mouse recipients for successful tumor engraftment and subsequent colonization to distant organs. It has been widely reported the tumour-promoting and tumour-suppressing roles of the immune system in cancer progression and metastasis. Therefore, next generation "personalized immune" mouse models will be needed to observe the impact of the autologous immune elements on cancer spreading. Of major interest, currently, is the development of preclinical models with reconstituted immune system from the donor patient. These so-called "humanized" mouse models with immune system reconstituted upon transplantation of hematopoietic stem cells aspirated from bone marrow of an individual cancer patient, may provide a new *In-vivo* system to study the molecular mechanisms mediating the anti-metastatic immune responses, as well as to test new immunomodulatory agents with aim to enhance the anti-tumour immune response.

5.1.2. Metastatic PDX models: a source for efficient enrichment of all human tumor populations involved in metastatic disease.

Cancer metastasis is a dynamic multi-step process, composed of distinct tumor cell populations. To understand the metastatic disease at cellular and molecular level, first it is important to develop an appropriate platform for enrichment and purification of the tumor populations involved in metastatic process. In clinical practice, the most common method for isolation of viable tumor cells of epithelial origin is based on using antibodies specific to epithelial membrane markers such as EpCAM among others. For example, CellSearch® is the only FDA-approved method for enumeration of CTCs of epithelial origin (CD45-, EpCAM+, and cytokeratins 8, 18+, and/or 19+) in whole blood. However, as discussed in chapter 2.2.3, the epithelial tumor cells need to undergo phenotypic changes to complete the entire metastatic cascade. Some of these changes are accompanied by loss of epithelial markers expression and acquisition of mesenchymal-associated genes, process known as EMT. In addition, we also observed that the primary tumors and metastatic lesions in 6 out of 7 metastatic PDX models contain cells positive for the classical

mesenchymal marker vimentin, suggesting that these cells may be undergoing EMT (see chapter 2.2.1). Therefore, the use of epithelial-marker-based enrichment approaches may lead to selective loss of some tumor populations.

For this reason the next goal of this thesis was to develop a method, that enables the identification of all human tumor populations involved in metastatic process. Taken into account the interspecies difference between the tumor and host cells in the PDX models, we searched for a ubiquitously expressed epithelial-independent human specific surface marker to discriminate the human tumor cells from host mouse cells. Among others, the HLA-ABC was a good candidate for enrichment of the human tumor cells, since it is robustly expressed on the surface of all nucleated cells. Indeed, flow cytometry analysis showed that the HLA marker was also abundantly expressed in tumor cells from two of the metastatic PDX models and therefore this allowed us to develop a highly sensitive, species-specific magnetic separation method, and enriched all human tumor populations from the mouse peripheral tissues (primary tumor, blood and metastatic organs) with negligible false-positive rate. HLA-ABC was also superior to the commonly used epithelial marker EpCAM (data no shown, lab observation). Unfortunately, this species-specific, epithelial-marker-independent method cannot be used for isolation of tumor cells including CTCs from patients samples, because all cells are of human origin. Therefore, future research is needed to identify new selection markers that are robustly expressed in pancreatic tumor cells and not subjected to phenotypic changes.

5.1.3. Pancreatic CTC populations contain tumor- and metastasis-initiating cells.

CTCs are a key intermediate event in metastatic process, which is indispensible for generation of the future metastatic lesions. It has been hypothesized that CTC populations in the blood of patients with carcinoma may contain cells with the clonal capacity to initiate metastatic growth in distant organs, thus behaving as MICs. Indeed, the presence of CTC in patient blood has been associated with metastatic disease and decreased overall survival in several types of carcinoma [144]. To date, only two studies were able to demonstrate that the CTCs populations isolated from breast and lung cancer patients possess tumorigenic and metastatic capacity upon transplantation in immunodeficient mice [139-140]. Although these findings support the hypothesis that CTC

populations contain MICs, the existence and functional characterization of circulating MICs in the context of pancreatic cancer have not been formally documented [145].

A major barrier to identify these circulating metastatic cells is that they might be present at very low number in blood of the pancreatic patients. In this regard, a recent study reported that the median CTCs number in the peripheral blood of PDAC patients is 3 CTCs/7.5 ml [146]. This low number of pancreatic CTCs might extremely limit their molecular and functional characterization. In fact, over the last 2 years our laboratory has been trying to generate PDX models from the blood of metastatic PDAC patients using "negative enrichment" approach with anti-CD45 antibody for depletion of the white blood cells. The CD45- fractions obtained from PDAC patients were unable to produce tumors in immunodeficient mice. The method for development of these desirable patient CTC-derived xenograft models is under continues improvement process, but up to date no patient CTC-derived xenograft model of pancreatic cancer has been generated.

To overcome this issue, we exploited the metastatic PDX models as an efficient *In-vivo* platform to produce sufficient number of human pancreatic CTCs for further molecular and functional studies. In truth, the positive HLA-ABC fraction isolated from a highly metastatic Panc265 model was $6x10^4$ cells/10 ml mouse blood and it was more than sufficient to investigate the *In-vivo* tumorigenic and metastatic capacity of these tumor cells. *In vivo* transplantation of human pancreatic CTCs in immunodeficient mice resulted in generation of human tumors in 7 out of 8 transplants and lung metastasis in all recipient animals, thus demonstrating that the human pancreatic CTC population is enriched of functional TICs and MICs. Moreover, the CTC-derived tumors retained the principal morphological characteristics of the parental tumor. Orthotopic implantation of fragments established from CTCs-derived tumors in small set of animals resulted in similar survival rate to that of the parental tumor and sporadic macro and micro metastasis in distant organs (data no shown, lab observation). Altogether, this data suggests that the CTCs population may also contain tumor cells with stem cell features capable of regenerating the entire parental tumor. In conclusion, we successfully demonstrated the existence of TICs and MICs within the pancreatic CTCs population isolated from a highly metastatic PDX model. However, future functional studies will be necessary to confirm their tumorigenic and metastatic capacity in the other metastatic models. Further phenotypic characterization of these rare, life-threatening cells

to identify pancreatic MIC-specific markers and their subsequent validation in prospective clinical studies, is also of crucial importance.

5.2. Single-cell dissection of the transcriptional heterogeneity during the metastatic progression of pancreatic cancer.

Cancer metastasis is a highly heterogeneous disease, composed of multiple cell populations distinct from one another, which are subjected to a continuously evolving process. This Intra-tumoral heterogeneity results from mutations, transcriptional changes and clonal selection dynamics during tumor growth, where individual tumor cells accumulate cell-specific genetic changes. This clonal heterogeneity is significantly associated with tumor progression and metastasis.

The recently developed single-cell sequencing technologies provide the highest-resolution analysis of intra-tumoral heterogeneity. In contrast to the conventional bulk-sequencing methods, these single-cell analysis are able to uncover the heterogeneous behaviors of rare tumor populations and therefore facilitate the identification of specific genetic alterations or gene expression signatures involved in the tumor progression and metastasis. Indeed, a recent study exploited the scRNA sequencing technology to decipher the transcriptional heterogeneity of breast cancer metastasis in mouse xenograft models [147]. The single-cell sequencing in this study revealed that low-burden metastatic lesions are composed of cells with stem-cell- ,EMT-, pro-survival- and dormancy-associated gene expression properties, whereas high-burden metastatic lesions contain cancer cells with similar gene expression signature with that of the primary tumor. However, despite these considerable advances in metastasis research, the transcriptional heterogeneity of metastatic disease in pancreatic cancer still remains poorly studied.

In this thesis, we exploited the metastatic PDX models of pancreatic cancer and the single-cell technology to answer the question whether the tumor populations (primary tumor, CTCs, liver metastatic cells) involved in tumor progression are transcriptionally distinct from one another. The single-cell analysis revealed considerable transcriptional heterogeneity between the three biological groups and the PCA plot demonstrated that the intra-population heterogeneity is more pronounced in CTC group, showing more dispersed pattern than the other two groups. Altogether these findings suggest that the metastatic disease of pancreatic cancer is a well-organized

evolutionary process, where cell subpopulations derived from the primary tumor are continuously modifying their transcriptomic program until they complete the entire metastatic cascade.

5.2.1 ECM interaction and focal adhesion, cell cycle and ribosome biogenesis signatures are the major aspects of the transcriptional intra-tumor heterogeneity during pancreatic cancer metastasis.

The characterization of the aspects (gene sets and biological pathways), which reflect the transcriptional intra-tumoral heterogeneity in the context of cancer is also needed for gaining more knowledge in cancer progression and metastasis. Using a recently developed bioinformatics method (PAGODA) for resolving the transcriptional diversity at single-cell level, we successfully characterize the previously uncovered transcriptional heterogeneity between the tumor populations involved in metastatic process. This bioinformatic analysis identified that three main biological patherns: ECM interaction and focal adhesion, Cell Cycle and Ribosome biogenesis define this intra-tumoral heterogeneity.

In contrast to the primary tumor cells, ECM interaction signature mainly composed of collagen genes is significantly down-regulated in CTCs and liver metastatic cells. The differential expression of these ECM-related genes could reflect the adaptation of the metastatic cells to the new tissue environment, where the stromal compartment and ECM composition are different from those in primary tumor niche. In fact, this result is coherent with findings of previous studies, which reported a significant variation in the expression of human extracellular matrix-related genes that were significantly down-regulated in xenografts compared with patients tumors [148].

The cell cycle is the second biological pattern, which was found to be repressed in CTC population. Moreover, in contrast to primary tumor and metastatic cells, the majority of the CTCs reside in G1 phase, thus suggesting that they might be in a state of dormancy. Indeed, many hypotheses have been proposed to explain this single-cell dormancy model. According to this model, individual cancer cell or cell clusters detach from primary tumor mass and arrive at the secondary homing sites, where they enter in a prolong dormant state by which they retard or suspend their replication completely until conditions favor their re-entry into the next-cell cycle. In this regard, recent studies supported this hypotheses by demonstrating that CTCs and metastatic cells from low-burden tissues isolated from pancreatic and breast cancer mouse models show low-

proliferative signature compared with their respective primary tumor and metastatic cells from high-burden tissues [106;147]. Altogether, these findings support that the pancreatic CTCs in this metastatic PDX model may remain dormant or slow-cycling with prolonged interphase until they establish overt metastasis at distant organs. However, additional studies are needed to confirm whether the CTCs exist in an inactive or active cycling state.

Interestingly, the third major aspect of the transcriptional heterogeneity is driven by a gene set associated with ribosome biogenesis, which is up-regulated in CTC population. It is well known that cell growth and proliferation are associated with changes in the rate of ribosome biogenesis. In fact, it was reported that the rRNA synthesis is increased during G1 phase and ribosome assembly is required for the protein synthesis during S phase. On other hand, downregulation of ribosome activity might be required during mitotic (M) phase for proper exit from the cell cycle. This was confirmed by other studies showing that the synthesis of rRNA reaches maximal levels in S phase and G2 phases, it is decreased in M phase and it is increased in G1 phase [149-151]. In agreement with these observations, the high expression levels of ribosome-associated genes in pancreatic CTC population might be tightly linked to their cell-cycle state. Indeed, in contrast to the primary tumor and metastatic population, which contain a large proportion of cells in G2/M phase, the majority of CTCs reside in G1 phase, therefore suggesting that they may remain in dormant or slow-cycling mode with prolonged interphase in which, as mentioned above, the rRNA synthesis is increased.

5.2.2. Single-cell RNA sequencing: a reliable method for identification of anti-metastatic targets.

The ultimate goal of studying the cancer metastasis is to develop effective anti-metastatic therapeutic strategies that will prolong the patient's survival. A large body of evidence suggests that metastasis is regulated by the expression of multiple genes necessary for completion of each step in the metastatic cascade and transcriptional regulation of metastasis-related genes is one possible mechanism to promote metastasis. This notion has encouraged many researchers to rely on gene-expression studies to pinpoint molecular mechanisms involved in metastatic process. Indeed, over the last few years, many studies discovered important metastasis-associated genes in different cancer types by exploring the gene-expression profiles of tumour populations, which

participate in metastatic process. For example, scRNA sequencing has been applied to decipher the transcriptional programs of the CTCs, where several metastasis-promoting genes have been identified to be up-regulated in CTCs population, and their knockdown in cancer cells suppress cell migration and invasiveness [105, 106].

Encouraged by these observations, we also considered that scRNA sequencing would be an appropriate approach to find relevant metastasis-associated genes, which can be further use for design of new and more effective therapeutic strategies against pancreatic cancer metastasis. Indeed, the detailed analysis of transcriptional program of the human pancreatic CTCs revealed numerous up-regulated genes and pathways such as BIRC5 (Survivin), AURKA, AURKB, PLK1, IL32 among others and the majority of them have been previously described in the literature to play important roles in cancer progression and metastasis. Moreover, pharmacological targeting of some of these genes (BIRC5, AURKA and AURKB) in our metastatic PDX models resulted in significant increase in survival of the treated animals and significant reduction in metastatic tumor burden. Altogether, these results are in agreement with the previous findings confirming that the scRNA-seq profiling of cancer cells with key roles in metastatic process might be a powerful and reliable tool for discovery of relevant metastasis-related genes, which in turns could contribute to improvement of the therapeutic strategies against metastatic disease.

5.2.3. Survivin: A therapeutic target for metastatic pancreatic cancer.

Survivin has been discovered to be one of the components of the chromosomal passenger complex (CPC) regulating chromomal segregation and cytokinesis during mitosis [152]. Loss of function of Survivin or of one of its partners (AURKB, INCENP and DASRA B) upon RNAi-mediated inhibition resulted in disturbed segregation of chromosomes and defective cytokinesis [153-157]. Furthermore, Survivin knock-out in yeasts and *C. elegans* confirmed the role of Survivin in mitosis. In vertebrates, the essential role of Survivin during mitosis has been confirmed in *Xenopus laevis* and mice [158-159]. On the other hand, besides its functions in mitosis Survivin is associated with multiple roles in apoptotic regulation [160-162]. However, within the N-terminus of Survivin, there is only one baculoviral inhibitor of apoptosis repeat (BIR) domain. Also Survivin contains no C-terminal RING finger domain which is common for members of the IAP

family [163-164]. Therefore, although overexpression of Survivin might act as an anti-apoptotic factor, it appears conceivable that the Survivin-knockout phenotypes which were interpreted as loss of anti-apoptotic function might be primarily linked to deregulated mitotic processes.

In the context of cancer disease, Survivin has been found to promote tumor progression by regulating cell division and apoptosis [165-166]. It has been also reported that its overexpression enhances tumor invasion and metastasis in several cancer types [167-168]. Moreover, it has been recently reported that Survivin is highly expressed in CTCs isolated from prostrate cancer patients [169], as well as another recent study demonstrated that the expression levels of detergent soluble cytoplasmic Survivin in colorectal cancer cell lines correlated inversely with anoikis susceptibility in colorectal cancer [170]. However despite these advances, the precise role of Survivin in pancreatic cancer progression and metastasis remains poorly understood.

In this thesis work, we first identified that the mRNA expression level of Survivin was significantly higher in the human pancreatic CTCs compared to that in primary tumor cells. Second, Survivin was also expressed at protein level in the CTCs, primary tumor and metastatic cells derived from a highly metastatic Panc265 model. The protein expression of Survivin was assessed in the other metastatic models, showing the presence of Survivin-positive cells in primary tumor and metastatic sites of all metastatic models. The protein expression pattern of Survivin in all models was nuclear, thus suggesting that its function might be linked to cell division. Third, the pharmacological targeting of Survivin by using a small-molecule inhibitor YM155 (currently in clinical trials) resulted in significant improvement in survival of treated mice implanted with two of our metastatic models(Panc265 and Panc198), prolonged survival of the animals that were subjected to partial pancreatectomy for removal of primary tumor graft, and significant reduction in metastatic tumor burden. Altogether, this data give reasons to think that Survivin might play a role in tumor cell division during the metastasis progression of pancreatic cancer.

Despite these convincing results, however, additional studies are necessary to better elucidate the precise role of Survivin in pancreatic cancer metastasis. This includes the following: 1) Evaluation of Survivin protein expression in CTCs derived from the other metastatic PDX models; 2) Knock-down of Survivin in pancreatic metastasis-competent cancer cell lines by using shRNAs in order to

determine whether suppression of Survivin expression would impair their metastatic properties after tail-vein injection in immunodeficient mice; 3) Assessment of Survivin protein expression in pancreatic tumor patient specimens with aim to determine whether high expression of Survivin correlates with poor prognosis in PDAC patients. Moreover, the median survival of YM155 (survivin inhibitor) monotherapy was similar to that of Abraxane monotherapy, as well as the combo treatment with Abraxane resulted in a significant increase in median survival compared to the monotherapy regimens. Therefore, these data provide the rational for further investigation of anti-tumoral and anti-metastatic activity of this combo therapy in pancreatic cancer.

5.3. The role of tumor-derived exosomes in organotropic metastasis.

One salient feature of cancer metastasis is that some cancer cells preferentially metastasize to specific organs, under the control of multiple cellular and molecular mechanisms. Many studies focused largely on pinpointing intrinsic cancer cell properties which determine this organotropic metastasis, including genes, chemokine receptors expressed on cancer cells or tumor-secreted systemic factors. In recent years, tumor-derived exosomes have been demonstrated to promote cancer progression. In fact, recent studies have reported that the tumor exosomes which express specific integrins can determine the organotropic metastasis in various cancer types by preparing the pre-metastatic niche via their integrins-mediated fusion with organ-specific resident cells [80].

Based on these recent research findings, we also hypothesized that the tumor-derived exosomes may have a role in determining the metastatic organotropism observed in metastatic PDX models of pancreatic cancer. In collaboration with Hector Peinado`s group and Proteomics unit from CNIO, we were able to isolate and purify exosomes from different tissues and quantitative MS was able to identify proteins of human origin extracted from the exosomes derived from primary tumor and metastatic sites. Moreover, the unsupervised hierarchical clustering of the significantly abundant human proteins resulted in clear distinction between primary tumors, liver and lung proteome profiles. However, this type of analysis was unable to completely separate the exosomal protein signature of the aggressive models from that of less-agressive models. This could be due to the small number of differentially abundant human proteins identified in the liver and lung organs, as well as the small number of metastatic models used in this study(in total five PDX models – 2 aggressive and 3 less-agressive).

Next, we interrogated these "organ-specific" exosome protein signatures to search for potential protein candidates that might be associated with the metastatic disease and organotropic metastasis. Interestingly, the proteomics analysis identified that $ITGa_{6,}$ S100A11 and Vimentin proteins are abundantly expressed in primary tumor- and lung-tropic exosomes, but not in the exosomes from the liver organs. $ITGa_6$ is a member of transmembrane proteins, whose function is associated with cell adhesion, proliferation, cell differentiation and cell migration [171]. In fact, recent study identified enrichment of several integrin proteins including $ITGa_6$ in human exosomes derived from multiple organotropic tumor models [80]. Notably, $ITGa_6$ was abundantly expressed in the exosomes of breast, osteosarcoma, rhabdomyosacoma, Wilms'tumor and melanoma cell lines, which have propensity to metastasize to the lung, as well as in the exosomes derived from uveal melanoma, pancreatic and gastric cancer cells that colonize primarily to the liver. On the other hand, S100A11 is a member of the S100 calcium binding family and it has been associated with lymph node metastasis in metastatic non-small cell lung cancer, metastatic hepatocellular carcinoma and pancreatic adenocarcinoma [172-173]. Recently, S100A11 together with other S100 proteins was identified in mesothelioma cell-derived exosomes [174]. Vimentin is a type III intermediate filament protein, which has been reported to regulate a number of key cancer biological functions including EMT, cell migration and invasion, cell-cell and cell-substrate adhesion among others. However, despite the important role of this cytoskeletal protein in numerous processes implicated in metastatic disease, to the best of our knowledge, its precise role in organotropic metastasis has not been formally reported. Collectively, this data provides a scientific rationale for further investigating the role of these three exosomal proteins in pancreatic cancer spreading and metastatic organotropism.

In summary, the PDX metastatic models of pancreatic cancer developed in this thesis work provide an efficient, faithful and reproducible *In-vivo* system for modeling of the entire metastatic process. This *In-vivo* platform allowed the identification and isolation of all tumor populations involved in metastatic process, which in turns facilitated the transcriptional dissection of the metastatic disease at single-cell level, as well as the discovery of novel therapeutic targets for pancreatic cancer metastasis. Also, the use of these metastatic PDX models facilitated the molecular characterization of the tumor-secreted exosomes, which helped to better understand their role in organotropic metastasis.

VI. CONCLUSIONS

1. The metastatic PDX models of pancreatic cancer developed in this thesis provide an efficient and reproducible *In-vivo* platform for accurate modeling of the entire multi-step metastatic process and for isolation of all tumor populations involved in metastatic disease.

2. The human pancreatic circulating tumor cells (CTCs) possess high tumorigenic and metastatic capacity. The CTC-derived tumors preserve the morphological characteristics of parental tumor.

3. The metastatic disease of pancreatic cancer is a well-organized evolutionary process, where the primary tumor cells, metastatic cells and CTCs are transcriptionally distinct from one another. The transcriptional heterogeneity between these three biological groups is defined by three biological patterns which are ECM interaction and focal adhesion, Cell cycle and ribosome biogenesis.

4. The single-cell transcriptome dissection of metastatic disease was able to uncover numerous deregulated metastasis-associated genes. Survivin is one of these metastasis-related genes which is up-regulated in CTCs and the pharmacological targeting of this gene was able to reduce the metastatic tumor burden and improve the median survival of the metastatic PDX models of pancreatic cancer. Additionally, protein expression of Survivin was detected in primary tumors and metastatic sites of all metastatic PDX models, which suggests that Survivin can be a prognostic marker and anti-metastatic therapeutic target for pancreatic cancer metastasis.

5. Although the protein profiling of the exosomes purified from primary tumors and metastatic sites of metastatic PDX models failed to separate the “aggressive” from “less-aggressive” models, this proteomic analysis identified an “organ-specific” exosomal protein signatures with abundant expression of several metastasis-associated exosome proteins.

REFERENCES:

1. Siegel RL, Miller KD, Jemal A. Cancer Statistics, 2017. CA Cancer J Clin. 2017;67(1):7-30.
2. Neoptolemos JP, Cunningham D, Friess H, et al. Adjuvant therapy in pancreatic cancer: historical and current perspectives. Ann Oncol. 2003;14(5):675-92.
3. Davies K, Conlon KC. Neuroendocrine tumors of the pancreas. *Current gastroenterology reports* 2009, 11:119-127.
4. Ghaneh P, Costello E, Neoptolemos JP. Biology and management of pancreatic cancer. *Postgrad Med J* 2008, 84:478-497.
5. Klöppel G, Solcia E, Longnecker DS, Capella C, Sobin LH. *Histological typing of tumours of the exocrine pancreas.* Springer. 1996.
6. Sobin LH, Gospodarowicz MK, Wittekind C. *TNM classification of malignant tumours.* Wiley. 2011.
7. Matthaei H, Dal molin M, Maitra A. Identification and analysis of precursors to invasive pancreatic cancer. Methods Mol Biol. 2013;980:1-12.
8. Hruban RH, Maitra A, Kern SE, Goggins M. Precursors to pancreatic cancer. Gastroenterol Clin North Am. 2007;36(4):831-49, vi.
9. Cubilla AL, Fitzgerald PJ. Morphological lesions associated with human primary invasive nonendocrine pancreas cancer. Cancer Res. 1976;36(7 PT 2):2690-8.
10. Klöppel G, Bommer G, Rückert K, Seifert G. Intraductal proliferation in the pancreas and its relationship to human and experimental carcinogenesis. Virchows Arch A Pathol Anat Histol. 1980;387(2):221-33.
11. Andea A, Sarkar F, Adsay VN. Clinicopathological correlates of pancreatic intraepithelial neoplasia: a comparative analysis of 82 cases with and 152 cases without pancreatic ductal adenocarcinoma. Mod Pathol. 2003;16(10):996-1006.
12. Macgregor-das AM, Iacobuzio-donahue CA. Molecular pathways in pancreatic carcinogenesis. J Surg Oncol. 2013;107(1):8-14.
13. Feldmann G, Beaty R, Hruban RH, Maitra A. Molecular genetics of pancreatic intraepithelial neoplasia. J Hepatobiliary Pancreat Surg. 2007;14(3):224-32.
14. Mitelman F, Mertens F, Johansson B. Prevalence estimates of recurrent balanced cytogenetic aberrations and gene fusions in unselected patients with neoplastic disorders. Genes Chromosomes Cancer. 2005;43(4):350-66.

15. Calhoun ES, Hucl T, Gallmeier E, et al. Identifying allelic loss and homozygous deletions in pancreatic cancer without matched normals using high-density single-nucleotide polymorphism arrays. Cancer Res. 2006;66(16):7920-8.
16. Karhu R, Mahlamäki E, Kallioniemi A. Pancreatic adenocarcinoma -- genetic portrait from chromosomes to microarrays. Genes Chromosomes Cancer. 2006;45(8):721-30
17. Hahn SA, Kern SE. Molecular genetics of exocrine pancreatic neoplasms. Surg Clin North Am. 1995;75(5):857-69.
18. Ellis CA, Clark G. The importance of being K-Ras. Cell Signal. 2000;12(7):425-34.
19. Edkins S, O'meara S, Parker A, et al. Recurrent KRAS codon 146 mutations in human colorectal cancer. Cancer Biol Ther. 2006;5(8):928-32.
20. Caldas C, Hahn SA, Da costa LT, et al. Frequent somatic mutations and homozygous deletions of the p16 (MTS1) gene in pancreatic adenocarcinoma. Nat Genet. 1994;8(1):27-32.
21. Schutte M, Hruban RH, Geradts J, et al. Abrogation of the Rb/p16 tumor-suppressive pathway in virtually all pancreatic carcinomas. Cancer Res. 1997;57(15):3126-30.
22. Redston MS, Caldas C, Seymour AB, et al. p53 mutations in pancreatic carcinoma and evidence of common involvement of homocopolymer tracts in DNA microdeletions. Cancer Res. 1994;54(11):3025-33.
23. Latham KM, Eastman SW, Wong A, Hinds PW. Inhibition of p53-mediated growth arrest by overexpression of cyclin-dependent kinases. Mol Cell Biol. 1996;16(8):4445-55.
24. Hahn SA, Schutte M, Hoque AT, et al. DPC4, a candidate tumor suppressor gene at human chromosome 18q21.1. Science. 1996;271(5247):350-3.
25. Schutte M, Hruban RH, Hedrick L, et al. DPC4 gene in various tumor types. Cancer Res. 1996;56(11):2527-30.
26. Thiagalingam S, Lengauer C, Leach FS, et al. Evaluation of candidate tumour suppressor genes on chromosome 18 in colorectal cancers. Nat Genet. 1996;13(3):343-6.
27. Miyaki M, Kuroki T. Role of Smad4 (DPC4) inactivation in human cancer. Biochem Biophys Res Commun. 2003;306(4):799-804.
28. Bierie B, Moses HL. Tumour microenvironment: TGFbeta: the molecular Jekyll and Hyde of cancer. Nat Rev Cancer. 2006;6(7):506-20.
29. Massagué J, Blain SW, Lo RS. TGFbeta signaling in growth control, cancer, and heritable disorders. Cell. 2000;103(2):295-309.

30. Garrido-laguna I, Hidalgo M. Pancreatic cancer: from state-of-the-art treatments to promising novel therapies. Nat Rev Clin Oncol. 2015;12(6):319-34.
31. Harada T, Chelala C, Bhakta V, et al. Genome-wide DNA copy number analysis in pancreatic cancer using high-density single nucleotide polymorphism arrays. Oncogene. 2008;27(13):1951-60.
32. Hidalgo M. New insights into pancreatic cancer biology. Ann Oncol. 2012;23 Suppl 10:x135-8.
33. Jemal A, Siegel R, Xu J, Ward E. Cancer statistics, 2010. CA Cancer J Clin. 2010;60(5):277-300.
34. Klein CA. Cancer. The metastasis cascade. Science. 2008;321(5897):1785-7.
35. Ramaswamy S, Ross KN, Lander ES, Golub TR. A molecular signature of metastasis in primary solid tumors. Nat Genet. 2003;33(1):49-54.
36. Kim, M.Y., Oskarsson, T., Acharyya, S., Nguyen, D.X., Zhang, X.H., Norton, L., and Massague, J. (2009). Tumor self-seeding by circulating cancer cells. Cell *139*, 1315-1326.
37. Shah SP, Morin RD, Khattra J, et al. Mutational evolution in a lobular breast tumour profiled at single nucleotide resolution. Nature. 2009;461(7265):809-13.
38. Yachida S, Jones S, Bozic I, et al. Distant metastasis occurs late during the genetic evolution of pancreatic cancer. Nature. 2010;467(7319):1114-7.
39. Makohon-moore AP, Zhang M, Reiter JG, et al. Limited heterogeneity of known driver gene mutations among the metastases of individual patients with pancreatic cancer. Nat Genet. 2017;49(3):358-366.
40. Mcdonald OG, Li X, Saunders T, et al. Epigenomic reprogramming during pancreatic cancer progression links anabolic glucose metabolism to distant metastasis. Nat Genet. 2017;49(3):367-376.
41. Klein CA. Parallel progression of primary tumours and metastases. Nat Rev Cancer. 2009;9(4):302-12.
42. Stoecklein NH, Klein CA. Genetic disparity between primary tumours, disseminated tumour cells, and manifest metastasis. Int J Cancer. 2010;126(3):589-98.
43. Coghlin C, Murray GI. Current and emerging concepts in tumour metastasis. J Pathol. 2010;222(1):1 15.

44. Nguyen DX, Bos PD, Massagué J. Metastasis: from dissemination to organ-specific colonization. Nat Rev Cancer. 2009;9(4):274-84.
45. Chaffer CL, Weinberg RA. A perspective on cancer cell metastasis. Science. 2011;331(6024):1559-64.
46. Kalluri R, Weinberg RA. The basics of epithelial-mesenchymal transition. J Clin Invest. 2009;119(6):1420-8.
47. Moreno-bueno G, Portillo F, Cano A. Transcriptional regulation of cell polarity in EMT and cancer. Oncogene. 2008;27(55):6958-69.
48. Gregory PA, Bracken CP, Bert AG, Goodall GJ. MicroRNAs as regulators of epithelial-mesenchymal transition. Cell Cycle. 2008;7(20):3112-8.
49. Bhowmick NA, Neilson EG, Moses HL. Stromal fibroblasts in cancer initiation and progression. Nature. 2004;432(7015):332-7.
50. Egeblad M, Werb Z. New functions for the matrix metalloproteinases in cancer progression. Nat Rev Cancer. 2002;2(3):161-74.
51. Coussens LM, Fingleton B, Matrisian LM. Matrix metalloproteinase inhibitors and cancer: trials and tribulations. Science. 2002;295(5564):2387-92.
52. Jain RK, Munn LL, Fukumura D. Dissecting tumour pathophysiology using intravital microscopy. Nat Rev Cancer. 2002;2(4):266-76.
53. Gupta GP, Nguyen DX, Chiang AC, et al. Mediators of vascular remodelling co-opted for sequential steps in lung metastasis. Nature. 2007;446(7137):765-70.
54. Padua D, Zhang XH, Wang Q, et al. TGFbeta primes breast tumors for lung metastasis seeding through angiopoietin-like 4. Cell. 2008;133(1):66-77.
55. Weiss L. Metastatic inefficiency. Adv Cancer Res. 1990;54:159-211.
56. Stupack DG, Teitz T, Potter MD, et al. Potentiation of neuroblastoma metastasis by loss of caspase-8. Nature. 2006;439(7072):95-9.
57. Nicolson GL. Organ specificity of tumor metastasis: role of preferential adhesion, invasion and growth of malignant cells at specific secondary sites. Cancer Metastasis Rev. 1988;7(2):143-88.
58. Minn AJ, Gupta GP, Siegel PM, et al. Genes that mediate breast cancer metastasis to lung. Nature. 2005;436(7050):518-24.

59. Matsuda Y, Schlange T, Oakeley EJ, Boulay A, Hynes NE. WNT signaling enhances breast cancer cell motility and blockade of the WNT pathway by sFRP1 suppresses MDA-MB-231 xenograft growth. Breast Cancer Res. 2009;11(3):R32.

60. Padua, D. *et al.* TGFβ primes breast tumors for lung metastasis seeding through angiopoietin-like 4. *Cell* 133, 66–77 (2008).

61. Gupta, G. P. *et al.* Mediators of vascular remodelling co-opted for sequential steps in lung metastasis. *Nature* 446, 765–770 (2007).

62. Tichet, M. *et al.* Tumour-derived SPARC drives vascular permeability and extravasation through endothelial VCAM1 signalling to promote metastasis. *Nature Commun.* 6, 6993 (2015).

63. Weis, S., Cui, J., Barnes, L. & Cheresh, D. Endothelial barrier disruption by VEGF-mediated Src activity potentiates tumor cell extravasation and metastasis. *J. Cell Biol.* 167, 223–229 (2004).

64. Schumacher, D., Strilic, B., Sivaraj, K. K., Wettschureck, N. & Offermanns, S. Platelet-derived nucleotides promote tumor-cell transendothelial migration and metastasis via P2Y2 receptor. *Cancer Cell* 24, 130–137 (2013).

65. Labelle, M., Begum, S. & Hynes, R. O. Direct signaling between platelets and cancer cells induces an epithelial-mesenchymal-like transition and promotes metastasis. *Cancer Cell* 20, 576–590 (2011).

66. Qian, B. Z. *et al.* CCL2 recruits inflammatory monocytes to facilitate breast-tumour metastasis. *Nature* 475, 222–225 (2011).

67. Braun, S. *et al.* A pooled analysis of bone marrow micrometastasis in breast cancer. *N. Engl. J. Med.* 353, 793–802 (2005).

68. McAllister SS, Gifford AM, Greiner AL, Kelleher SP, Saelzler MP, Ince TA, Reinhardt F, Harris LN, Hylander BL, Repasky EA, et al. Systemic endocrine instigation of indolent tumor growth requires osteopontin. Cell. 2008;133:994–1005

69. Hiratsuka S, Duda DG, Huang Y, Goel S, Sugiyama T, Nagasawa T, Fukumura D, Jain RK. C-X-C receptor type 4 promotes metastasis by activating p38 mitogen-activated protein kinase in myeloid differentiation antigen (Gr-1)-positive cells. Proc Natl Acad Sci USA. 2011a;108:302–307.

70. Chambers AF, Groom AC, MacDonald IC. Dissemination and growth of cancer cells in metastatic sites. Nat Rev Cancer. 2002;2:563–572.
71. Kang SY, Halvorsen OJ, Gravdal K, Bhattacharya N, Lee JM, Liu NW, Johnston BT, Johnston AB, Haukaas SA, Aamodt K, et al. Prosaposin inhibits tumor metastasis via paracrine and endocrine stimulation of stromal p53 and Tsp-1. Proc Natl Acad Sci USA. 2009;106:12115–12120.
72. Mazzieri R, Pucci F, Moi D, Zonari E, Ranghetti A, Berti A, Politi LS, Gentner B, Brown JL, Naldini L, et al. Targeting the ANG2/TIE2 axis inhibits tumor growth and metastasis by impairing angiogenesis and disabling rebounds of proangiogenic myeloid cells. Cancer Cell. 2011;19:512–526.
73. Pantel K, Brakenhoff RH. Dissecting the metastatic cascade. Nat Rev Cancer. 2004;4(6):448-56.
74. Weiss L. Comments on hematogenous metastatic patterns in humans as revealed by autopsy. Clin Exp Metastasis. 1992;10(3):191-9.
75. Denève E, Riethdorf S, Ramos J, et al. Capture of viable circulating tumor cells in the liver of colorectal cancer patients. Clin Chem. 2013;59(9):1384-92.
76. Paget S. The distribution of secondary growths in cancer of the breast. 1889. Cancer Metastasis Rev. 1989;8(2):98-101.
77. Ruoslahti E. Vascular zip codes in angiogenesis and metastasis. Biochem Soc Trans. 2004;32(Pt3):397-402.
78. Nicolson GL, Dulski KM. Organ specificity of metastatic tumor colonization is related to organ-selective growth properties of malignant cells. Int J Cancer. 1986;38(2):289-94.
79. Kaplan RN, Riba RD, Zacharoulis S, et al. VEGFR1-positive haematopoietic bone marrow progenitors initiate the pre-metastatic niche. Nature. 2005;438(7069):820-7
80. Hoshino A, Costa-silva B, Shen TL, et al. Tumour exosome integrins determine organotropic metastasis. Nature. 2015;527(7578):329-35.
81. Liu Y, Cao X. Organotropic metastasis: role of tumor exosomes. Cell Res. 2016;26(2):149-50.
82. Francia G, Cruz-munoz W, Man S, Xu P, Kerbel RS. Mouse models of advanced spontaneous metastasis for experimental therapeutics. Nat Rev Cancer. 2011;11(2):135-41
83. Kang Y, Siegel PM, Shu W, Drobnjak M, Kakonen SM, et al. (2003) A multigenic program mediating breast cancer metastasis to bone. Cancer Cell 3:537–49.

84. Bardeesy N, Aguirre AJ, Chu GC, et al. Both p16(Ink4a) and the p19(Arf)-p53 pathway constrain progression of pancreatic adenocarcinoma in the mouse. Proc Natl Acad Sci USA. 2006;103(15):5947-52.

85. Hidalgo M, Amant F, Biankin AV, et al. Patient-derived xenograft models: an emerging platform for translational cancer research. Cancer Discov. 2014;4(9):998-1013.

86. Fidler IJ. Rationale and methods for the use of nude mice to study the biology and therapy of human cancer metastasis. Cancer Metastasis Rev. 1986;5(1):29-49.

87. Fogh J, et al. Thirty-four lines of six human tumor categories established in nude mice. Journal of the National Cancer Institute. 1980;64(4):745–751.

88. Hoffman RM. Patient-derived orthotopic xenografts: better mimic of metastasis than subcutaneous xenografts. Nat Rev Cancer. 2015;15(8):451-2.

89. Munoz, R. *et al.* Highly efficacious non‐toxic treatment for advanced metastatic breast cancer using combination UFT‐cyclophosphamide metronomic chemotherapy. *Cancer Res.* 66, 3386–3391 (2006).

90. Furukawa T, Kubota T, Watanabe M, Kitajima M, Hoffman RM. A novel "patient-like" treatment model of human pancreatic cancer constructed using orthotopic transplantation of histologically intact human tumor tissue in nude mice. Cancer Res. 1993;53(13):3070-2.

91. Yabuuchi S, Pai SG, Campbell NR, de Wilde RF, De Oliveira E, Korangath P, Streppel MM, Rasheed ZA, Hidalgo M, Maitra A, et al. Notch signaling pathway targeted therapy suppresses tumor progression and metastatic spread in pancreatic cancer. Cancer Lett. 2013;335:41–51.

92. Paez-ribes M, Man S, Xu P, Kerbel RS. Development of Patient Derived Xenograft Models of Overt Spontaneous Breast Cancer Metastasis: A Cautionary Note. PLoS ONE. 2016;11(6):e0158034.

93. Francia G, et al. Long term progression and therapeutic response of visceral metastatic disease non-invasively monitored in mouse urine using β-hCG choriogonadotropin secreting tumor cell lines. Mol. Cancer Ther.2008;7:3452–3459

94. Morikawa K, Walker SM, Jessup JM, Fidler IJ. *In vivo* selection of highly metastatic cells from surgical specimens of different primary human colon carcinomas implanted into nude mice. Cancer Res. 1988;48:1943–1948.

95. Kubota T. Metastatic models of human cancer xenografted in the nude mouse: the importance of orthotopic transplantation. J. Cell. Biochem. 1994;56:4–8.

96. Nangia-Makker P, et al. Inhibition of human cancer cell growth and metastasis in nude mice by oral intake of modified citrus pectin. J. Natl Cancer Inst. 2002;94:1854–1862.

97. Cruz-Munoz W, Man S, Xu P, Kerbel RS. Development of a preclinical model of spontaneous human melanoma CNS metastasis. Cancer Res. 2008;68:4500–4505.

98. Kiguchi K, et al. A patient-like orthotopic implantation nude mouse model of highly metastatic human ovarian cancer. Clin. Exp. Metastasis. 1998;16:751–756

99. Almendro V, Marusyk A, Polyak K. Cellular heterogeneity and molecular evolution in cancer. Annu Rev Pathol. 2013;8:277-302.

100. Gerlinger M, Rowan AJ, Horswell S, et al. Intratumor heterogeneity and branched evolution revealed by multiregion sequencing. N Engl J Med. 2012;366(10):883-92.

101. Swanton C. Intratumor heterogeneity: evolution through space and time. Cancer Res. 2012;72(19):4875-82.

102. L. Yan, M. Yang, H. Guo, L. Yang, J. Wu, R. Li, P. Liu, Y. Lian, X. Zheng, J . Yan, J. Huang, M. Li, X. Wu, L. Wen, K. Lao, R. Li, J. Qiao, and F. Tang. Single cell RNA-Seq profiling of human preimplantation embryos and embryonic stem cells. Nat Struct Mol Biol, 20(9):1131–9, Sep 2013.

103. Grindberg RV, Yee-greenbaum JL, Mcconnell MJ, et al. RNA-sequencing from single nuclei. Proc Natl Acad Sci USA. 2013;110(49):19802-7.

104. Ramsköld D, Luo S, Wang YC, et al. Full-length mRNA-Seq from single-cell levels of RNA and individual circulating tumor cells. Nat Biotechnol. 2012;30(8):777-82.

105. Aceto N, Bardia A, Miyamoto DT, et al. Circulating tumor cell clusters are oligoclonal precursors of breast cancer metastasis. Cell. 2014;158(5):1110-22.

106. Ting DT, Wittner BS, Ligorio M, et al. Single-cell RNA sequencing identifies extracellular matrix gene expression by pancreatic circulating tumor cells. Cell Rep. 2014;8(6):1905-18.

107. Hidalgo M, Bruckheimer E, Rajeshkumar NV, Garrido-Laguna I, De Oliveira E, Rubio-Viqueira B, et al. A pilot clinical study of treatment guided by personalized tumorgrafts in patients with advanced cancer. Mol Cancer Ther 2011;10:1311–6.

108. Rowold DJ, Herrera RJ. Alu elements and the human genome. Genetica. 2000;108(1):57-72.

109. Van der horst EH, Leupold JH, Schubbert R, Ullrich A, Allgayer H. TaqMan-based quantification of invasive cells in the chick embryo metastasis assay. BioTechniques. 2004;37(6):940-2, 944, 946.

110. Steven Wingett. FastQ screen, available online at: http://www.bioinformatics.babraham.ac.uk/projects/fastq_screen/
111. Trapnell C, Pachter L, Salzberg SL. TopHat: discovering splice junctions with RNA-Seq. Bioinformatics 2009;25:1105–11.
112. Anders S, Pyl PT, Huber W. HTSeq-a Python framework to work with high-throughput sequencing data. Bioinformatics 2015;31:166–9.
113. Kharchenko PV, Silberstein L, Scadden DT. Bayesian approach to single-cell differential expression analysis. Nat Methods. 2014 Jul;11(7):740-2.
114. Benjamini, Y., and Hochberg, Y. (1995). Controlling the false discovery rate: a practical and powerful approach to multiple testing. Journal of the Royal Statistical Society Series B 57, 289–300.
115. Subramanian A, Tamayo P, Mootha VK, Mukherjee S, Ebert BL, Gillette MA, Paulovich A, Pomeroy SL, Golub TR, Lander ES, Mesirov JP. Gene set enrichment analysis: a knowledge-based approach for interpreting genome-wide expression profiles. Proc Natl Acad Sci U S A. 2005 Oct 25;102(43):15545-50.
116. Lamb J, Crawford ED, Peck D, Modell JW, Blat IC, Wrobel MJ, Lerner J, Brunet JP, Subramanian A, Ross KN, Reich M, Hieronymus H, Wei G, Armstrong SA, Haggarty SJ, Clemons PA, Wei R, Carr SA, Lander ES, Golub TR. The Connectivity Map: using gene-expression signatures to connect small molecules, genes, and disease. Science. 2006 Sep 29;313(5795):1929-35.
117. BROAD INSTITUTE LINCS CENTER FOR TRANSCRIPTOMICS. https://projectreporter.nih.gov/project_description.cfm?projectnumber=1U54HL127366-01
118. Smyth, G. K. (2004). Linear models and empirical Bayes methods for assessing differential expression in microarray experiments. Statistical Applications in Genetics and Molecular Biology Volume 3, Issue 1, Article 3.
119. Benten D, Keller G, Quaas A, et al. Aurora kinase inhibitor PHA-739358 suppresses growth of hepatocellular carcinoma in vitro and in a xenograft mouse model. Neoplasia. 2009;11(9):934-44.
120. Nakahara T, Kita A, Yamanaka K, et al. YM155, a novel small-molecule survivin suppressant, induces regression of established human hormone-refractory prostate tumor xenografts. Cancer Res. 2007;67(17):8014-21.

121. Wang F, Wang L, Zhao Y, et al. A novel small-molecule activator of procaspase-3 induces apoptosis in cancer cells and reduces tumor growth in human breast, liver and gallbladder cancer xenografts. Mol Oncol. 2014;8(8):1640-52.

122. Yahata T, Ando K, Nakamura Y, et al. Functional human T lymphocyte development from cord blood CD34+ cells in nonobese diabetic/Shi-scid, IL-2 receptor gamma null mice. J Immunol. 2002;169(1):204-9.

123. Xing F, Kobayashi A, Okuda H, et al. Reactive astrocytes promote the metastatic growth of breast cancer stem-like cells by activating Notch signalling in brain. EMBO Mol Med. 2013;5(3):384-96.

124. Li M, Zhang B, Sun B, et al. A novel function for vimentin: the potential biomarker for predicting melanoma hematogenous metastasis. J Exp Clin Cancer Res. 2010;29:109

125. Korsching E, Packeisen J, Liedtke C, et al. The origin of vimentin expression in invasive breast cancer: epithelial-mesenchymal transition, myoepithelial histogenesis or histogenesis from progenitor cells with bilinear differentiation potential? J Pathol. 2005;206:451–7

126. Jin H, Morohashi S, Sato F, et al. Vimentin expression of esophageal squamous cell carcinoma and its aggressive potential for lymph node metastasis. Biomed Res. 2010;31(2):105-12.

127. Hu L, Lau SH, Tzang CH, et al. Association of Vimentin overexpression and hepatocellular carcinoma metastasis. Oncogene. 2004;23:298–302.

128. Hoorens A, Prenzel K, Lemoine NR, Klöppel G: Undifferentiated carcinoma of the pancreas: analysis of intermediate filament profile and Ki-ras mutations provides evidence of a ductal origin. J Pathol 185 :53-60 (1998).

129. Nakajima S, Doi R, Toyoda E, et al. N-cadherin expression and epithelial-mesenchymal transition in pancreatic carcinoma. Clin Cancer Res. 2004;10(12 Pt 1):4125-33.

130. Hendrix MJ, Seftor EA, Seftor RE, Trevor KT. Experimental co-expression of vimentin and keratin intermediate filaments in human breast cancer cells results in phenotypic interconversion and increased invasive behavior. Am J Pathol. 1997;150:483–495.

131. Gilles C, Polette M, Piette J, et al. Vimentin expression in cervical carcinomas: association with invasive and migratory potential. J Pathol. 1996;180(2):175-80

132. Raymond WA, Leong AS. Co-expression of cytokeratin and vimentin intermediate filament proteins in benign and neoplastic breast epithelium. J Pathol. 1989;157(4):299-306.

133. Lee J, Hahm ER, Marcus AI, Singh SV. Withaferin A inhibits experimental epithelial-mesenchymal transition in MCF-10A cells and suppresses vimentin protein level in vivo in breast tumors. Mol Carcinog. 2015;54(6):417-29.

134. Hong B, Zu Y. Detecting circulating tumor cells: current challenges and new trends. Theranostics. 2013; 3:377–394.

135. Liu Z, Fusi A, Klopocki E, Schmittel A, Tinhofer I, Nonnenmacher A, Keilholz U. Negative enrichment by immunomagnetic nanobeads for unbiased characterization of circulating tumor cells from peripheral blood of cancer patients. J Transl Med. 2011; 9:70.

136. Doak SH, Jenkins GJ, Parry EM, D'Souza FR, Griffiths AP, Toffazal N, Shah V, Baxter JN, Parry JM. Chromosome 4 hyperploidy represents an early genetic aberration in premalignant Barrett's oesophagus. Gut. 2003; 52:623–628.

137. Allaway RJ, Fischer DA, De abreu FB, et al. Genomic characterization of patient-derived xenograft models established from fine needle aspirate biopsies of a primary pancreatic ductal adenocarcinoma and from patient-matched metastatic sites. Oncotarget. 2016;7(13):17087-102.

138. Paez-ribes M, Man S, Xu P, Kerbel RS. Development of Patient Derived Xenograft Models of Overt Spontaneous Breast Cancer Metastasis: A Cautionary Note. PLoS ONE. 2016;11(6):e0158034.

139. Hodgkinson CL, Morrow CJ, Li Y, et al. Tumorigenicity and genetic profiling of circulating tumor cells in small-cell lung cancer. Nat Med. 2014;20(8):897-903.

140. Baccelli I, Schneeweiss A, Riethdorf S, et al. Identification of a population of blood circulating tumor cells from breast cancer patients that initiates metastasis in a xenograft assay. Nat Biotechnol. 2013;31(6):539-44.

141. Fan J, Salathia N, Liu R, et al. Characterizing transcriptional heterogeneity through pathway and gene set overdispersion analysis. Nat Methods. 2016;13(3):241-4.

142. Scialdone A, Natarajan KN, Saraiva LR, et al. Computational assignment of cell-cycle stage from single-cell transcriptome data. Methods. 2015;85:54-61

143. Milsom CC, Lee CR, Hackl C, Man S, Kerbel RS. Differential post-surgical metastasis and survival in SCID, NOD-SCID and NOD-SCID-IL-2Rγ(null) mice with parental and subline variants of human breast cancer: implications for host defense mechanisms regulating metastasis. PLoS ONE. 2013;8(8):e71270.

144. Krebs MG, Hou JM, Ward TH, Blackhall FH, Dive C. Circulating tumour cells: their utility in cancer management and predicting outcomes. Ther Adv Med Oncol. 2010;2(6):351-65.
145. Cen P, Ni X, Yang J, Graham DY, Li M. Circulating tumor cells in the diagnosis and management of pancreatic cancer. *Biochimica et Biophysica Acta*. 2012;1826(2):350–356.
146. Gao Y, Zhu Y, Zhang Z, Zhang C, Huang X, Yuan Z. Clinical significance of pancreatic circulating tumor cells using combined negative enrichment and immunostaining-fluorescence in situ hybridization. J Exp Clin Cancer Res. 2016;35:66.
147. Lawson DA, Bhakta NR, Kessenbrock K, et al. Single-cell analysis reveals a stem-cell program in human metastatic breast cancer cells. Nature. 2015;526(7571):131-5.
148. Martinez-garcia R, Juan D, Rausell A, et al. Transcriptional dissection of pancreatic tumors engrafted in mice. Genome Med. 2014;6(4):27.
149. Grummt I. Regulation of mammalian ribosomal gene transcription by RNA polymerase I. Prog Nucleic Acid Res Mol Biol. 1999;62:109-54.
150. Kief DR, Warner JR. Coordinate control of syntheses of ribosomal ribonucleic acid and ribosomal proteins during nutritional shift-up in Saccharomyces cerevisiae. Mol Cell Biol. 1981;1(11):1007-15.
151. Klein J, Grummt I. Cell cycle-dependent regulation of RNA polymerase I transcription: the nucleolar transcription factor UBF is inactive in mitosis and early G1. Proc Natl Acad Sci USA. 1999;96(11):6096-101.
152. Ruchaud S, Carmena M, Earnshaw WC. Chromosomal passengers: conducting cell division. Nat Rev Mol Cell Biol. 2007;8(10):798-812.
153. Li F, Ackermann EJ, Bennett CF, et al. Pleiotropic cell-division defects and apoptosis induced by interference with survivin function. Nat Cell Biol. 1999;1(8):461-6.
154. Temme A, Rieger M, Reber F, et al. Localization, dynamics, and function of survivin revealed by expression of functional survivinDsRed fusion proteins in the living cell. Mol Biol Cell. 2003;14(1):78-92.
155. Hendruschk S, Wiedemuth R, Aigner A, et al. RNA interference targeting survivin exerts antitumoral effects in vitro and in established glioma xenografts in vivo. Neuro-oncology. 2011;13(10):1074-89.

156. Tatsuka M, Katayama H, Ota T, et al. Multinuclearity and increased ploidy caused by overexpression of the aurora- and Ipl1-like midbody-associated protein mitotic kinase in human cancer cells. Cancer Res. 1998;58(21):4811-6.

157. Temme A, Herzig E, Weigle B, et al. Inhibition of malignant glioma cell growth by a survivin mutant retrovirus. Hum Gene Ther. 2005;16(2):209-22.

158. Uren AG, Wong L, Pakusch M, et al. Survivin and the inner centromere protein INCENP show similar cell-cycle localization and gene knockout phenotype. Curr Biol. 2000;10(21):1319-28.

159. Bolton MA, Lan W, Powers SE, Mccleland ML, Kuang J, Stukenberg PT. Aurora B kinase exists in a complex with survivin and INCENP and its kinase activity is stimulated by survivin binding and phosphorylation. Mol Biol Cell. 2002;13(9):3064-77.

160. Altieri DC. The case for survivin as a regulator of microtubule dynamics and cell-death decisions. Curr Opin Cell Biol. 2006;18(6):609-15.

161. Reed JC. The Survivin saga goes in vivo. J Clin Invest. 2001;108(7):965-9

162. Wheatley SP, Mcneish IA. Survivin: a protein with dual roles in mitosis and apoptosis. Int Rev Cytol. 2005;247:35-88.

163. Altieri DC. Survivin and IAP proteins in cell-death mechanisms. Biochem J. 2010;430(2):199-205.

164. Ambrosini G, Adida C, Altieri DC. A novel anti-apoptosis gene, survivin, expressed in cancer and lymphoma. Nat Med. 1997;3(8):917-21.

165. Mita AC, Mita MM, Nawrocki ST, Giles FJ. Survivin: key regulator of mitosis and apoptosis and novel target for cancer therapeutics. Clin Cancer Res. 2008;14(16):5000-5.

166. Mehrotra S, Languino LR, Raskett CM, Mercurio AM, Dohi T, Altieri DC. IAP regulation of metastasis. Cancer Cell. 2010;17(1):53-64.

167. Chu XY, Chen LB, Wang JH, et al. Overexpression of survivin is correlated with increased invasion and metastasis of colorectal cancer. J Surg Oncol. 2012;105(6):520-8.

168. Zhang M, Coen JJ, Suzuki Y, et al. Survivin is a potential mediator of prostate cancer metastasis. Int J Radiat Oncol Biol Phys. 2010;78(4):1095-103.

169. Cann GM, Gulzar ZG, Cooper S, et al. mRNA-Seq of single prostate cancer circulating tumor cells reveals recapitulation of gene expression and pathways found in prostate cancer. PLoS ONE. 2012;7(11):e49144.

170. Hori M, Miki T, Okamoto M, et al. The detergent-soluble cytoplasmic pool of survivin suppresses anoikis and its expression is associated with metastatic disease of human colon cancer. PLoS ONE. 2013;8(2):e55710.
171. Srichai, M.B., and Zent, R. “Integrin Structure and Function.” Cell-Extracellular Matrix Interactions in Cancer. (2010): 19-41.
172. Tian T, Hao J, Xu A, et al. Determination of metastasis-associated proteins in non-small cell lung cancer by comparative proteomic analysis. Cancer Sci. 2007;98(8):1265-74.
173. Chen H, Xu C, Jin Q, Liu Z. S100 protein family in human cancer. Am J Cancer Res. 2014;4(2):89-115.
174. Greening DW, Ji H, Chen M, et al. Secreted primary human malignant mesothelioma exosome signature reflects oncogenic cargo. Sci Rep. 2016;6:32643.

ANNEXE I – Supplementary material

Table S1. TNM staging classification for exocrine pancreatic cancer. This table demostrates the anatomic stage of the disease and the prognostic groups.

Definition	
Primary tumor(T)	
Tx	Primary tumor cannot be evaluated.
T0	No evidence of primary tumor.
Tis	Carcinoma in situ, including “PanIII“ classification.
T1	Tumor limited to the pancreas ≤ 2 cm in greatest diameter
T2	Tumor limited to the pancreas > 2 cm in greatest diameter
T3	Tumor extends beyond the pancreas without involvement of the celiac axis or superior mesenteric artery.
T4	Tumor involves the celiac axis or the superior mesenteric artery (unresectable primary tumor).
Regional Lymph Nodes (N)	
NX	Regional lymph nodes cannot be evaluated
N0	No regional node metastasis
N1	Regional lymph node metastasis
Distal Metastasis (M)	
MX	Distant metastasis cannot be evaluated.
M0	No distant metastasis
M1	Distant metastasis

Stage grouping			
Stage 0	Tis	N0	M0
Stage IA	T1	N0	M0
Stage IB	T2	N0	M0
Stage IIA	T3	N0	M0
Stage IIB	T1	N1	M0
	T2	N1	M0
	T3	N1	M0
Stage III	T4	Any N	M0
Stage IV	Any T	Any N	M1

Table S2. This table summarizes the statistically significant deregulated genes identified by scRNA-seq in CTCs versus primary tumor cells.

Symbol	log2 fold change	direction	FDR
FOS	-10.2	down-regulated	8.5008E-09
TGFBI	-11.4	down-regulated	8.5008E-09
COL1A2	-9.2	down-regulated	1.0596E-05
EGR1	-11.0	down-regulated	1.1231E-05
SAT1	-3.5	down-regulated	4.3182E-05
KLF6	-3.0	down-regulated	0.00011433
IL32	4.2	up-regulated	0.00014097
SCD	-10.2	down-regulated	0.00058038
COL1A1	-10.1	down-regulated	0.00102859
CD44	-2.1	down-regulated	0.00230985
MAN2A1	-7.3	down-regulated	0.00411704
SLC39A11	-9.5	down-regulated	0.00411704
HSP90B1	-2.0	down-regulated	0.00429505
ITGB8	-3.2	down-regulated	0.00429505
TSC22D1	-8.2	down-regulated	0.00429505
TAPBP	-2.6	down-regulated	0.00507435
PTTG1	2.5	up-regulated	0.00519431
CD109	-8.5	down-regulated	0.00547216

GLRX	2.6	up-regulated	0.00547216
MARCKS	-2.7	down-regulated	0.00659957
TNS3	-7.4	down-regulated	0.00659957
COL6A3	-3.8	down-regulated	0.00750599
DNMT3A	-7.2	down-regulated	0.00750599
CCNB1	3.1	up-regulated	0.00842524
FOSB	-6.9	down-regulated	0.00842524
IGFBP3	-8.5	down-regulated	0.00842524
STEAP3	-6.9	down-regulated	0.00895967
DHRS3	-7.8	down-regulated	0.00925168
AMIGO2	-6.9	down-regulated	0.01023283
LIPA	-7.0	down-regulated	0.01160081
CDKN3	3.0	up-regulated	0.01176546
SLC5A3	-9.3	down-regulated	0.01291935
KIAA1109	-6.7	down-regulated	0.01304171
THBS1	-6.9	down-regulated	0.01304171
ZFP36	-3.1	down-regulated	0.01411937
SPARC	-2.8	down-regulated	0.01693196
PCMTD1	-7.3	down-regulated	0.01854657
COL11A1	-6.8	down-regulated	0.01930312
COL3A1	-6.6	down-regulated	0.02172881
NFKBIZ	-6.8	down-regulated	0.02351611
NR4A2	-6.5	down-regulated	0.02416221
BIRC5	3.2	up-regulated	0.02880758
BAG2	2.4	up-regulated	0.0302595
ELP2	-6.6	down-regulated	0.03576705
CTSC	-2.3	down-regulated	0.04264083
CALU	-3.1	down-regulated	0.04532532
SRPX	-7.7	down-regulated	0.04532532

Table S3. This table summarizes the differentially deregulated genes identified by scRNA-seq in CTCs versus liver metastatic tumor cells.

Symbol	log2 fold change	direction	FDR
KLF6	-2,6	down-regulated	0,045742
SPARC	-3,2	down-regulated	0,096095
EIF5	2,4	up-regulated	0,129277
CD44	-1,7	down-regulated	0,188729
TNS3	-7,2	down-regulated	0,188729

EGR1	-10,1	down-regulated	0,19307
CAPZA1	1,4	up-regulated	0,253283
LIPA	-6,6	down-regulated	0,253283
SLC1A5	-6,3	down-regulated	0,263756
EYA3	2,1	up-regulated	0,295456
KIAA1109	-6,1	down-regulated	0,360318
EPDR1	-5,9	down-regulated	0,367628
EXT2	-5,9	down-regulated	0,367628
HSPA5	-3,3	down-regulated	0,367628
PPP1CB	1,4	up-regulated	0,367628
PPP6R3	1,9	up-regulated	0,367628
YWHAE	1,6	up-regulated	0,367628
CDC42	1,4	up-regulated	0,423215
COL1A2	-5,6	down-regulated	0,423215
CTSC	-2,1	down-regulated	0,423215
MAN2A1	-5,7	down-regulated	0,423215
OS9	-5,9	down-regulated	0,423215
RPN2	-2,2	down-regulated	0,423215
SAR1A	1,4	up-regulated	0,423215
DNMT3A	-5,6	down-regulated	0,486752
HSP90B1	-1,5	down-regulated	0,486752
NR4A2	-5,4	down-regulated	0,486752
SRPX	-7,0	down-regulated	0,486752
ZFP36	-2,9	down-regulated	0,486752
FOS	-8,1	down-regulated	0,51287
GLRX	1,9	up-regulated	0,51287
TAPBP	-2,0	down-regulated	0,51287
TGFBR1	-5,7	down-regulated	0,536809
ARL8B	2,1	up-regulated	0,537001
CTSB	-2,0	down-regulated	0,537001
DYNC2H1	-6,7	down-regulated	0,537001
GLT25D2	-5,4	down-regulated	0,537001
IL32	2,2	up-regulated	0,537001
LEPRE1	-5,2	down-regulated	0,537001
PIGU	-5,4	down-regulated	0,537001
TNFAIP2	-5,3	down-regulated	0,537001
ZBTB11	-5,4	down-regulated	0,537001
ZW10	-6,1	down-regulated	0,537001
MAP1A	-5,2	down-regulated	0,547961
STEAP3	-5,3	down-regulated	0,547961
ABCC1	-6,3	down-regulated	0,565401
ARHGEF10	-4,4	down-regulated	0,565401
ARHGEF9	-4,6	down-regulated	0,565401
ARPC4	1,4	up-regulated	0,565401
ARRB1	-4,6	down-regulated	0,565401

ATL2	-4,8	down-regulated	0,565401
BAG2	1,6	up-regulated	0,565401
BRD3	-4,9	down-regulated	0,565401
CALU	-2,4	down-regulated	0,565401
CCDC93	2,7	up-regulated	0,565401
CCL2	-4,8	down-regulated	0,565401
CHIC1	-4,8	down-regulated	0,565401
COL11A1	-4,5	down-regulated	0,565401
COL1A1	-5,7	down-regulated	0,565401
DHRS1	-4,9	down-regulated	0,565401
DHX38	-4,9	down-regulated	0,565401
DRAP1	1,8	up-regulated	0,565401
DUSP1	-7,1	down-regulated	0,565401
EIF5A	1,7	up-regulated	0,565401
ELP2	-5,2	down-regulated	0,565401
EMR1	-5,4	down-regulated	0,565401
ESYT1	-6,3	down-regulated	0,565401
FAM204A	1,6	up-regulated	0,565401
FAS	-6,5	down-regulated	0,565401
FASTKD5	-4,7	down-regulated	0,565401
G6PC3	-5,1	down-regulated	0,565401
GALNT14	-5,0	down-regulated	0,565401
GFPT2	-4,5	down-regulated	0,565401
GIPC2	0,1	up-regulated	0,565401
GLMN	-5,2	down-regulated	0,565401
HIST1H2BD	-5,0	down-regulated	0,565401
HIST1H4C	-1,7	down-regulated	0,565401
ILVBL	-4,7	down-regulated	0,565401
ITPR2	-5,0	down-regulated	0,565401
LOC729013	-4,9	down-regulated	0,565401
MAGEH1	-4,3	down-regulated	0,565401
MPDU1	-5,1	down-regulated	0,565401
MRS2	-5,0	down-regulated	0,565401
MTRNR2L8	-2,8	down-regulated	0,565401
NEK11	-4,7	down-regulated	0,565401
NUCB1	-4,8	down-regulated	0,565401
P4HA2	-7,7	down-regulated	0,565401
PEX11B	-4,9	down-regulated	0,565401
PIGL	-4,7	down-regulated	0,565401
QKI	1,7	up-regulated	0,565401
RCE1	-5,0	down-regulated	0,565401
RGMB	-4,7	down-regulated	0,565401
RPN1	-1,7	down-regulated	0,565401
SERPINA3	-4,5	down-regulated	0,565401
SERPINE1	-2,0	down-regulated	0,565401

SERPINI1	-5,0	down-regulated	0,565401
SIL1	-5,4	down-regulated	0,565401
SLC35C2	-4,7	down-regulated	0,565401
SLC4A2	-4,7	down-regulated	0,565401
SNORA61	-4,9	down-regulated	0,565401
TBL2	-5,0	down-regulated	0,565401
TGFBI	-8,5	down-regulated	0,565401
TMBIM6	-1,7	down-regulated	0,565401
TMEM109	-4,9	down-regulated	0,565401
TMEM205	-6,3	down-regulated	0,565401
TMEM25	-4,9	down-regulated	0,565401
TSPAN3	-6,2	down-regulated	0,565401
UNC5C	-4,7	down-regulated	0,565401
WDR19	-4,7	down-regulated	0,565401
ZAK	1,8	up-regulated	0,565401
ZFAND2A	-5,1	down-regulated	0,565401
ZFP90	-4,7	down-regulated	0,565401
ZNF184	-4,9	down-regulated	0,565401
GPATCH2	-4,5	down-regulated	0,565542
SESN1	-4,5	down-regulated	0,567814
DGKH	-4,3	down-regulated	0,572791
HIST1H2BG	-4,4	down-regulated	0,572791
ZCCHC14	-4,8	down-regulated	0,572791
MTRNR2L2	-2,6	down-regulated	0,581013
RGS2	-4,4	down-regulated	0,587162
ASAP2	1,9	up-regulated	0,587522
MYO9A	-5,0	down-regulated	0,587522
PGRMC1	-5,9	down-regulated	0,587522
SLC2A12	-4,6	down-regulated	0,587522
TTL	2,2	up-regulated	0,587522
YES1	2,0	up-regulated	0,587522
FUT11	-4,4	down-regulated	0,590232
TOR1B	-4,5	down-regulated	0,590232
ZNF473	-4,3	down-regulated	0,590232
SAP30BP	1,5	up-regulated	0,599247
AACS	-4,3	down-regulated	0,608199
ADAMTS3	-4,2	down-regulated	0,608199
AGL	-5,8	down-regulated	0,608199
ALYREF	2,2	up-regulated	0,608199
APH1B	-4,4	down-regulated	0,608199
BBS12	-4,3	down-regulated	0,608199
CCDC15	-4,2	down-regulated	0,608199
CCDC150	-4,1	down-regulated	0,608199
CETN3	1,7	up-regulated	0,608199
CHST14	-4,0	down-regulated	0,608199

CNPY4	-4,2	down-regulated	0,608199
CSPG4	-4,7	down-regulated	0,608199
CSRNP1	-4,1	down-regulated	0,608199
CYB561	-5,2	down-regulated	0,608199
DSC2	-4,4	down-regulated	0,608199
ELMOD2	-4,9	down-regulated	0,608199
FAM57A	-4,6	down-regulated	0,608199
FBXL4	-4,2	down-regulated	0,608199
FOSB	-4,4	down-regulated	0,608199
FSTL1	-4,1	down-regulated	0,608199
GPR107	-4,2	down-regulated	0,608199
HDDC3	-4,2	down-regulated	0,608199
HIVEP3	-4,4	down-regulated	0,608199
HYOU1	-6,8	down-regulated	0,608199
JUNB	-4,6	down-regulated	0,608199
LINC00461	-4,2	down-regulated	0,608199
LRRC6	-4,4	down-regulated	0,608199
NDST2	-4,2	down-regulated	0,608199
NRM	-6,2	down-regulated	0,608199
NUCKS1	1,8	up-regulated	0,608199
NUDT12	-4,2	down-regulated	0,608199
PPT2	-4,0	down-regulated	0,608199
PROCR	-6,9	down-regulated	0,608199
RALGAPA2	-4,2	down-regulated	0,608199
RBFA	2,0	up-regulated	0,608199
RRNAD1	-4,2	down-regulated	0,608199
SCFD2	-4,7	down-regulated	0,608199
SET	1,2	up-regulated	0,608199
SNF8	1,7	up-regulated	0,608199
SP110	-4,2	down-regulated	0,608199
TESK2	-4,3	down-regulated	0,608199
TIAM2	-4,1	down-regulated	0,608199
TM9SF4	-6,0	down-regulated	0,608199
TMEM87B	-4,3	down-regulated	0,608199
UBE2J1	2,8	up-regulated	0,608199
UXS1	-5,6	down-regulated	0,608199
ZFP91	1,9	up-regulated	0,608199
KDELR3	-6,1	down-regulated	0,615725
LOX	-5,6	down-regulated	0,615725
PCMTD1	-5,8	down-regulated	0,61794
TTC13	-4,1	down-regulated	0,626415
ADCY7	-4,5	down-regulated	0,627955
AGBL2	-3,7	down-regulated	0,627955
B9D1	-4,7	down-regulated	0,627955
BCAP31	-1,8	down-regulated	0,627955

CBX3	1,3	up-regulated	0,627955
FYCO1	-4,0	down-regulated	0,627955
GPX3	-3,9	down-regulated	0,627955
HARBI1	-4,3	down-regulated	0,627955
MTBP	-4,0	down-regulated	0,627955
PDSS1	-4,1	down-regulated	0,627955
SFT2D2	-3,8	down-regulated	0,627955
BHLHE40	-7,9	down-regulated	0,629459
CXCL2	-4,5	down-regulated	0,629459
ELL3	-3,7	down-regulated	0,629459
EMC10	-3,7	down-regulated	0,629459
GSTM4	-3,8	down-regulated	0,629459
HIST1H3H	-3,9	down-regulated	0,629459
KLHDC2	-3,9	down-regulated	0,629459
PLOD1	-1,9	down-regulated	0,629459
PRMT6	-4,2	down-regulated	0,629459
SNHG5	1,3	up-regulated	0,629459
TBCCD1	2,2	up-regulated	0,629459
VPS26A	1,5	up-regulated	0,629459
ACYP2	-3,3	down-regulated	0,629574
APCDD1L	-3,7	down-regulated	0,629574
ATAT1	-3,9	down-regulated	0,629574
BBS2	-4,1	down-regulated	0,629574
BIRC5	1,3	up-regulated	0,629574

Table S4. This table summarizes the statistically significant deregulated genes identified by scRNA-seq in liver metastatic cells versus primary tumor cells.

Symbol	log2 fold change	direction	FDR
ADAM19	-2.5	down-regulated	2.8403E-09
ARRDC3	-3.3	down-regulated	2.8403E-09
MARCKS	-2.5	down-regulated	2.8403E-09
PPP1CB	-1.6	down-regulated	2.8403E-09
TGFBI	-2.9	down-regulated	2.8403E-09
TIMP3	-5.2	down-regulated	2.8403E-09
SAR1A	-1.4	down-regulated	5.205E-09
DMD	-4.9	down-regulated	1.2617E-08
PCDH10	3.8	up-regulated	9.119E-08
AMIGO2	-6.6	down-regulated	3.0982E-07

EGLN3	-4.7	down-regulated	3.0982E-07
FKBP9	-2.1	down-regulated	7.4802E-07
OGT	-2.1	down-regulated	8.8619E-07
HTR7	-4.2	down-regulated	1.086E-06
SCG2	-4.7	down-regulated	1.6584E-06
HNRNPH1	-1.5	down-regulated	2.1047E-06
NNMT	-4.1	down-regulated	3.1587E-06
FAP	-6.1	down-regulated	1.085E-05
HAS2	-5.1	down-regulated	1.9916E-05
EIF2S3	-1.2	down-regulated	3.1781E-05
SCD	-2.6	down-regulated	3.1781E-05
MAP1B	-1.2	down-regulated	4.5832E-05
YWHAE	-1.2	down-regulated	6.3675E-05
TMEM255B	-4.4	down-regulated	7.9097E-05
SLC5A3	-3.0	down-regulated	9.2085E-05
PTPRS	-3.3	down-regulated	0.00011948
SLC38A2	-1.8	down-regulated	0.00011948
CCNB1	2.8	up-regulated	0.0001224
WSB1	-1.9	down-regulated	0.00014495
EDEM1	-1.8	down-regulated	0.00015393
MFAP5	-5.2	down-regulated	0.00015393
EMP1	-1.9	down-regulated	0.00016158
SERINC5	-1.6	down-regulated	0.00016801
NBPF7	-2.4	down-regulated	0.00021388
TUBB4B	1.9	up-regulated	0.00024854
CTTN	-1.0	down-regulated	0.0005519
GNAT2	-3.6	down-regulated	0.00071133
TRA2A	-1.4	down-regulated	0.00071133
ITGB1	-0.9	down-regulated	0.00081994
LUC7L3	-1.4	down-regulated	0.00081994
DHRS3	-3.7	down-regulated	0.00087735
AKR1B1	6.4	up-regulated	0.00095662
PTTG1	1.9	up-regulated	0.00095662
NCOA3	-2.2	down-regulated	0.0009694
CDC20	2.9	up-regulated	0.00097208
ISG20	-4.4	down-regulated	0.00101281
ITGB8	-3.0	down-regulated	0.00101281
NDRG1	-5.0	down-regulated	0.00106938
EML4	-1.9	down-regulated	0.00115579
PHLDA1	-1.6	down-regulated	0.00126871
H2AFZ	1.1	up-regulated	0.00131256
MMP2	-6.0	down-regulated	0.00131256
MEDAG	-2.1	down-regulated	0.0013541
ANKRD10	-2.3	down-regulated	0.00152615
LPCAT2	-2.3	down-regulated	0.00155481

SLC39A11	-1.5	down-regulated	0.00158768
THBS1	-3.1	down-regulated	0.00158768
TRPS1	-1.8	down-regulated	0.00158768
ZNF624	-3.8	down-regulated	0.00158768
ZNF860	-4.2	down-regulated	0.00158768
CDK5R1	-3.8	down-regulated	0.00165957
SNORA21	-2.3	down-regulated	0.00193537
PIP4K2A	-1.3	down-regulated	0.0019448
GOLGB1	-1.5	down-regulated	0.00214186
STRN3	-1.5	down-regulated	0.00214186
FOSB	-2.4	down-regulated	0.00238158
DDAH1	-1.3	down-regulated	0.00240829
POC1A	2.9	up-regulated	0.00243587
REEP3	-1.2	down-regulated	0.00251206
TTC3	-1.7	down-regulated	0.00268344
BDH2	-3.9	down-regulated	0.00292976
TMEM41B	-1.5	down-regulated	0.00300527
PTP4A2	-1.1	down-regulated	0.00335196
MALAT1	-1.5	down-regulated	0.00341394
B4GALT1	-1.1	down-regulated	0.00346242
LOC284454	-2.3	down-regulated	0.00346242
VMP1	-1.2	down-regulated	0.00357634
RGCC	-3.0	down-regulated	0.00387567
CDH11	-5.4	down-regulated	0.00402644
CXCL5	3.7	up-regulated	0.00499098
CTNNB1	-1.2	down-regulated	0.00529025
QKI	-1.2	down-regulated	0.00529025
STAT2	-1.5	down-regulated	0.00529025
USP34	-1.4	down-regulated	0.00529025
FLRT2	-0.5	down-regulated	0.00543632
R3HDM2	-1.4	down-regulated	0.00561332
SAT1	-1.8	down-regulated	0.00561923
HMOX2	1.6	up-regulated	0.00599731
IGF1R	-1.8	down-regulated	0.0061133
C10orf54	-3.3	down-regulated	0.00641251
LTBP1	-5.4	down-regulated	0.00684805
POP5	1.6	up-regulated	0.00684805
MKI67	2.8	up-regulated	0.00687913
PSRC1	4.4	up-regulated	0.00747682
RUVBL2	1.7	up-regulated	0.00775024
GPRC5A	-4.7	down-regulated	0.00788746
BCAT1	-1.1	down-regulated	0.0081639
COL6A3	-1.4	down-regulated	0.00846345
EIF4B	-1.2	down-regulated	0.00846345
KPNA2	1.8	up-regulated	0.0088105

MRPS12	1.2	up-regulated	0.00913211
NTSR1	-3.8	down-regulated	0.00913211
AKAP12	-1.2	down-regulated	0.0094233
LOXL1	-5.1	down-regulated	0.00948594
PDGFA	-3.9	down-regulated	0.00986067
TSC22D1	-2.7	down-regulated	0.01036084
PDGFC	-1.7	down-regulated	0.01046011
CALD1	-4.1	down-regulated	0.01048367
TIMP1	-1.4	down-regulated	0.0105297
TMEM154	-4.0	down-regulated	0.01066111
NOG	-4.0	down-regulated	0.0107623
CA12	-4.4	down-regulated	0.01084554
ARL4C	-1.6	down-regulated	0.01097926
CD109	-1.6	down-regulated	0.01141628
SYNE1	-2.1	down-regulated	0.01162825
CNIH3	-4.2	down-regulated	0.01215826
RAP2C	-1.2	down-regulated	0.01215826
RIN2	-1.4	down-regulated	0.01215826
PTHLH	-2.6	down-regulated	0.01252327
KIF4A	2.3	up-regulated	0.01314675
RBPJ	-1.8	down-regulated	0.01314675
USP18	4.2	up-regulated	0.01314675
FOS	-2.1	down-regulated	0.0132021
PLOD2	-1.9	down-regulated	0.01327152
KLF12	-4.5	down-regulated	0.01354669
LPP	-1.4	down-regulated	0.01356365
ARPC4	-1.1	down-regulated	0.01408836
HAS2-AS1	-0.7	down-regulated	0.01408836
UBR1	-2.1	down-regulated	0.01408836
SYT1	-2.1	down-regulated	0.01427144
ARF6	-1.2	down-regulated	0.01526575
FBN1	-2.6	down-regulated	0.01624549
SLC2A1	-2.2	down-regulated	0.01669102
CDC42	-0.8	down-regulated	0.0170762
PMEPA1	-1.9	down-regulated	0.0170762
PON3	-2.8	down-regulated	0.0170762
TLK1	-1.1	down-regulated	0.0170762
H3F3B	0.7	up-regulated	0.01709381
ZC3HC1	2.6	up-regulated	0.01722442
CDCA3	2.5	up-regulated	0.01744472
EDEM3	-1.7	down-regulated	0.01744472
SKIL	-1.5	down-regulated	0.01836637
SLC20A1	-1.3	down-regulated	0.01845839
ATRX	-1.2	down-regulated	0.0193895
PAQR7	-1.6	down-regulated	0.01947123

PJA2	-1.4	down-regulated	0.01947123
RNF144A	-2.3	down-regulated	0.01947123
SERINC1	-1.2	down-regulated	0.01947123
TSPYL1	-0.9	down-regulated	0.01947123
CAPZA1	-0.7	down-regulated	0.01959184
PRR5L	-4.4	down-regulated	0.02004494
SEMA3C	-1.7	down-regulated	0.02004494
NFKBIZ	-3.3	down-regulated	0.0200719
CDCA8	2.5	up-regulated	0.02008844
IQGAP1	-1.0	down-regulated	0.02072443
ARHGAP1	-1.4	down-regulated	0.02073285
MIR4714	-1.9	down-regulated	0.02076434
TOB1	-1.4	down-regulated	0.02116123
MATN3	-3.7	down-regulated	0.02126894
MLL3	-2.0	down-regulated	0.02126894
FAM3C	-1.3	down-regulated	0.02161174
ITGB5	-2.0	down-regulated	0.02184877
AURKB	2.5	up-regulated	0.02193636
ITPR3	-5.3	down-regulated	0.02193636
TUBA1C	1.0	up-regulated	0.02193636
MIER1	-1.1	down-regulated	0.02211827
TUBB	0.8	up-regulated	0.02222688
PSMC4	0.7	up-regulated	0.02370362
THAP5	-1.2	down-regulated	0.02370362
PSMB5	0.9	up-regulated	0.0245046
TPX2	2.0	up-regulated	0.0245046
FNIP1	-1.4	down-regulated	0.02462276
GPR183	-0.4	down-regulated	0.02515702
SNTB2	-1.3	down-regulated	0.02515702
TUFM	1.4	up-regulated	0.02515702
ENTPD5	-4.0	down-regulated	0.02553252
COL3A1	-2.3	down-regulated	0.0258858
PPL	-4.8	down-regulated	0.0258858
RNF26	2.4	up-regulated	0.0258858
HSF2BP	4.1	up-regulated	0.02720888
TUBA1A	-0.9	down-regulated	0.02748426
SEC22B	-0.9	down-regulated	0.02826093
NDC80	2.1	up-regulated	0.02827151
CCDC164	-2.0	down-regulated	0.0303265
COG1	-3.3	down-regulated	0.0303265
COPS6	1.2	up-regulated	0.0303265
TMPO	1.5	up-regulated	0.0303265
UBE2D3	1.1	up-regulated	0.0303265
CDCA5	1.9	up-regulated	0.03041914
TGFBR2	-2.0	down-regulated	0.03041914

DST	-0.9	down-regulated	0.03065429
DLGAP5	2.1	up-regulated	0.03076129
BUB3	0.9	up-regulated	0.03093549
MAD2L1	2.1	up-regulated	0.03144197
MYADM	-1.2	down-regulated	0.03155583
FAM32A	1.6	up-regulated	0.03250276
KCTD18	-3.0	down-regulated	0.03431073
TUBA1B	0.8	up-regulated	0.03490438
GADD45A	2.9	up-regulated	0.03639458
GLS	-1.4	down-regulated	0.03803619
CABYR	3.0	up-regulated	0.0393121
ITPRIPL2	-1.2	down-regulated	0.03934289
YWHAZ	-0.6	down-regulated	0.03934289
HN1	1.1	up-regulated	0.03938609
PDCD4	-1.2	down-regulated	0.0401303
SRSF6	-1.2	down-regulated	0.0410698
GOLGA3	-1.2	down-regulated	0.04138667
TRPM7	-1.4	down-regulated	0.04139845
N4BP2L2	-1.5	down-regulated	0.04173372
C12orf23	-1.3	down-regulated	0.04215506
CCNB2	2.4	up-regulated	0.04215506
DEPDC1	2.3	up-regulated	0.04215506
MGA	-1.6	down-regulated	0.04215506
SLC30A1	-3.5	down-regulated	0.04215506
TAF1D	-1.4	down-regulated	0.04215506
AHI1	-1.4	down-regulated	0.04239187
EFNA5	-1.4	down-regulated	0.04239201
PPP6R3	-1.0	down-regulated	0.04293361
AGBL2	3.3	up-regulated	0.04361627
HMGB2	1.6	up-regulated	0.04361627
KIF5A	-3.2	down-regulated	0.04394212
GLIPR1	-2.5	down-regulated	0.04429346
WIPF1	-4.6	down-regulated	0.04698874
RFX2	-0.5	down-regulated	0.04716232
ADAM20	-0.5	down-regulated	0.04811704
ANKRD40	-0.9	down-regulated	0.04811704
TOP2A	2.4	up-regulated	0.049078
CEP55	1.8	up-regulated	0.04922169
ELOF1	2.3	up-regulated	0.04922169
PRKD1	-5.0	down-regulated	0.04922169
SYNGR2	3.1	up-regulated	0.04922169

Table S5. This table summarizes the 37 human proteins present in at least 70% of lung-tropic exosome samples.

Gene names	Organism	Welch's T-test q-value liver vs pdac	Welch's T-test Difference liver_vs pdac	Welch's T-test q-value lung vs pdac	Welch's T-test Difference lung vs pdac	Welch's T-test q-value Lung vs Liver Agress	Welch's T-test Difference Lung vs Liver Agress
MUC5AC	Human	0,000	-8,619	0,000	-9,481	0,582034	-1,34754
FLG2	Human	0,052	0,783	0,651	0,504	0,942197	-0,16826
SBSN	Human	1,000	0,000	0,016	-0,904	0,412	-0,73624
SPHK2	Human	1,000	0,000	0,000	3,143	0,000	2,517859
OSBP	Human	0,471	-0,230	0,667	-0,140	0,605753	0,271438
HMGA2	Both (H)	0,000	-1,986	0,000	-1,400	0,385279	0,548807
AHNAK	Human	0,000	-4,242	0,000	1,890	0,000	6,051396
ITGA6	Both (H)	0,000	-3,582	0,000	-3,196	0,811296	0,270408
SELENBP1	Human	1,000	0,000	0,000	4,961	0,003055	2,995849
CAT	Human	0,992	0,030	0,010	1,241	0,810952	0,738166
GYG2	Human	1,000	0,000	0,000	4,222	0,000	4,236656
VIM	Human	0,000	-5,175	0,000	-4,475	0,263803	0,787262
FLNA	Both (H)	0,000	-5,294	0,000	-7,476	0,000229	-2,83524
FASN	Human	0,000	-11,249	0,000	-11,441	0,978201	-0,04014
PKM	Human	0,000	-7,812	0,000	-5,603	0,023483	1,999727
GAPDH	Human	0,000	-6,791	0,000	-3,978	0,001096	2,959638
PYGB	Human	0,000	-6,410	0,000	-2,635	0,000	3,659831
TUBB8	Human	0,000	-5,416	0,295	-0,664	0,000	4,052232
HSP90AA1	Human	0,000	-7,234	0,000	-6,746	0,969518	-0,05596
HSP90AB2P	Human	0,015	0,530	0,307	-0,274	0,000	-0,72257
EEF1G	Human	0,000	-6,334	0,000	-6,076	0,920133	-0,14221
COPA	Human	0,000	-1,950	0,000	-1,080	0,008813	1,118923
FARSA	Human	0,000	-3,804	0,000	-1,643	0,000164	2,091284
S100A11	Both (H)	0,000	-4,794	0,727	0,256	0,000	4,79905
ALDH1A1	Human	0,002	2,520	0,000	3,550	0,710454	0,222613

MVP	Human	0,000	-8,378	0,000	-9,633	0,009234	-1,81275
PFN1	Human	0,000	-7,630	0,000	-7,446	0,772751	-0,75945
PLEC	Human	0,000	-8,778	0,000	-8,704	0,737791	-0,2451
ENO1	Human	0,000	-6,217	0,000	-5,080	0,281622	0,670389
PGK1	Both (H)	0,000	-7,713	0,000	-6,203	0,888656	0,415717
PFKP	Human	0,000	-7,510	0,000	-7,888	0,860276	-0,37297
HSPB1	Human	0,000	-8,726	0,000	-8,023	0,037227	0,859078
ESD	Human	0,000	-8,853	0,000	-7,679	0,000662	1,55881
UBA1	Both (H)	0,000	-8,959	0,000	-8,381	0,066775	0,837086
WDR1	Human	0,000	-2,719	0,000	-2,818	0,135165	-0,21826
CLIC1	Human	0,000	-7,899	0,000	-6,231	0,071362	1,386115

ANNEXE II – Conference presentations

Abstract B42: Patient-derived metastatic models of pancreatic cancer: An in-vivo system for modeling metastasis and preclinical drug screening.

Spas Dimitrov, Manuel Muñoz, Natalia Baños, Camino Menéndez, Victoria Bonilla, Yolanda Dur an, Rodrigo Toledo, Francesca Sarno, Javier Perales-Patón, Fátima Al-Shahrour, Pedro P. Lopez-Casas and Manuel Hidalgo

DOI: 10.1158/1557-3265.PDX16-B42 Published August 2016.

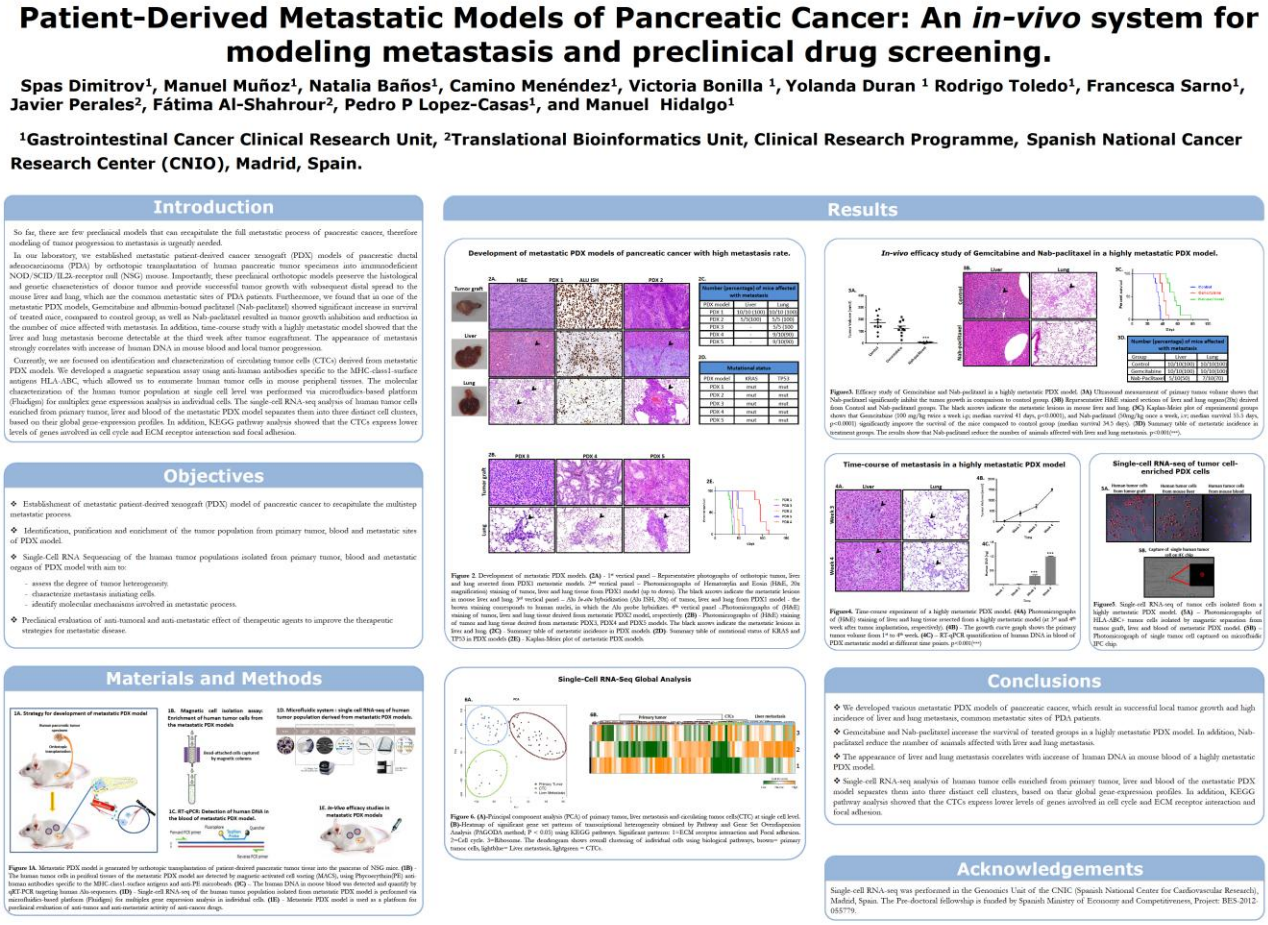

VI. CONCLUSIONES

1. Los modelos metastásicos PDX de cáncer de páncreas desarrollados en esta tesis proporcionan una plataforma *in-vivo* eficiente y reproducible para modelar de forma precisa todo el proceso metastásico y para el aislamiento de todas las poblaciones tumorales implicadas en la enfermedad metastásica.

2. Las células tumorales circulantes (CTC) pancreáticas humanas poseen alta capacidad tumorigénica y metastásica. Los tumores derivados de CTC preservan las características morfológicas del tumor parental.

3. La enfermedad metastásica del cáncer de páncreas es un proceso evolutivo bien organizado, donde las células tumorales primarias, las células metastásicas y los CTC son transcripcionalmente distintos entre sí. La heterogeneidad transcripcional entre estos tres grupos biológicos se define por tres patrones biológicos que son la interacción ECM y la adhesión focal, el ciclo celular y la biogénesis ribosómica.

4. La disección de transcriptoma al nivel individual de la enfermedad metastásica fue capaz de descubrir numerosos genes desregulados asociados con la metástasis. Survivina es uno de estos genes relacionados con la metástasis que está sobreexpresado en CTC y el bloqueo farmacológico de este gen fue capaz de reducir la carga tumoral metastásica y mejorar la supervivencia media de los modelos metastáticos PDX de cáncer de páncreas. Además, la expresión de la proteína survivina se detectó en los tumores primarios y sitios metastásicos de todos los modelos metastásicos PDX, lo que sugiere que survivina puede ser un marcador pronóstico y una diana terapéutica anti-metastásica para la metástasis del cáncer pancreático.

5. Aunque el perfil proteico de los exosomas purificados de los tumores primarios y sitios metastásicos de los modelos metastásicos PDX no logró separar los modelos "agresivos" de "menos agresivos", este análisis proteómico identificó firmas proteómicas "órgano-específicas" con abundante expresión de varias proteínas exosomales asociadas con la metástasis.